

ANALYSIS OF MOMENT TRANSFER IN  
MULTI-SPAN WEB SYSTEMS

By

ANUGU ARJUN REDDY

Bachelor of Technology in Mechanical Engineering

Jawaharlal Nehru Technology University

Hyderabad, Andhra Pradesh

2007

Submitted to the Faculty of the  
Graduate College of the  
Oklahoma State University  
in partial fulfillment of  
the requirements for  
the Degree of  
MASTER OF SCIENCE  
May, 2010

ANALYSIS OF MOMENT TRANSFER IN  
MULTI-SPAN WEB SYSTEMS

Thesis Approved:

Dr. J.K. Good

---

Thesis Adviser

Dr. R.D. Delahoussaye

---

Dr. S.P. Harimkar

---

Dr. A. Gordon Emslie

---

Dean of the Graduate College

## **ACKNOWLEDGMENTS**

I wish to express my sincere and utmost gratitude to my mentor, advisor and thesis chair, Dr. James K. Good for his insightful guidance, encouraging confidence and immeasurable kindness throughout my graduate program. I highly appreciate the time he spent discussing my research, especially when I was stuck. This research would not have been possible without his help. In addition, I would like to thank him for his concern and guidance towards my future career plans.

I would like to thank Dr. Ronald D. Delahoussaye and Dr. Sandip P. Harimkar for serving on my graduate committee.

I am indebted to Mr. Ron Markum, Senior Research Engineer at WHRC, for his invaluable time and immense cooperation throughout my work. I would like to thank him for his significant assistance with the design of experimental setups and for teaching all the odds and evens of machining.

I thank the WHRC sponsors for making my research possible.

Finally, I wish to express my sincere thanks to my parents, Gopal R. Anugu and Uma, my sister, Archana and my friends for their constant words of encouragement, unfailing support and patience through the entire duration of this research and all my other endeavors.

## TABLE OF CONTENTS

Chapter	Page
1. Introduction.....	1
2. Literature Review.....	6
2.1 Research Objective: .....	13
3. Experimental Procedure.....	14
3.1 Laser Doppler Velocimeters .....	14
3.1.1 Overview .....	14
3.1.2 Principle of operation .....	15
3.1.3 Using LDVs for Moment measurements.....	17
3.2 Developing a calibration rig for LDVs .....	19
3.2.1 Data Acquisition system for the calibration rig: .....	24
3.3 Preliminary tests.....	26
3.4 Building the new Test Rig: .....	31
3.5 Crucial parts installed on the machine:.....	38
3.6 Troubleshooting and the instruments used .....	42
3.7 A Summary of the Capabilities of the Machine: .....	45
3.8 Web Properties Testing:.....	49
3.8.1 Measurement of the Tangential Modulus of Elasticity: .....	49
3.8.2 Measurement of Coefficient of Static Friction:.....	51
3.8.3 Surface Roughness Tests (on roller B):.....	52
3.9 Evaluating different misalignment values for roller C .....	55
4. Experimental Results and Discussion.....	58
4.1 Calculating Moments: .....	59
4.2 Cosine error in measurements and correction:.....	62
4.3 Results in span B.....	66
4.4 Results on roller B: .....	69
4.5 Results in span A: .....	71
4.6 Results from Keyence sensors .....	74
5. A New FEM Model .....	77
5.1 Introduction.....	77
5.2 Defining the Model.....	78

5.3 Applying Boundary Conditions .....	81
5.4 Executing the Problem.....	84
5.5 Results from FEM model.....	85
6. Summary and Conclusions .....	90
6.1 Summary .....	90
6.2 Conclusions.....	90
6.3 Future Work.....	91
7. REFERENCES .....	92
8. APPENDICES .....	94

## LIST OF TABLES

<b>Table</b>		<b>Page</b>
Table 3.1	Specifications of the LDV .....	16
Table 3.2	Test specifications for preliminary tests.....	28
Table 3.3	Allowable tensions at various speeds .....	54
Table 3.4	Test specifications .....	55
Table 4.1	Test positions on roller B .....	69
Table 4.2	Lateral deflection on roller B .....	76
Table 5.1	Various Misalignment cases.....	78
Table 5.2	Inputs for the model .....	80
Table 5.3	Lateral deformations at various nodes.....	86
Table 5.4	A comparison of web edge deflections .....	87

## LIST OF FIGURES

<b>Figure</b>		<b>Page</b>
Figure 1.1	Misaligned roller .....	2
Figure 1.2	A two span web system .....	3
Figure 1.3	Tension distribution before and after slippage at roller B ( $\theta_1 < \theta_2$ ) .....	5
Figure 2.1	When the traction between the roller B and the web is enough to contain the moment generated within span B .....	7
Figure 2.2	When the traction between the roller B and the web is NOT enough to contain the moment generated within span B .....	8
Figure 2.3	Beam element showing sign convention for Loads and Deformations .....	9
Figure 3.1	Two types of LDVs .....	15
Figure 3.2	Fringe pattern formed by LDV .....	16
Figure 3.3	Using LDVs to estimate CMD strains .....	18
Figure 3.4	Basic principle of the experiment (with cosine error) .....	20
Figure 3.5	Side view of LDV showing the Rotation Stage with Micrometer .....	21
Figure 3.6	Setup with both the LDVs shooting on the shaft simultaneously .....	23
Figure 3.7	(a)Data from the LS8000 LDVs .....	25
Figure 3.7	(b)Data from the LS200 LDVs .....	25

Figure 3.8	Sketch showing span B.....	26
Figure 3.9	Test setup for measuring strains in a web with the help of LDVs .....	27
Figure 3.10	Micrometer assembly .....	28
Figure 3.11	Positioning of the LDVs.....	30
Figure 3.12	Sketch of the apparatus modeled with Inventor® .....	33
Figure 3.13	LDVs taking data in entering span (span B) .....	34
Figure 3.14	LDVs taking data over roller B .....	35
Figure 3.15	Schematic diagram of the web line through the test setup .....	37
Figure 3.16	Combined assembly of the test rig and the winder .....	38
Figure 3.17	Linear variable differential transformers.....	39
Figure 3.18	A Keyence sensor with its controller .....	40
Figure 3.20	Picture of a FIFE guide assembly.....	41
Figure 3.19	Schematic diagram of a web guide.....	41
Figure 3.21	Use of Dial indicators for align LDV arm in line to the roller B .....	43
Figure 3.22	Crow’s foot micrometer with its extension rods .....	44
Figure 3.23	Custom made micrometer for aligning roller B and roller C .....	45
Figure 3.24	18' Starrett® Machinists' Level .....	45
Figure 3.25	LDVs taking data in all three spans.....	46
Figure 3.26	Top view of the span B showing edge sensors.....	47
Figure 3.27	Lateral deformation in the pre-entering span .....	48
Figure 3.29	Schematic diagram showing Stretch test.....	50
Figure 3.31	Setup for measurement of Co-efficient of Static Friction .....	51
Figure 3.32	Surface roughness tester.....	54



Figure 4.1	Free body diagram web in span B .....	61
Figure 4.2	Plot of moments before correcting cosine error .....	62
Figure 4.3	Cosine error in LDV measurements .....	63
Figure 4.4	Modification in test setup to correct cosine error .....	65
Figure 4.5	Moment at 30' from roller B in span B at $\theta=0.074$ degrees .....	66
Figure 4.6	Moments in span B, when $\theta=0.074$ degrees .....	67
Figure 4.7	Moments in span B, when $\theta=0.223$ degrees .....	67
Figure 4.8	Moments in span B, when $\theta=0.446$ degrees .....	68
Figure 4.9	Different locations on roller B .....	69
Figure 4.10	Moments on roller B .....	70
Figure 4.11	Moments in Span A ( $0.446^\circ$ ) .....	72
Figure 4.12	Shear and moment diagram for a constrained beam .....	73
Figure 4.14	Data recorded from S1 and S2 .....	75
Figure 5.1	Distribution of nodes on the web .....	79
Figure 5.2	Lateral deformations at various nodes .....	86
Figure 5.3	Moments on roller B from FE model .....	89

# **CHAPTER I**

## **Introduction**

Any material made from paper, textiles, metals or composites in continuous flexible strip form is called a web. Webs are manufactured and then wound in a roll for storage and transportation. Web handling is the mechanics involved in transporting web materials through process machinery. If the handling is done correctly the losses and defects should be minimal. Web processes include coating, laminating, drying, calendaring, embossing, slitting, and metalizing. During processing, losses of web material occur mainly due to improper winding, wrinkling, misalignment, web deformations, breakage and slitting processes.

Webs pass over numerous rollers in web processing machinery. A common problem is the formation of troughs and wrinkles in webs. A web span is an unsupported length of web between two rollers. Any out-of-plane web deformation in a span is called a trough and if this trough passes over a roller it may form a wrinkle. A major reason for the formation of troughs and wrinkles is the misalignment of the downstream roller in a span, as shown in Figure 1.1. Lorig [3] found that webs always try to enter a downstream roller normally. Due to the misalignment, shear forces are generated in the test span which produces compressive stresses in cross machine direction (CMD) of the web.

Increasing the amount of misalignment causes increases in the CMD stresses when these compressive stresses exceed the critical buckling stress for the web in the free span, troughs will result.

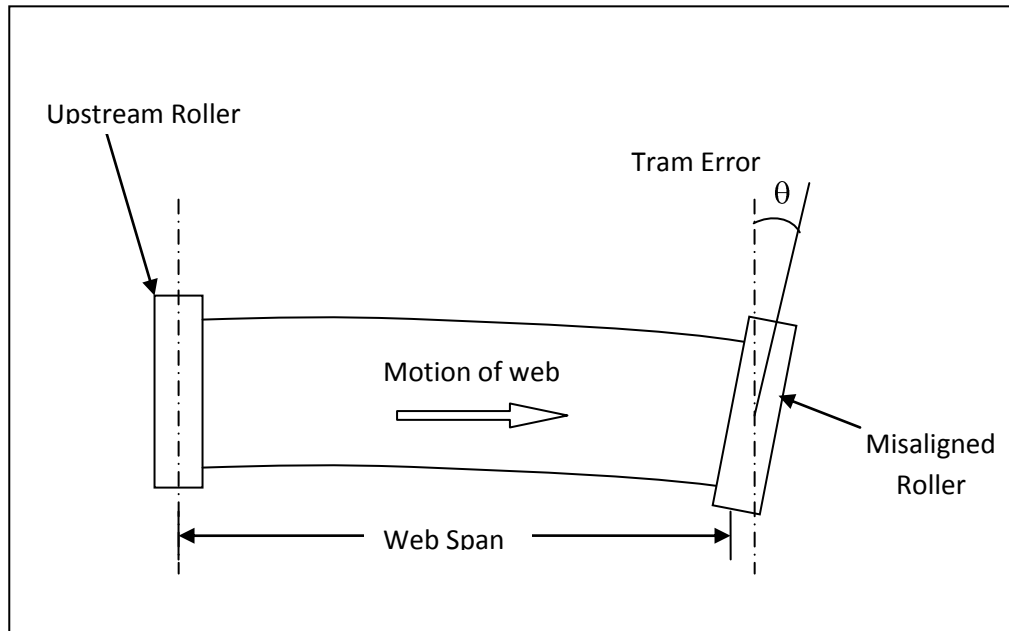


*Figure 1.1 Misaligned roller*

A web between an upstream roller and a misaligned downstream roller behaves as a cantilever beam subjected to an end load. Shelton [1] determined that the moment in the web span is zero at the misaligned roller and increases linearly towards the upstream roller. Shelton's findings depend on the adequate friction between the web and the upstream roller to provide the displacement and slope constraints at the cantilever root.

The assumptions made for the analysis of single span web systems may not be valid when multiple span web systems are considered. For instance the assumption of cantilever support at the upstream roller in a single span would require infinite friction between the web and the upstream roller. If the assumption of the cantilever support is

relaxed we must begin to consider a web as a structure whose lateral deformation is governed by frictional forces that result web/roller interaction. In analysis the next step of complexity is a two span system where the lateral behavior of the web is now governed by three rollers as shown in Figure 1.2. The three rollers A, B and C are shown in a single plane but in reality web makes a 90° wrap angle around each roller. Whenever roller C is misaligned, a bending moment is developed in span B. The bending moment is maximum at roller B and decreases linearly to zero as we approach roller C. The value of the

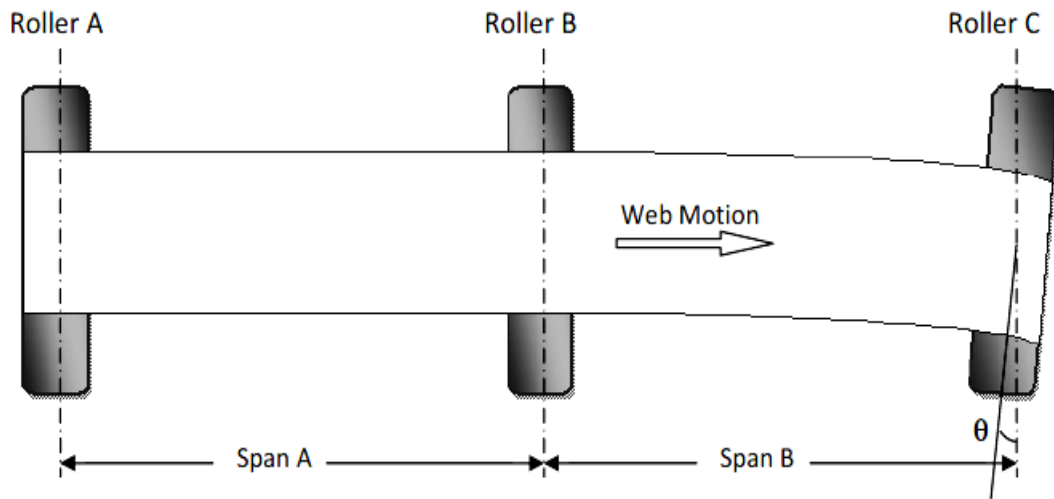


Figure 1.2 A two span web system

bending moment in the web at roller B increases with the increased misalignment of roller C, and goes to maximum value  $M_r$ . Good [2] has shown that:

$$M_r = \frac{\mu T \beta W}{4}$$

where,  $\mu$  is coefficient of friction between roller B and web material, T is tension in the web,  $\beta$  is angle of wrap of web around roller B and W is width of web. As the moment at

roller B increases traction between the roller and web decreases causing slippage over the roller and when bending moment at roller B ( $M_{bi}$ ) goes beyond  $M_r$ , bending moment begins to transfer across roller B from span B to span A. This can be seen in Figure 1.3. Also an attempt has been made to show the tension distribution at each roller with the increase in misalignment or bending moment.

The focus of this research is to study moment transfers from a span to its upstream span which is induced due to a misaligned downstream roller. An experimental setup was built to quantify amount of moments transferred and to validate the above expression for predicting  $M_r$  with help of the data taken. A finite element model was developed for a better understanding of moments and moment transfer in a multispan web system due to a misaligned downstream roller.

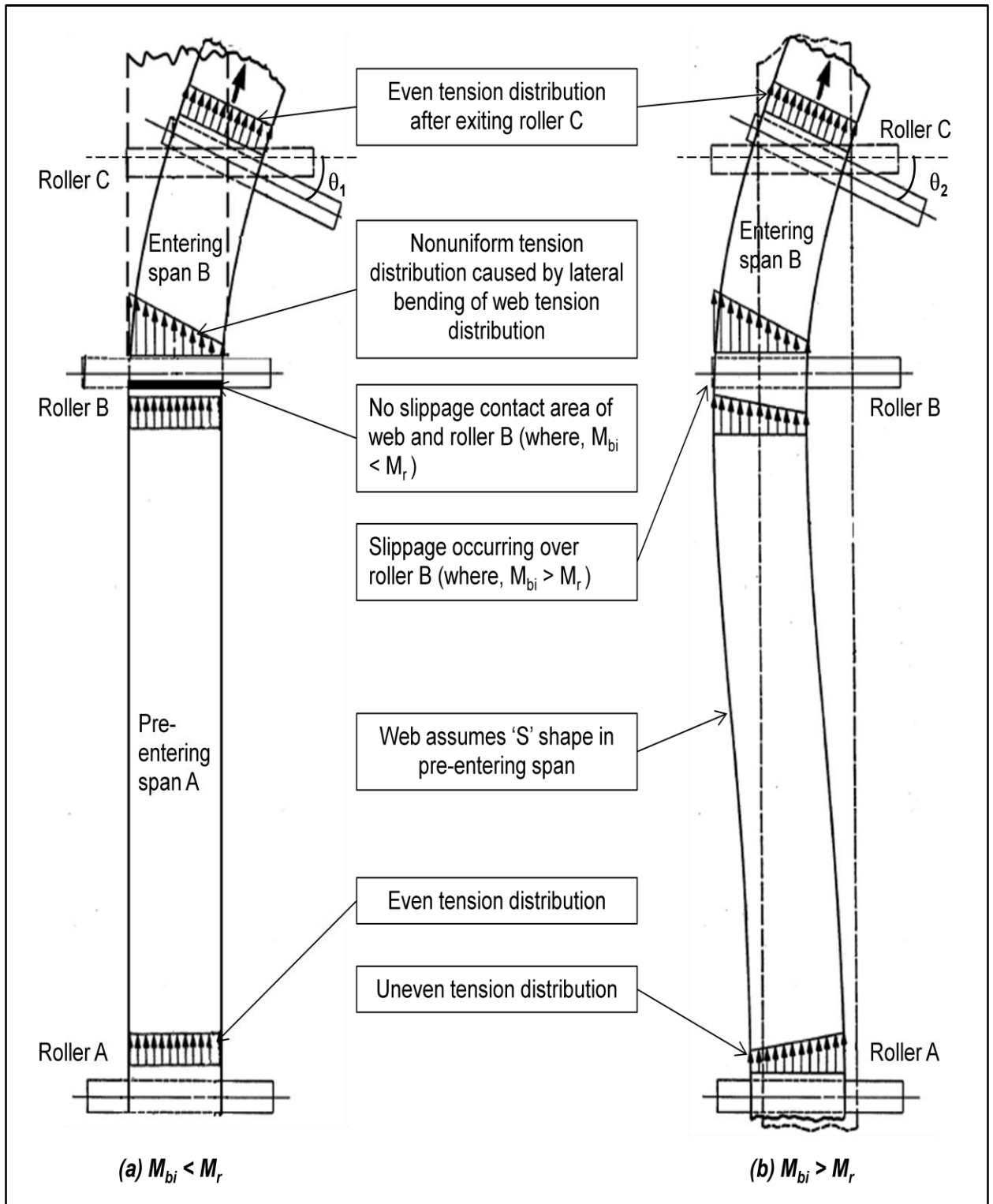


Figure 1.3 Tension distribution before and after slippage at roller B ( $\theta_1 < \theta_2$ )

## **CHAPTER II**

### **Literature Review**

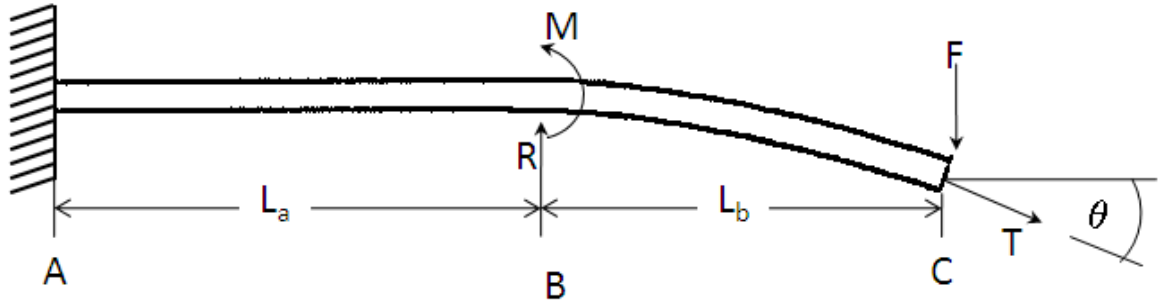
A study of the previous research was conducted on moments generated in webs due to misaligned rollers and interaction between two web spans due to a downstream misaligned roller.

In 1950, Lorig [3] suggested the concept of normal entry of a web to a downstream roller. He focused on the steering of the web due to crowned, concave and self centered rollers. Though he was able to explain the theory behind the normal entry of the web, he could not formulate or generate any model to predict lateral displacements in the web. In his doctoral thesis, Shelton [1] addressed the same problem, where the steering of the web was caused by a misaligned downstream roller. He developed a model in which the web was treated as a simply supported beam. Moment generated due to misaligned downstream roller was found to be zero at the end of the span. Shelton developed an experimental setup to verify his models. He provided methods to find web material properties and coefficient of friction between the web and the rollers.

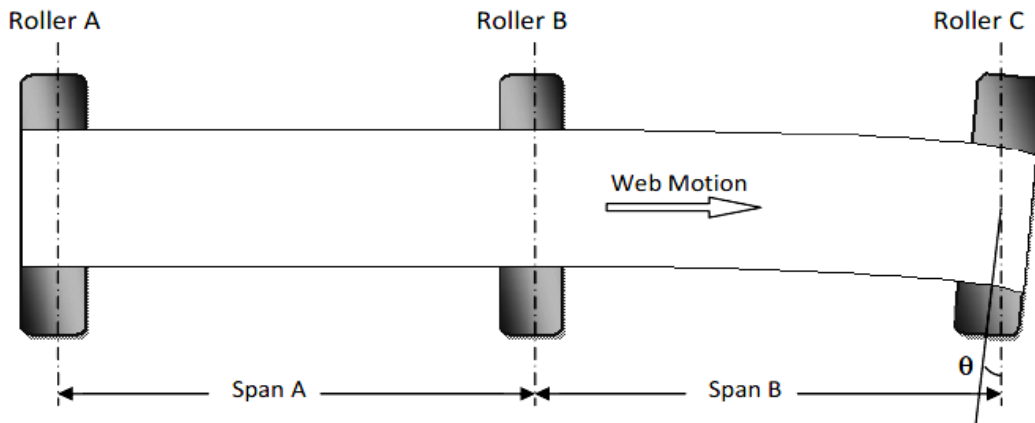
Gehlbach, et al. [4] studied shear wrinkles (which were then defined as the wrinkles due to misaligned roller) in isolated spans in web lines. A model was created by

applying plate buckling theories to a web in a free span. From this model, one can determine when an edge of the web will be slack, or have zero tension in the machine direction. Model is verified by comparing predicted occurrences with experimental data.

Dobbs and Kedl [6] investigated the effect of slippage on wrinkle formation. A model was presented to predict the onset of moment transfer based on equilibrium equation for a beam in bending, and web roller traction. Figure 2.1 shows the case with misaligned roller B wherein all the forces and deformations imposed on the web are reconciled in the span B.



(a) Beam with bending in span B only

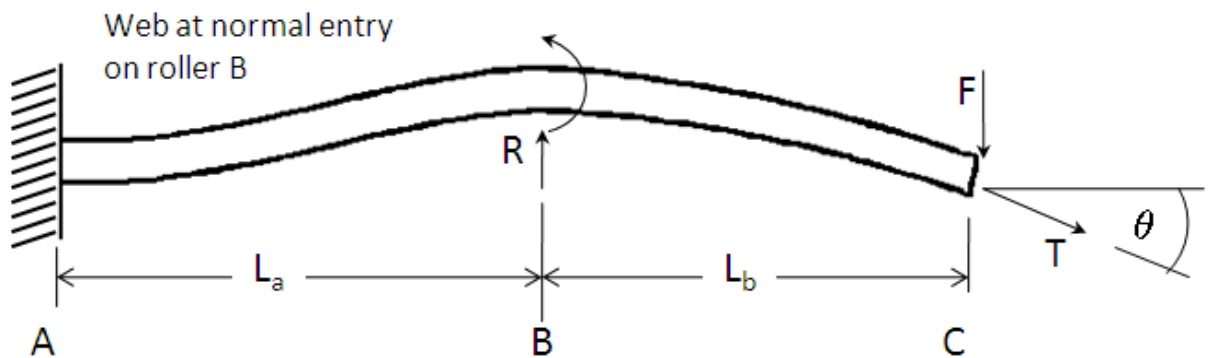


(b) No span interaction

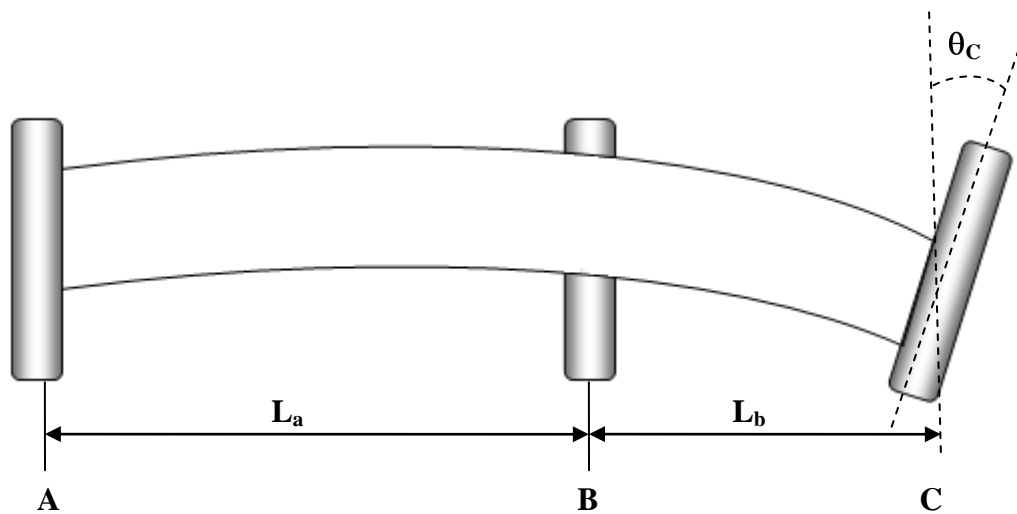
Figure 2.1 When the traction between the roller B and the web is enough to contain the moment generated within span B



In figure 2.2, roller B can no longer support moment generated by the shear force and the web twists. As long as there is sufficient friction, web will move laterally and regains normal entry into roller B. If the traction is not sufficient, the web no longer approaches roller B normally (Fig 2.2(b))



(a) Beam bending with moment transfer



(b) Web spans with moment interaction

Figure 2.2 When the traction between the roller B and the web is NOT enough to contain the moment generated within span B

Good [2] in his paper on “Shear in multispan web systems” focused on possible interaction of multiple web spans due to a downstream misaligned roller. Friction between the web and the roller dividing the two spans was considered to be a pivotal factor for web interactions to occur. An algorithm for  $M_r$  (the critical moment at which moment gets transferred to the upstream span) was developed to predict moment transfer. Expression for  $M_r$  was given by:

$$M_r = \frac{\mu T \beta W}{4} \quad (2.1)$$

Where,  $T$  is the nominal web tension in units of load,  $\mu$  is coefficient of friction between upstream roller and web material,  $\beta$  is angle of wrap made by web on upstream roller and  $W$  is the web width. To determine the moments generated and lateral deflection in the web due to span interactions, Good used a stiffness matrix developed by Przemieniecki [5] for beams stiffened by tension. In the following figure such a beam element is shown.

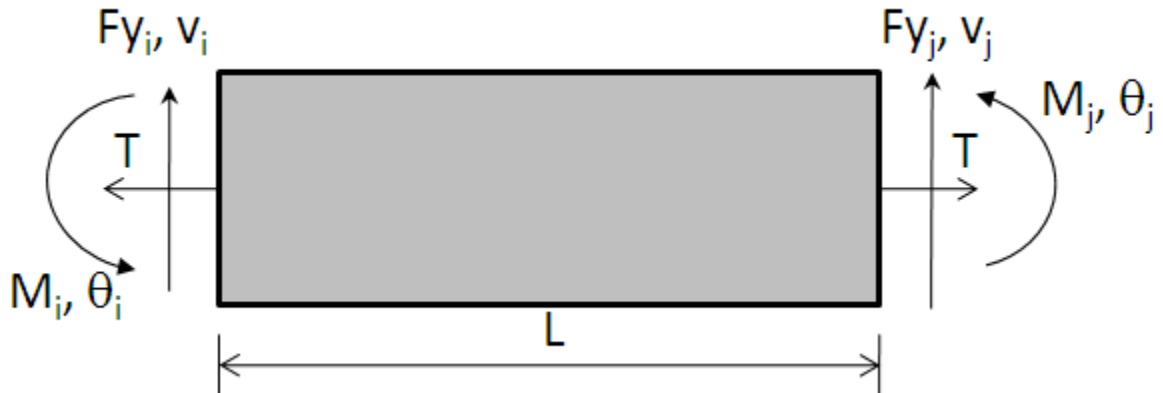


Figure 2.3 Beam element showing sign convention for Loads and Deformations

The stiffness matrix for this beam is given by:

$$\begin{Bmatrix} f_{yi} \\ M_i \\ f_{yj} \\ M_j \end{Bmatrix} = \begin{bmatrix} \frac{12EI}{L^3} + \frac{6T}{5L} & \frac{6EI}{L^2} + \frac{T}{10} & -\frac{12EI}{L^3} - \frac{6T}{5L} & \frac{6EI}{L^2} + \frac{T}{10} \\ \frac{6EI}{L^2} + \frac{T}{10} & \frac{4EI}{L} + \frac{2TL}{15} & -\frac{6EI}{L^2} - \frac{T}{10} & \frac{2EI}{L} - \frac{TL}{30} \\ -\frac{12EI}{L^3} - \frac{6T}{5L} & -\frac{6EI}{L^2} - \frac{T}{10} & \frac{12EI}{L^3} + \frac{6T}{5L} & -\frac{6EI}{L^2} - \frac{T}{10} \\ \frac{6EI}{L^2} + \frac{T}{10} & \frac{2EI}{L} - \frac{TL}{30} & -\frac{6EI}{L^2} - \frac{T}{10} & \frac{4EI}{L} + \frac{2TL}{15} \end{bmatrix} \begin{Bmatrix} v_i \\ \theta_i \\ v_j \\ \theta_j \end{Bmatrix} \quad (2.2)$$

Where, E is young's modulus of the web material, I is moment of inertia of cross-section of the web, T is tension applied to the web span and L is span length. The above equation is applied to span A and span B (figure 1.2) independently to find moments generated and lateral deflections in the web in both the spans. For span B, assumption was first made that the friction between the roller B and the web is high enough to contain the moment within span B. As there were no span interactions  $v_{bi}$  and  $\theta_{bi}$  are zero and from Shelton [1] the moment ( $M_{bj}$ ) at the misaligned roller C is zero. The last equation of the matrix above yields:

$$0 = \left[ \frac{-6EI}{L_b^2} - \frac{T}{10} \right] v_{bj} + \left[ \frac{4EI}{L_b} + \frac{2TL_b}{15} \right] \theta \quad (2.3)$$

where,  $\theta$  is misalignment given to roller C. Now we can write the expression for lateral deflection in the web as:

$$v_{bj} = \left[ \frac{\frac{4EI}{L_b} + \frac{2TL_b}{15}}{\frac{6EI}{L_b^2} + \frac{T}{10}} \right] \theta_c = \frac{4(30EIL_b + TL_b^3)}{3(60EI + TL_b^2)} \theta_c \quad (2.4)$$

Then the expressions for shear force  $V_b$  and moment  $M_{bi}$  can be written as:

$$F_{byi} = V_b = -\frac{240(EI)^2 + 104EIL_b^2T + 3L_b^4T^2}{2L_b^2(60EI + TL_b^2)} \theta_c \quad (2.5)$$

$$M = \left[ \frac{2EI}{L_b} + \frac{TL_b}{6} \right] \theta_c \quad (2.6)$$

Expression (2.2) can be applied to span A assuming that there is some moment transferred from span B due to insufficient frictional forces between web and roller B. The expressions for the moment at roller B as the web exits span A were developed by Shelton [1] as follows:

$$\begin{aligned} M_{aj} &= 0 && \text{when } M_{bi} < |M_r| \\ M_{aj} &= -[M_{bi} - M_r] && \text{when } M_{bi} > M_r \text{ and } M_{bi}(+) \\ M_{aj} &= -[M_{bi} + M_r] && \text{when } |M_{bi}| > M_r \text{ and } M_{bi}(-) \end{aligned} \quad (2.7)$$

Assuming that  $v_{ai}$ ,  $\theta_{ai}$ , and  $\theta_{aj}$  are zero. From (2.2) lateral deflection in span A at roller B,  $v_{aj}$  is:

$$v_{aj} = -\frac{M_{aj}}{\frac{6EI}{L_a^2} + \frac{T}{10}} \quad (2.8)$$

Now the effect on web lateral deflection due to moment transfer from span B to span A can be calculated by adding equations 2.8 and 2.4 as:

$$v_{bj}(total) = v_{bj}(2.3) + v_{aj}(2.7) \quad (2.9)$$

Good also focused on air entrainment between a moving web and the roller and its effect on web to roller traction. He incorporated the effect of slack edge into his model for a downstream misaligned roller in a multispan system. Experimental verification was provided. These expressions prescribe the first stage of the moment transfer where  $M_{bi} > M_r$  but  $\theta_{aj}$  can still be assumed zero. As the misalignment of the roller C increases yet further  $M_{bi}$  will still exceed  $M_r$  but now  $\theta_{aj}$  will become nonzero. Note that in the first

stage of the moment transfer that the lateral deflection of the web is decreased at roller C ( $v_{bj}$ ) due to the negative deflection of the web in span A. In the second stage of moment interaction the web deflection in span A will be positive and will sum with the positive deformation of the web in the span B.

Shelton [7] studied the interactions between two web spans because of a misaligned downstream roller. He analyzed the lateral forces and moment on a web at a roller where the slippage is occurring. He suggested recommendations in the design of process lines to eliminate interaction between spans. He simultaneously solved a two span system and discussed the influence on preceding web guides. Shelton compared his theory to Good's and other test results.

Beisel [8] developed a theory to predict the formation of troughs and wrinkles due to a downstream misaligned roller. He derived a model by considering orthotropic material properties. His experimental data provided starting point for correlating troughs with wrinkles. A linear relation was found between  $\theta_{\text{trough}}$  (misalignment required to generate a trough) and  $\theta_{\text{wrinkle}}$  (misalignment required to generate a wrinkle). Webb [9] found that  $\theta_{\text{wrinkle}}$  is twice that of  $\theta_{\text{trough}}$ . He tested a variety of materials and found that the correlation between trough and wrinkle formation was constant. Good and Beisel [10] showed that a closed form solution could be found for prediction of trough formation, but wrinkle formation would require a post buckling analysis. Beisel was able to develop a closed form expression that predicted the misalignment required to induce troughs in orthotropic webs. He developed a modeling method employing a commercial nonlinear

finite element code using wrinkle-membrane elements that provided the first successful computations of the misalignment required to wrinkle webs on rollers. Later Yurtcu [15] developed a standalone code that was able to perform similar computations.

### **2.1 Research Objective:**

The objective of this research is to analyze moment transfer in multispan web systems due to a misaligned downstream roller. New tools (Laser Doppler Velocimeters) have become available that allow the moments within webs to be determined accurately. With these tools the moments within webs transiting rollers will be explored for the first time. These tools will be held to discern where slippage is occurring and what level of moment is associated with that slippage.

## **CHAPTER III**

### **Experimental Procedure**

The research required numerous stages of experimentation before achieving the objective. All the steps and setups with their experimental procedures are explained in this chapter. To study the span interaction in web systems due to a misaligned downstream roller, moment measurements were made in entering span, pre-entering span, and on the roller dividing those two spans.

#### **3.1 Laser Doppler Velocimeters**

##### **3.1.1 Overview**

Laser Doppler Velocimeter (LDV) is an industrial instrument that can measure the velocity and the deformed length of a moving material. Due to the nature of the laser-based measurement, there is no physical contact with the material. The model LS200 LaserSpeed® Noncontact Length and Speed Gauge manufactured by BETA LaserMike was used for experimentation. The LS200 measures length and speed with accuracy

better than  $\pm 0.05\%$ . Figure 3.1 shows the picture of two different LDVs, LS200 (Model 240201) and LS8000-3.



*Figure 3.1 Two types of LDVs*

### **3.1.2 Principle of operation**

The LS200 utilizes dual beam interferometer technology to provide accurate velocity readings. The opto-electronic portion of the LS200 generates a monochromatic laser beam that is split (to ensure coherency between the two) and then crossed in space to form a measurement region. The two beams are made to intersect at their waists (the focal point of a laser beam), where they interfere and generate a fringe pattern that is orthogonal to the plane of two beams. As the product (web, in this research) moves, light is scattered back to the LaserSpeed at a frequency proportional to the speed of the material. The frequency is measured, converted to a speed and pulses are generated at a rate proportional to the speed. External counters or PLCs count the pulse to determine length. National Instruments 'NI 6602 counter/timer board' was used for data acquisition. Working of this data acquisition system will be explained later in the section 3.2.1.



The fringe spacing ( $d$ ), shown in figure 3.2, is known from calibration and is a function of laser wavelength ( $\lambda$ ) and beam angle ( $\theta$ ):

$$d = \frac{\lambda}{2 \sin \theta}$$

If ' $f$ ' is the frequency of the signal received at the detector, velocity of the material is

$$v = d \times f$$

Velocity is integrated to find length,  $L = \int_0^T v \cdot dt$

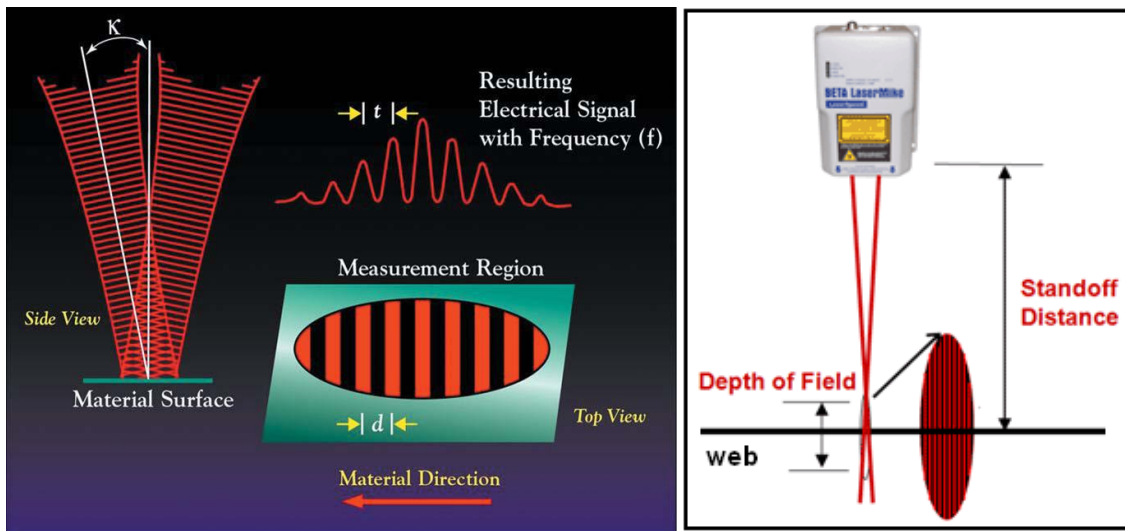


Figure 3.2 Fringe pattern formed by LDV

Figure 3.2 shows the fringe patterns formed by two intersecting lasers and table 3.1 gives some specifications of the LDV.

<b>LS200 (SENSOR 240201)</b>	
Depth of field	1.38 in (35mm)
Standoff Distance	11.81 in (300mm)
Output	1000 counts/foot

Table 3.1 Specifications of the LDV

- Depth of field: Vertical measurement region of the gauge. Measurements are taken within this range.

- Standoff distance: Distance from the base of the LDV to the center of the depth of field.
- Output: The LS200 has different types of output that are accessed through various ports.

One type of output that will be employed in this research is a TTL output that is associated with the length of the web material that has passed the measurement sight. This output can be set to 1000 pulses per foot or 1000 pulses per meter. To take advantage of the greater resolution, 1000 pulses per foot was chosen. If we attempted to infer strain level after 1 foot of the web had passed the LDV target site and resolution in strain would be 1 part in thousand, or .001 in/in. This resolution in strain is unacceptable. For a web material such as polyester film whose Young's Modulus is approximately 600,000 psi, this would yield a resolution in stress of 600 psi. Polyester's yield stress is on the order of 6000-8000 psi and the ability to resolve only 10 increments in stress prior to material yield is unacceptable. This problem is solved by allowing several feet of web to pass the LDV target site prior to stopping the counter measurement. In most cases 100 feet of web were allowed to pass. Now our resolution in strain has improved from 1/1000 to 1/100,000 and our resolution of stresses in a polyester web is now 6 psi.

### **3.1.3 Using LDVs for Moment measurements**

LDVs are capable of measuring the length of the material moving beneath them. For calculating the moment induced in a web span due to a misaligned downstream roller a set of two LDVs was used. They were mounted above the web span side by side in CMD as shown in the figure 3.3. The LDV's capability to measure length was used to calculate relative strain in a web. LDVs give 1000pulses/foot of material. Whenever there

is some misalignment in a span, one edge of the web moves faster when compared to other edge due to the principle of normal entry.

The principle of normal entry states that a web will always seek entry to a downstream roller such that the elastic axis of the web will be normal to the axis of rotation of the roller. For a misaligned roller Shelton found that the internal moment increased from zero at the misaligned roller to a maximum value at the upstream roller [1]. This means that as a result of bending moment, the length of the strained web that passes the target site of one LDV will be greater than the length of strained web that passes the other LDV. Hence a difference in the TTL output of the two LDVs is expected that can be correlated to the level of bending moment.

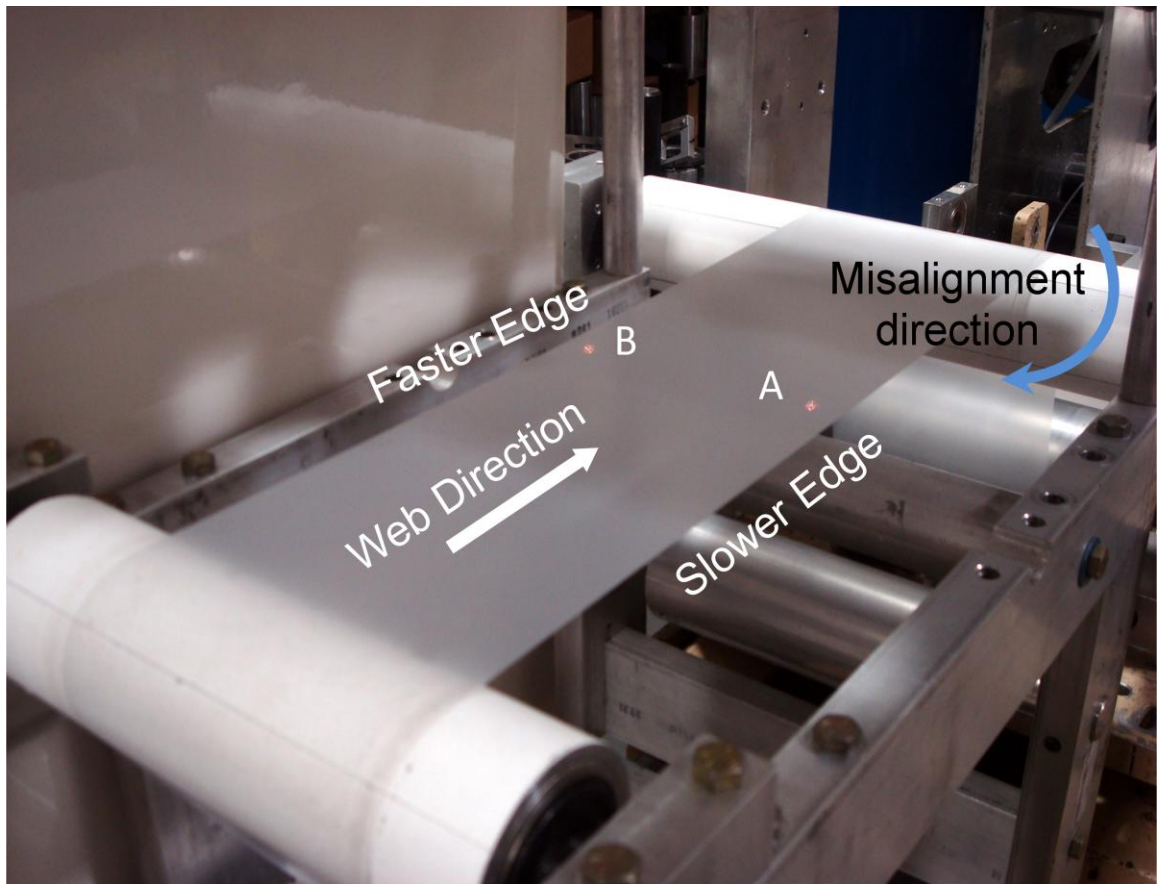


Figure 3.3 Using LDVs to estimate CMD strains

As it can be seen in the figure 3.3, material below LDV A is moving slower, resulting in higher pulse output when compared to LDV B, which is shooting on faster edge of the web material. Difference in the counts of these LDVs is directly proportional to the strain in the web in CMD. Moments at various points in the span were then calculated from the strain data obtained from LDVs.

Beisel [13] used LDVs to measure MD strains generated in a web span due to crowned rollers. Beisel used the LS200 LDVs previously described. Output from the LDVs is in the form of pulses and they can give a maximum output of 1000 pulses per foot of material. A new set of LDVs (LS8000) were obtained from BETA LaserMike and were superior to LS200 as their output could be adjusted to a maximum of 100,000 pulses per foot. So the idea was to use these new LDVs with higher capability to calculate the relative strain in the web with higher accuracy.

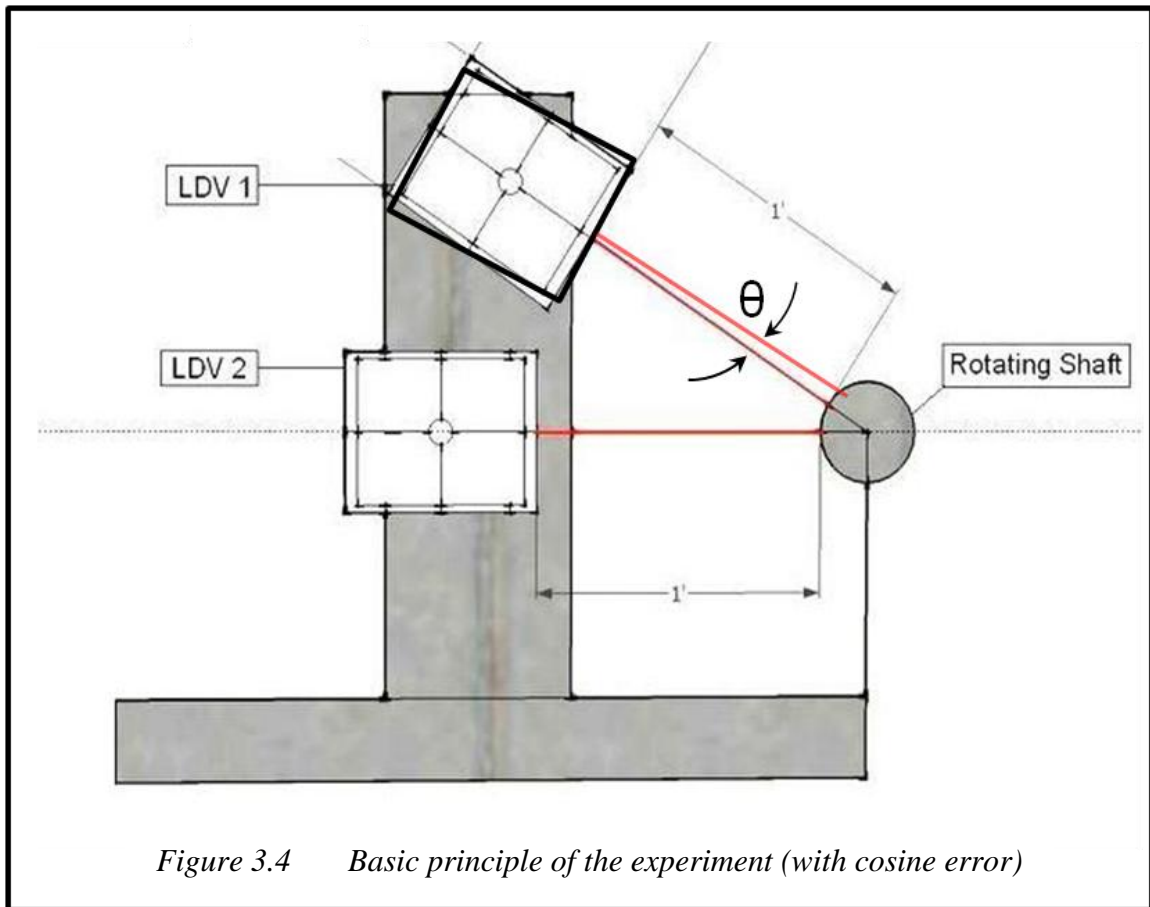
A rig was designed to calibrate these LDVs. This process is explained in the following section. During the process of calibration it was found that one of the two LS8000s gave inconsistent output when compared to LS200s. So, two of the LS200s were used for the experimentation purposes of this research.

### **3.2 Developing a calibration rig for LDVs**

The purpose of using LDVs was to estimate the relative stresses and hence moments in a web. Two LDVs were used side by side in CMD at various positions in a span. Both of the new LDVs (Model LS8000) have a selectable pulse output ranging from 1000 pulses/foot to 100,000 pulses/foot. Whenever these LDVs are made to shoot simultaneously on a material moving with a constant speed across its width the difference in the pulse rate should be zero. But, usually these LDVs have some offset and a setup

was designed to calibrate these LDVs. The pulse output from both the LDVs was set to 1000 pulses/foot.

The LDVs were targeted on an air supported rotating shaft. This shaft was connected to a motor which had adjustable speed control. Schematic diagram of the calibration rig is shown below (figure 3.4).



The calibration rig had a vertical aluminum plate on which two LDVs were attached. As it can be observed from the diagram, Standoff distance of 12 inches was maintained between the LDVs and the shaft. If a circle with 12in radius and center on the axis of rotation of the shaft is drawn, then the bottoms (point from where the laser comes out of the LDV) of LDVs would lie on the circumference of that circle.

A rotation stage is installed in between the LDVs and the metal plate (figure 3.5). The purpose of this instrument is to rotate the LDVs till the laser coming out of them is perpendicular to the tangent to the rotating shaft. The rotary stage is equipped with a micrometer for small variations.

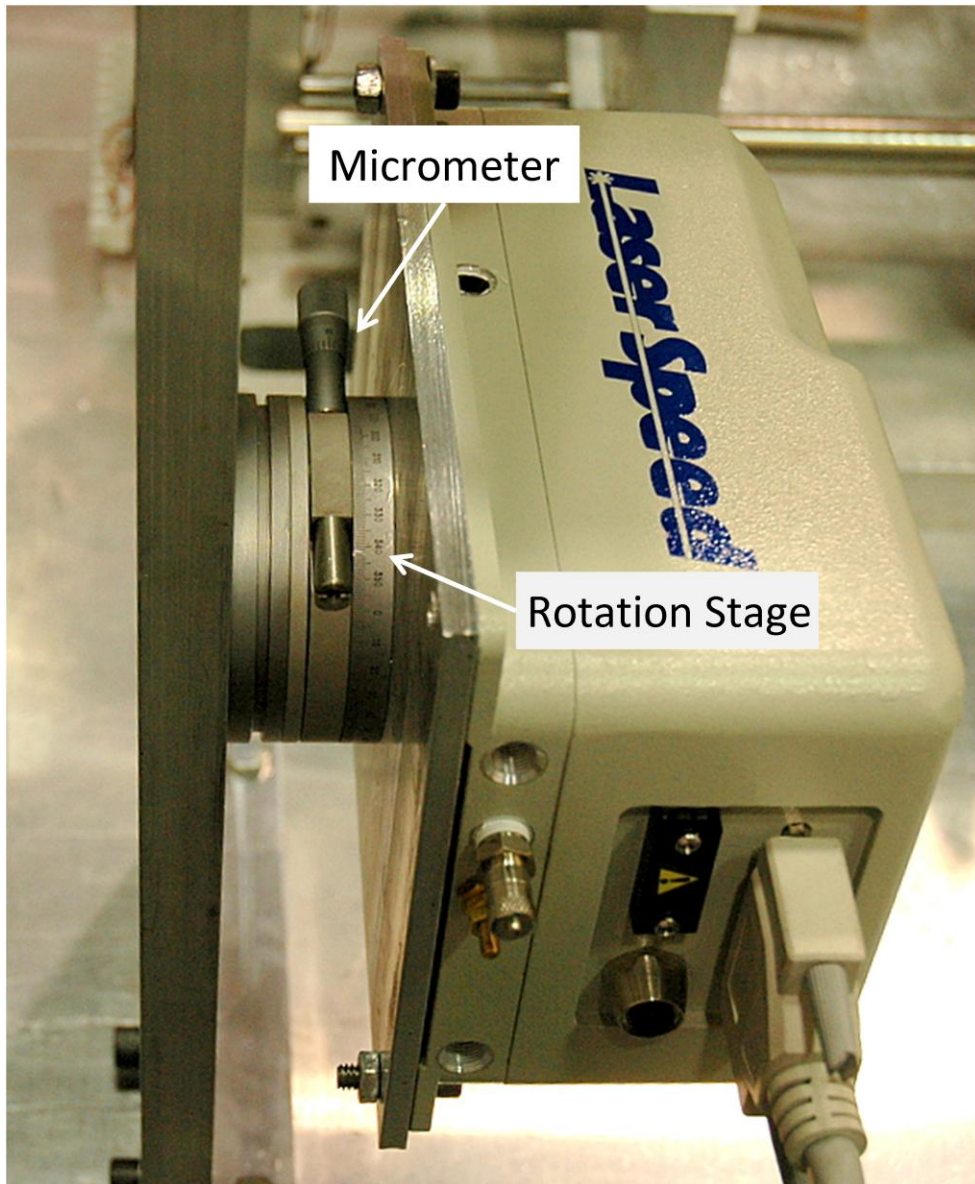


*Figure 3.5 Side view of LDV showing the Rotation Stage with Micrometer*

To make sure that the LDVs are shooting perpendicularly on the surface of rotating shaft, we used the *LaserTrak 4.0* software. This is BETALASERMIKE's proprietary software. This software displays the surface velocity of the shaft and the quality factor of the measurements being made. The quality factor is an indicator of how good the velocity measurements are. LDVs do not work well, for instance, on surfaces with little surface roughness and in such cases the quality factor would appear low. It was found that whenever a LDV shoots laser perpendicular to the shaft, the velocity goes to a maximum value. At angles other than perpendicular there is a cosine error and the indicated velocity ( $V_I$ ) will be less than the tangent velocity ( $V_T$ ):

$$V_I = V_T \cos\theta$$

This cosine error is shown in figure (3.4). Then, each of the LDVs was connected to the computer separately and their angle of inclination was adjusted using the rotary stage until the velocity achieved a maximum value. It was then known that the LDVs were perpendicular to the tangent point on the circular shaft when the velocity was maximum.

The experimental setup with the LDVs shooting on the rotating sir supported shaft is shown in figure 3.6.

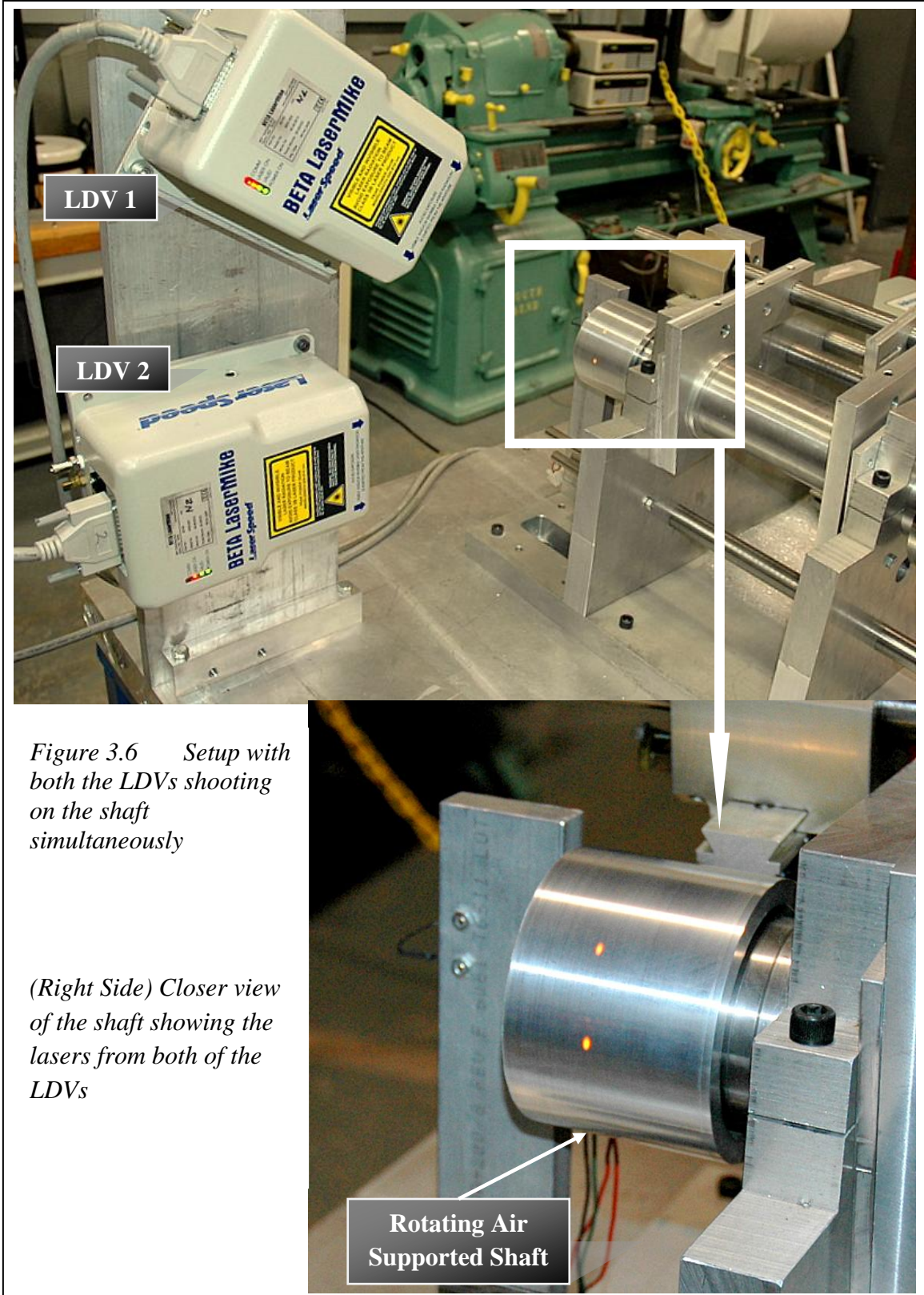


*Figure 3.6 Setup with both the LDVs shooting on the shaft simultaneously*

*(Right Side) Closer view of the shaft showing the lasers from both of the LDVs*



### **3.2.1 Data Acquisition system for the calibration rig:**

Once the LDVs were known to be perpendicular to the shaft surface, they were connected to a computer through a NI 6602 counter/timer board. A LabVIEW program was used to record the pulse data and to find the difference in the counts of the LDVs. The counter increments its event count every time a pulse comes into its source input and transfers that value to memory every time a pulse comes into its gate input. The data in memory is read continuously in the while loop until the Stop button is clicked. When we connect both the LDVs through NI 6602 board it records the pulse rates of the LDVs and the difference in their pulses. The data was stored in a text document after each test run.

Data was taken with both the LS200 and the LS8000 LDVs. The surface speed of the rotating shaft is kept constant at 188.5 feet/min (shaft of 4 inch diameter rotating at 180 rpm). Every set of data has almost 30 readings where each reading was taken while 100 feet of the surface of the rotating shaft passed the target sites of the LDVs. Four sets of data for both the models of LDVs were compared.

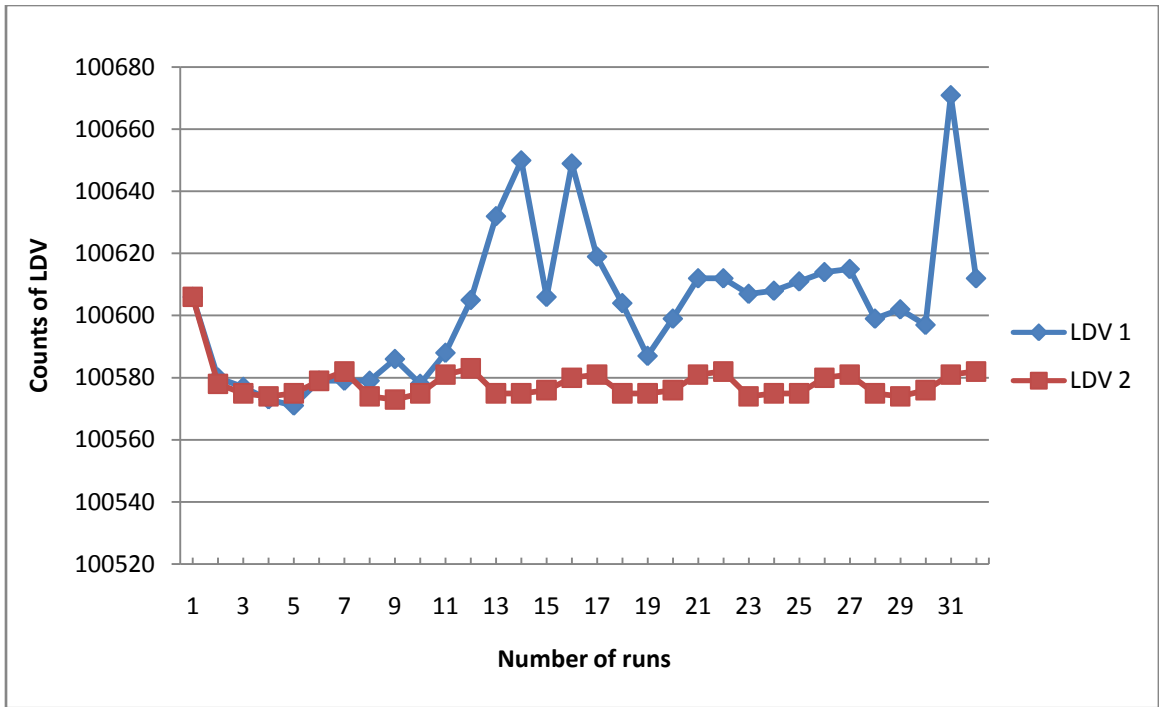


Figure 3.7 (a) Data from the LS8000 LDVs

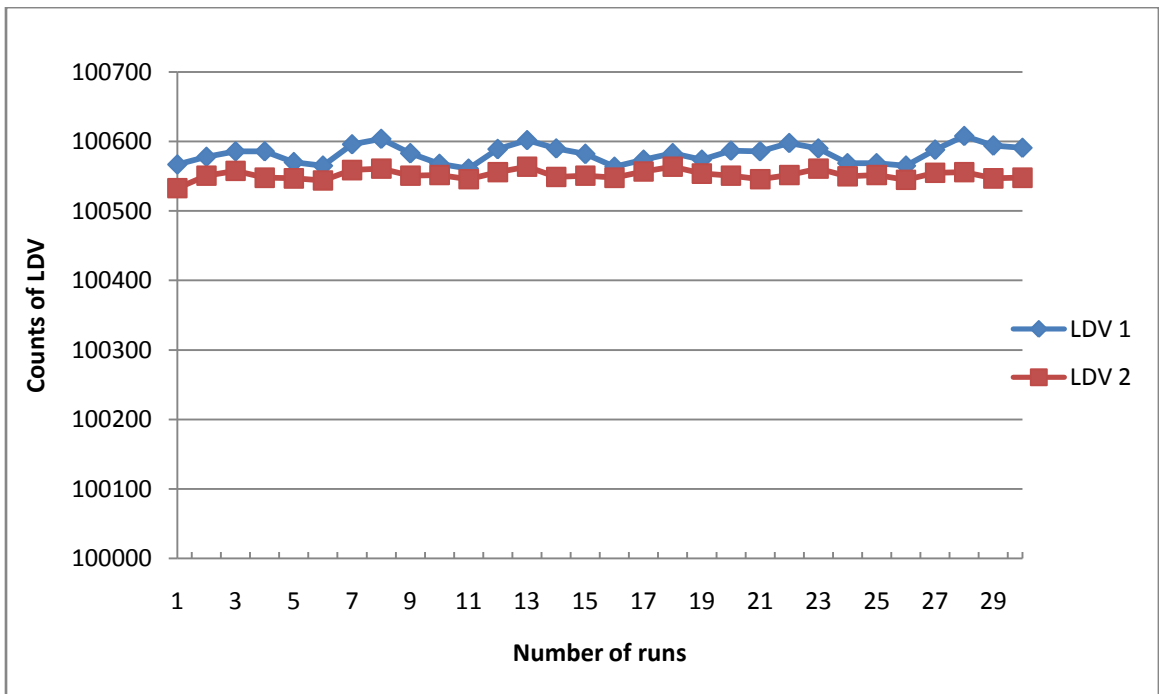
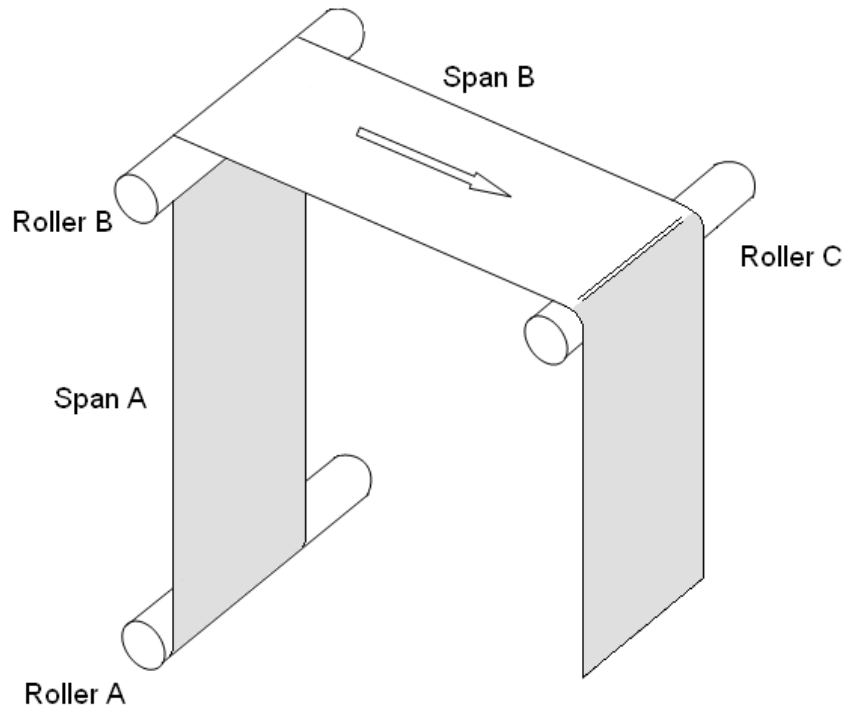


Figure 3.7 (b) Data from the LS200 LDVs

Figure (3.7) shows one of the four outputs for both sets of LDVs (LS200 and LS8000). From the plots, it can be observed that in the case of the LS8000 LDVs, LDV 1 did not follow the path of LDV 2, whereas from the plot of the LS200 LDVs both LDV 1 and LDV 2 followed almost the same pattern. As mentioned earlier, for strain calculations in a web a set of LDVs is required, so it was concluded that the older set of LDVs (Model LS200, previously used by Beisel [13]) gave consistent results and they were used for experiments in this research hereafter.

### **3.3 Preliminary tests**

During the initial stages moment measurements were made in the entering span using the Shelton Machine, a closed loop web transport system developed by Shelton [1] to verify his theories. In the figure 3.8, span B represents the entering span.



*Figure 3.8 Sketch showing span B*

The Shelton machine was a modified lathe bed, which had the capability of taking data for different span lengths. Beisel [8] made several modifications to study single span buckling in webs. The web comes off of the unwinder and passes over a series of rollers then into a web guide. The purpose of the web guide is to make sure that the web enters the upstream roller with no inclination and with a fixed lateral position. The web passes through the test span and is consumed at the winder. Throughout the web line the tension in the web is maintained with help of a tension control system. The velocity of the web is also controlled with the drive controls for the winder.

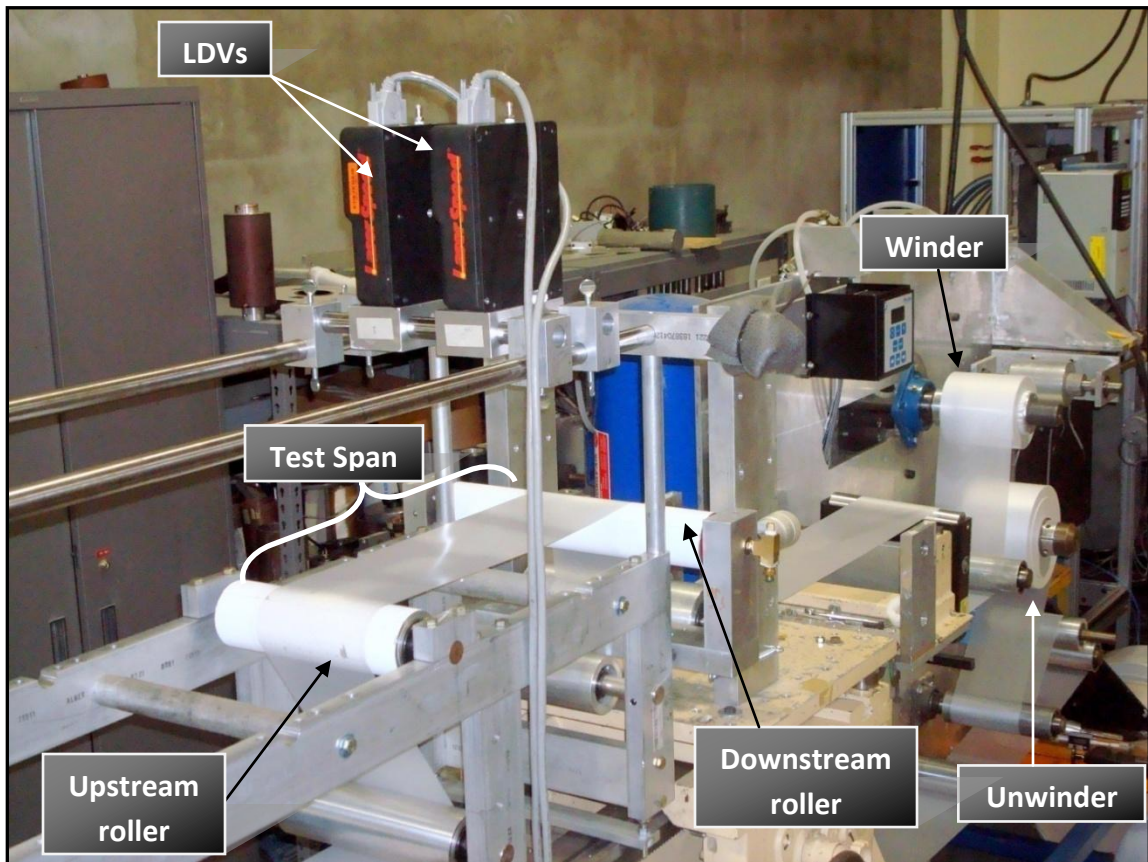


*Figure 3.9 Test setup for measuring strains in a web with the help of LDVs*

The setup can be seen the figure 3.9, where the two LDVs are mounted over the test span to estimate the strain difference between two points in the CMD. Misalignment was given

to the downstream roller and a micrometer was used to measure the angle of rotation. The micrometer assembly is shown in figure 3.10.

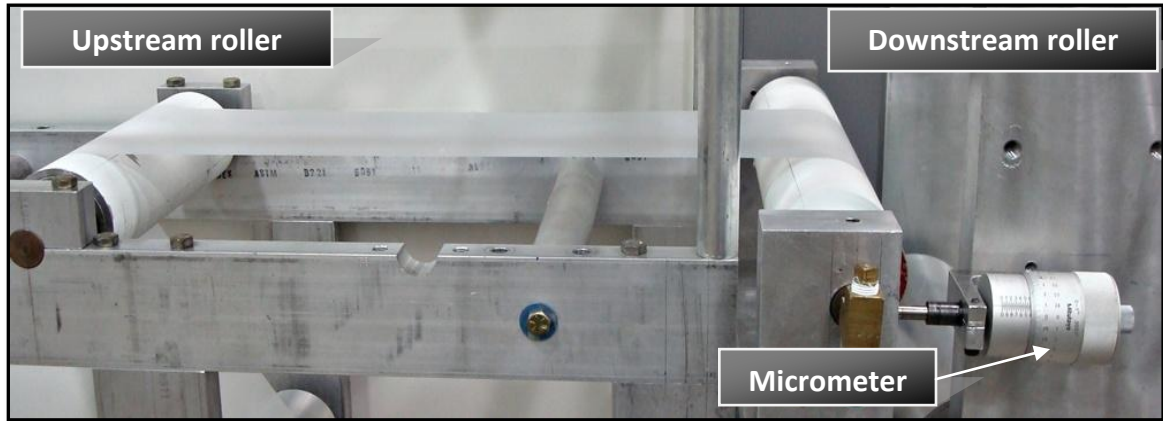


Figure 3.10 Micrometer assembly

<b>TEST SPECIFICATIONS</b>	
Material used	92 gage Polyester (PET)
Young's modulus (E)	710 000 psi
Width of web (w)	6 inches
Thickness of web (t)	.00092 inches
Length of test span (L)	20 inches
Distance between LDVs ( $\Delta y$ )	5 inches
Tension in web (T)	10 lb
LDV Type	BETA LaserMike LS200
Pulse rate of each LDV	1000 counts/foot
Standoff distance of LDV	12 inches

Table 3.2 Test specifications for preliminary tests

The initial tests were conducted on 92 gage polyester to find the moments generated in a web span due to a misaligned downstream roller. The test specifications

are shown in table 3.2. A 20 inch span length was chosen and moments were measured at different locations in the span. Measurements were not made right at the exit point at the upstream roller and right at the entry point to the misaligned roller. The opacity of the web material used was not high enough and there was a possibility of measuring the roller surface velocity rather than the web velocity.

The zero or null position of the downstream roller had to be established before the test could proceed. The downstream roller was rotated in a clockwise direction (looking down from the top) until a wrinkle was observed in the span and the micrometer reading was recorded. Then roller was rotated in counter-clockwise direction corresponding micrometer reading for wrinkle was recorded. The zero position must be half way between the two micrometer readings. This point on the micrometer was marked as zero. Once the zero position of the downstream roller was established, it was misaligned to a position where troughs just began to form. Now with the help of the micrometer reading and the distance between the micrometer and center of yoke supporting the downstream roller, value of misalignment was calculated in radians. From strength of materials:

$$\theta = \frac{FL^2}{2EI}$$

where,  $\theta$  is misalignment in radians, L is span length in inches, E is modulus of elasticity of web material in psi, F is forced applied on web due to misalignment in pounds and I is moment of inertia in  $\text{in}^4$ , which is given by:

$$I = \frac{tw^3}{12}$$

where,  $t$  is thickness of web (.00092 in) and  $w$  is width of the web (6 in). Theoretical moments in the span at various positions were calculated by:

$$M = \left( \frac{2EI\theta}{L^2} \right) (L - x)^2$$

where,  $x$  is distance from the upstream roller.

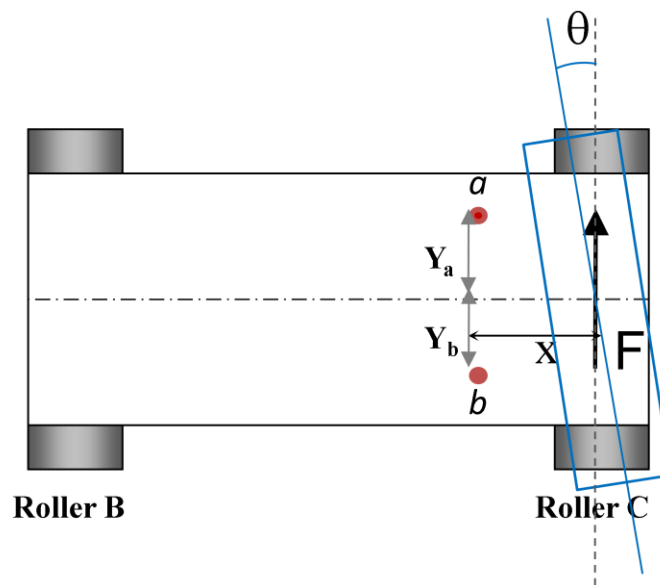


Figure 3.11 Positioning of the LDVs

The LDVs were set at various 'x' positions in the spans where moments were intended to be measured, see figure (3.11). Each LDV was made to shoot at a distance of 2.5 in above and below the centroidal axis of the web, so that distance between them is 5 inches. The moment inferred experimentally was calculated from:

$$M = EI \left( \frac{\text{strain}_a - \text{strain}_b}{Y_a - Y_b} \right)$$

Where,

$$strain_a - strain_b = \frac{LDV_a - LDV_b}{LDV_a}$$

When the downstream roller is aligned, the difference of counts of LDVs ( $LDV_a - LDV_b$ ) must be zero because of zero bending strain in the web. But it was found that the difference was a non-zero number which was taken as offset in the set of LDVs (this offset can be seen as the average difference of the traces in figure 3.7b). This offset was then subtracted from the count differences of LDVs. The LDVs (LS200) yield an output of 1000 counts per foot of passing web or 100,000 counts for 100 feet of web. At each 'x' position in the span, ten measurements were made where about 100 feet of web were allowed to pass the LDVs. The average of these ten measurements was taken to calculate experimental moments and was plotted against theoretical moments.

The Shelton machine would allow taking data only in the entering span, so there was a need of a new rig which could take data not only in entering span but also in pre-entering span and over roller B.

### **3.4 Building the new Test Rig:**

To study the moment transfer in a multispan web system a machine (test rig) was needed which would allow the misaligning of a downstream roller and letting the moments transfer upstream into the pre-entering span. As discussed earlier, the LDVs were used to measure moments developed in a web due to a misaligned downstream roller. The Shelton machine was setup to take LDV readings in the entering span (fig 3.9) only. The LDVs were moved on horizontal rails parallel to the web line. Due to the setup restrictions, the LDVs could not be moved around the upstream roller and into the pre-



entering span. This incapability of the Shelton machine to perform such a task lead to the development of a new test rig.

Various possible designs were considered for the setup, which would enable the movement of the LDVs in entering span, around the upstream roller (B) and in the pre-entering span. Finally, the design shown in figure (3.12) was selected. A commercial software called Autodesk® Inventor® was used to sketch this model. Inventor® provides a comprehensive and flexible set of software for 3D mechanical design, product simulation, tooling creation, and design communication.

In the sketch, span A is the pre-entering span and span B is the entering span. The web passes from span A over roller B into span B. The support system for the LDVs is designed in such a way that they always maintain the required standoff distance of 12'. The LDVs are positioned on a rotating arm which slides on a set of rails traversing span A, roller B and span B. The misalignment of roller C is precisely set with the help of a micrometer and a linear variable differential transformer (LVDT) was used to record the misalignment calibrated in degrees. Roller C sits on a carriage which slides on the horizontal rails to adjust the desired length for span B. A web guide was installed just before the web enters the pre-entering span A to steer the web to the center of the roller A.

Figures (3.12), (3.13) and (3.14) show the position of the LDVs when taking data in the pre-entering span (span A), the entering span (span B) and over roller B, respectively. Some of the parts of the machine are labeled for ease of understanding the working mechanism.

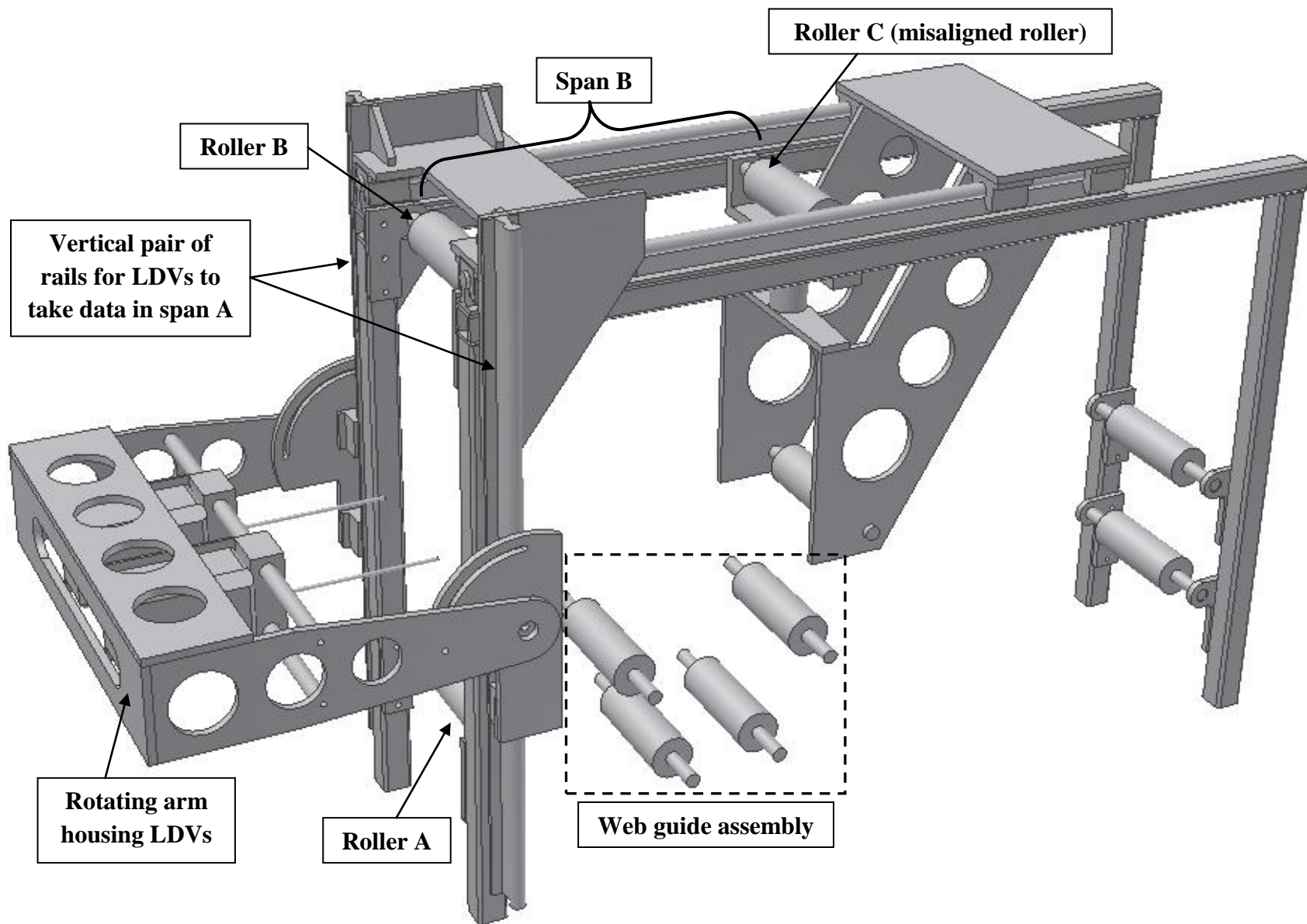


Figure 3.12 Sketch of the apparatus modeled with Inventor®

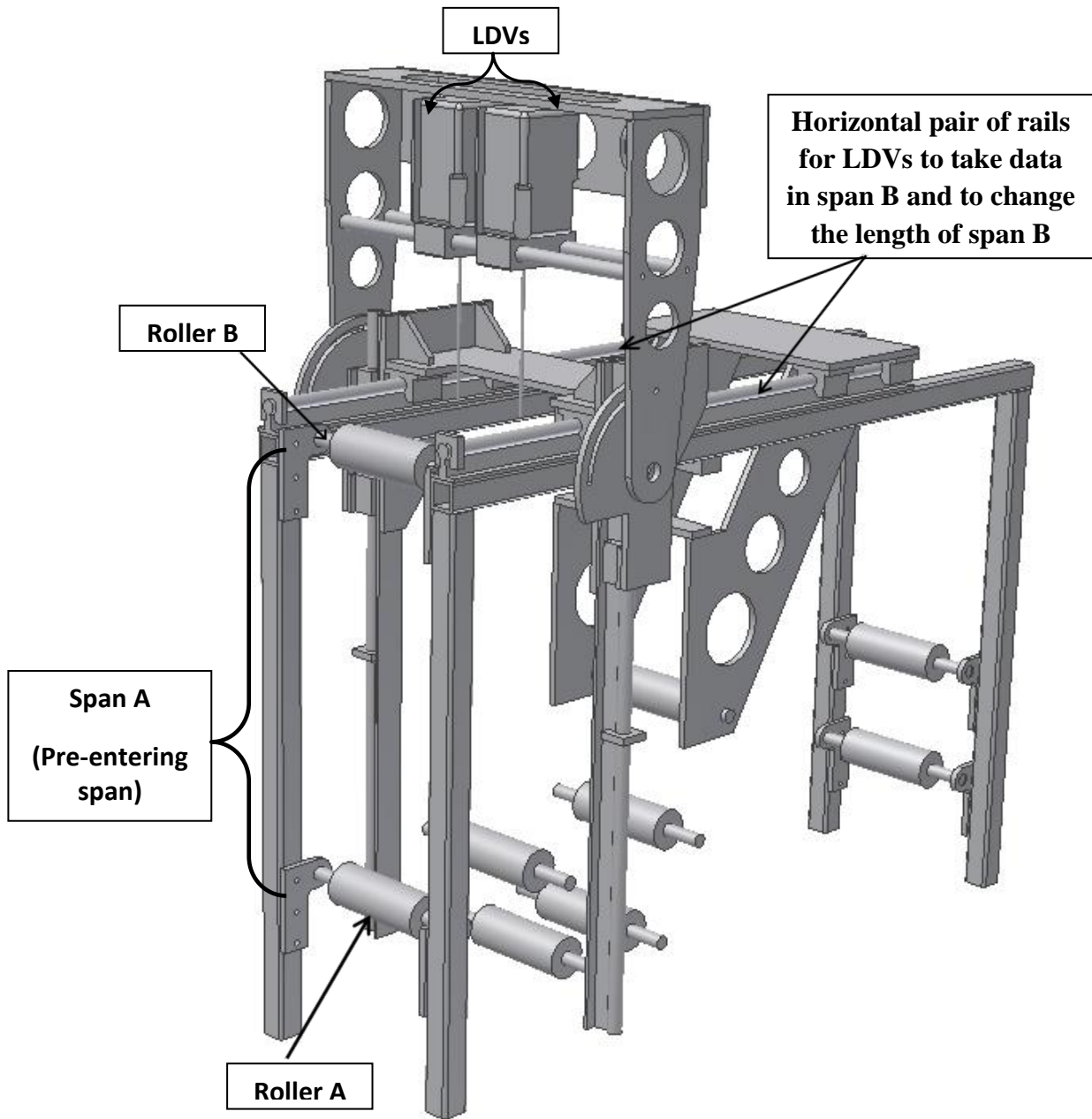
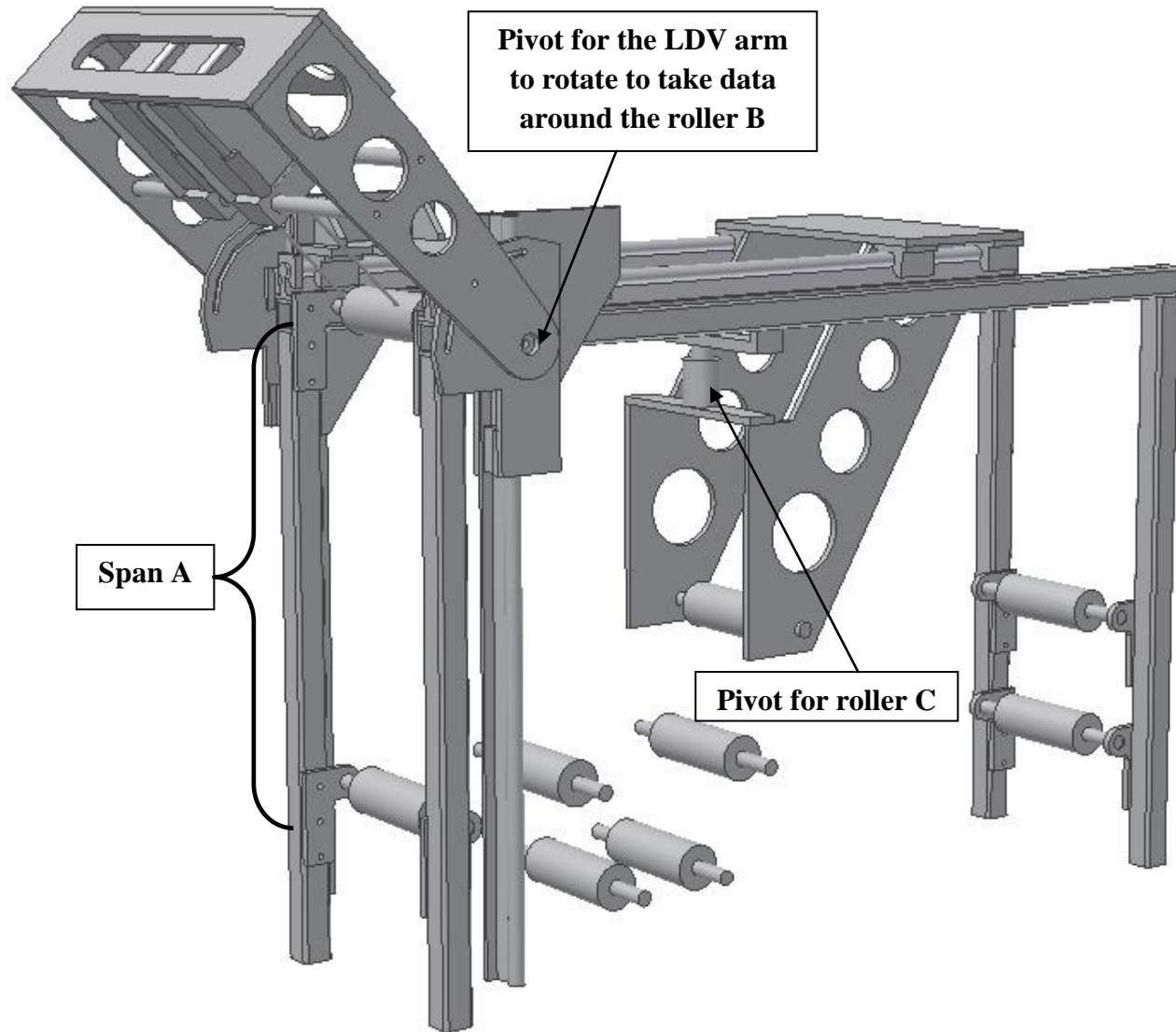


Figure 3.13 LDVs taking data in entering span (span B)



*Figure 3.14 LDVs taking data over roller B*

Most of the parts were machined out of 0.5 inch thick aluminum plate. Various milling, drilling and boring operations were performed on each part to machine to the required dimensions. The frame of the rig was made from hollow square tubing that was 2 inches by 2 inches and 1/8" thick. It was welded at the joints.

After all the parts were machined and assembled, the machine took the place of the Shelton Machine in the Web Handling Research Center. The new rig was then coupled with an existing winding/unwinding setup, on which the web rolls start unwinding and finally ends up being rewound after passing through the test rig. A schematic diagram of the entire web path is shown in figure (3.15). As it can be seen from the figure, a second web guide is installed before the web reaches the winder. Whenever there is some misalignment at roller C, the web tends to steer to one side of the rollers following the misaligned roller. The purpose of this web guide is to steer the web back to the center of the winding roll so that the same web could be used again. When the web starts unwinding at the unwinder it passes over a roller which has a load cell attached to it. The Load cell is used to maintain required tension in the web throughout the setup. The load cell signal is input to a controller that determines the current which is input to a magnetic hysteretic brake. This brake provides a resisting torque to the unwinding roll and in this way closed loop control of web tension in the test rig is achieved.

The finished assembly of the new rig and the winder setup is shown in figure (3.16).

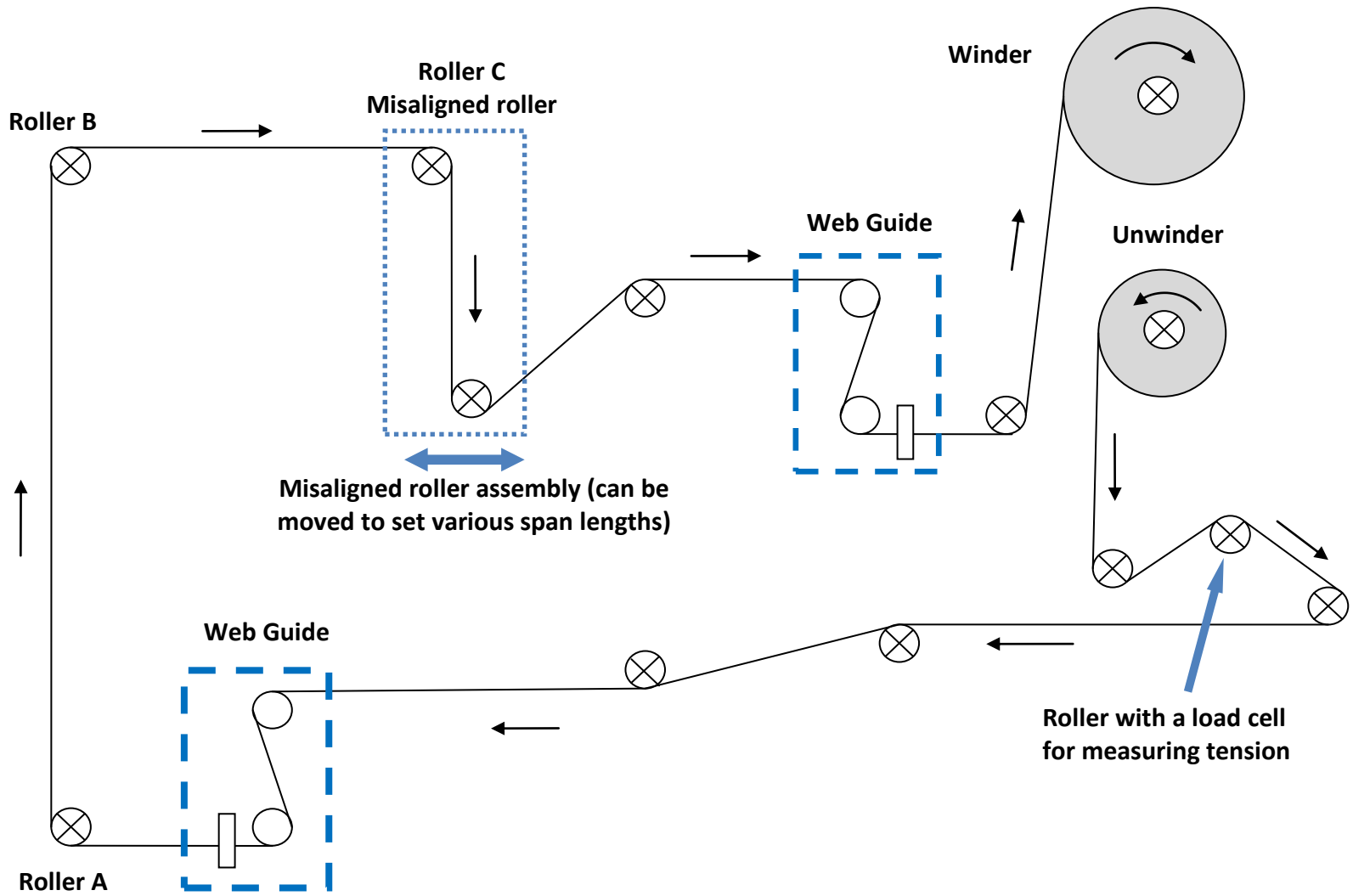


Figure 3.15 Schematic diagram of the web line through the test setup

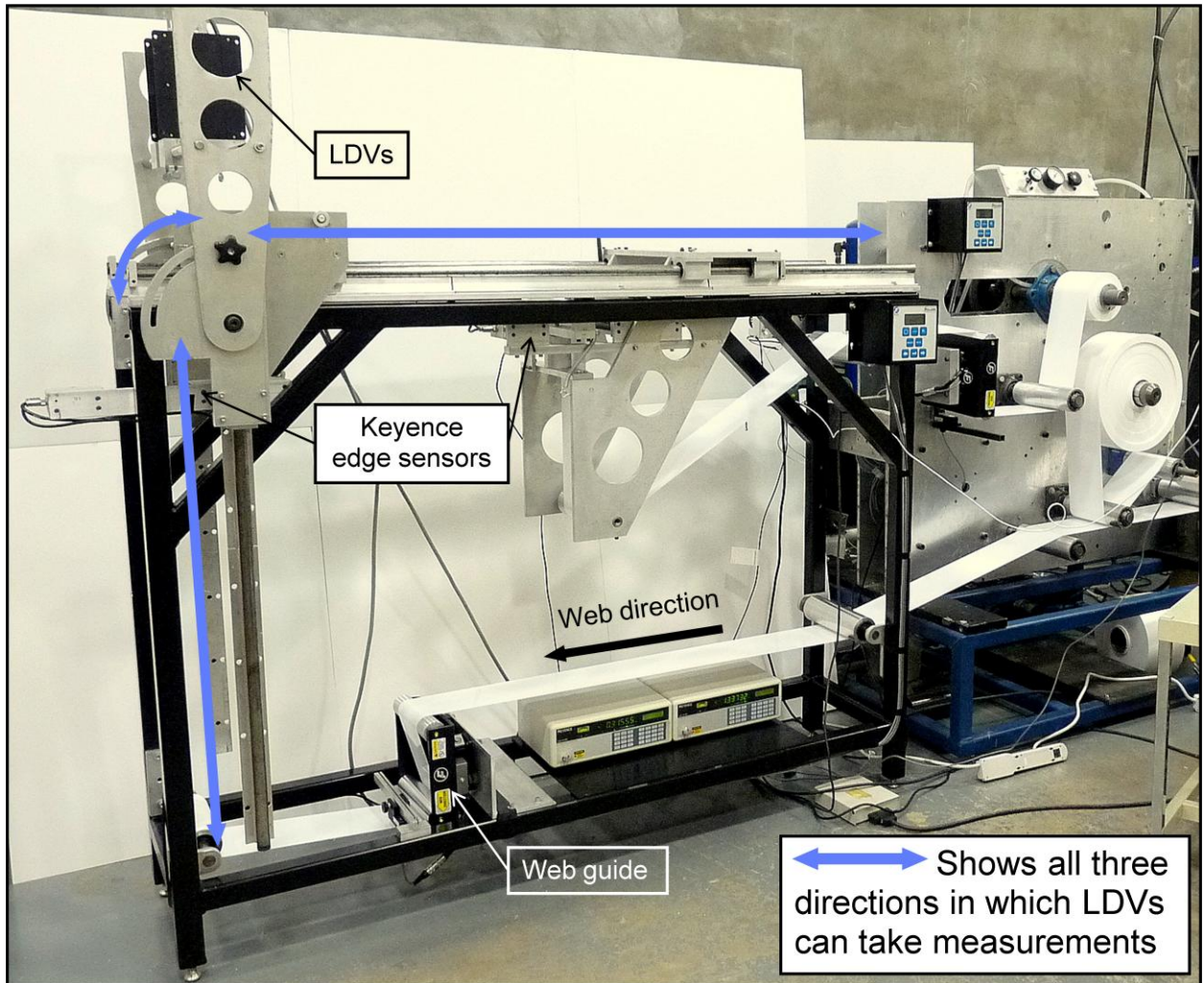


Figure 3.16 Combined assembly of the test rig and the winder

### **3.5 Crucial parts installed on the machine:**

Apart from LDVs, other critical parts such as an LVDT, web edge sensors and Web guides were also installed on the machine.

#### **(1) Linear variable differential transformer (LVDT)**

The LVDT is a type of sensor used for measuring linear displacement. It is installed beneath the roller C touching the base support plate of the roller. Whenever the

roller (C) is given an anti-clockwise or clockwise misalignment, the core of the LVDT moves in or out of the steel transformer housing. The result is that the roller misalignment can be precisely recorded during experiments. The LVDT installed on the machine is manufactured by Omega® (Model LD400-5). It has a stroke length of  $\pm 5.0$  mm (0.20"). Two LVDTs with different stroke lengths are shown below in figure (3.17).



*Figure 3.17 Linear variable differential transformers*

The LVDT is calibrated in such a way that it directly records the amount of misalignment in degrees on a computer with the help of a LabVIEW code.

## **(2) Edge Sensors:**

Two sets of Keyence® edge sensors (Model LS3060) were installed on the machine. The purpose of these sensors was to track the lateral deformation induced in the web due to the misalignment of roller C. One sensor was placed immediately after roller C to monitor the maximum edge deflection in the entering span (B). The second sensor



was placed at a fixed location upstream to roller B to track the web edge deflection in the pre-entering span (A) in the advent of moment transfer.



*Figure 3.18 A Keyence sensor with its controller*

These sensors have a measuring range of 0.003" to 4.72". A sensor with its controller is shown in figure (3.18).

### **(3) Web Guide:**

There are two FIFE electromechanical web guides installed on the setup, one on the new rig and the second on the winder setup. A web guide correctly steers the web onto the following roller. The position of the exiting web can be set by adjusting the sensor position or the offset of the controller.

After the Fife web guide was installed, the rollers of the offset pivot guide were aligned parallel to the rollers on the rig. During operation, the sensor installed in the exit span monitors the web position. If the web leaves the required position, an error signal is generated and recorded by a signal amplifier. This then activates a linear actuator that moves the offset pivot guide and thus corrects the web position.

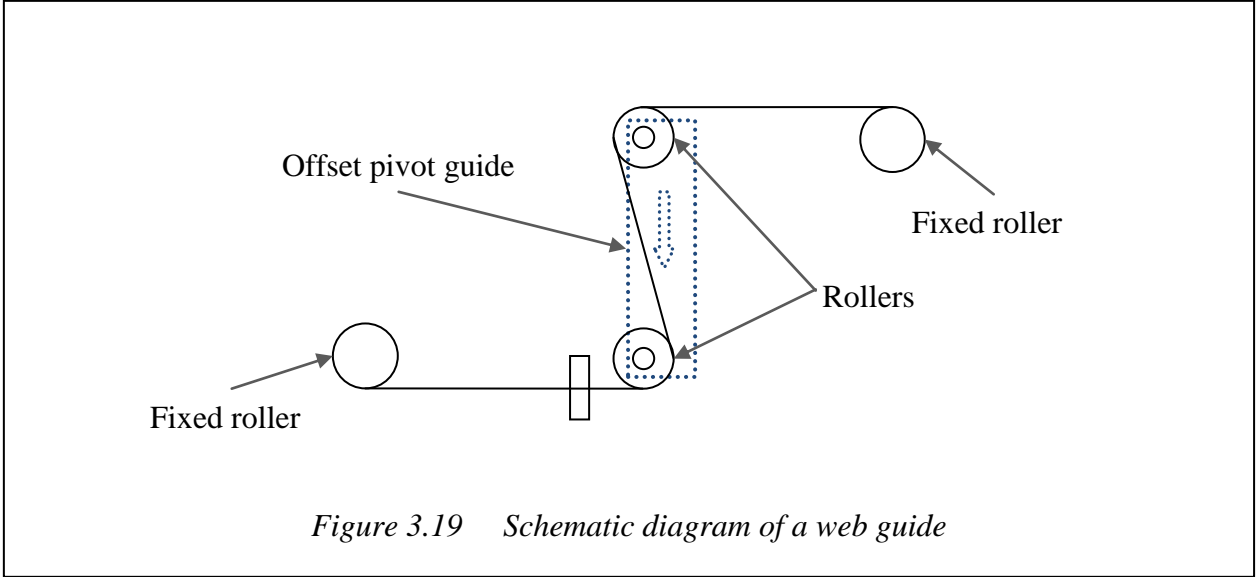


Figure 3.19 Schematic diagram of a web guide



Figure 3.20 Picture of a FIFE guide assembly

### **3.6 Troubleshooting and the instruments used:**

#### **Dial Indicator:**

The rig was designed in such a way that the set of LDVs could move over span A and span B. Before entering into span B, the LDVs would rotate around roller B (maintaining the standoff distance of 12') and take data over the roller. For this to happen, the center line of the roller B and both the hinges of the LDV arm should be in same line. A couple of dial indicators were used to set LDV arm to the desired position. In figure (3.21), white line represents the center line of the roller B.

Dial indicators are instruments used to accurately measure small linear distances. They are named so because the measurement results are displayed in a magnified way by means of a dial. Two dial indicators were mounted upside down as shown in the figure (3.21). Tip of the both the indicators were touching the roller at the ends. When the LDV arm is from vertical to horizontal position and if the roller and the line of rotation of the LDV arm were in the same line, the deflection in the dial indicator should be close to zero. So, the vertical and horizontal position of the LDV arm was adjusted accordingly to align it to the center line of roller B.



*Figure 3.21 Use of Dial indicators for align LDV arm in line to the roller B*

**Crow's foot micrometer:**

There are six rollers and a web guide installed on the rig. All the rollers should be parallel to each other to avoid any abnormality that may be induced in the web. The Crow's foot micrometer was used to align the rollers. It has a micrometer and a foot like front end which sits on the curved surface of the rollers. It has a set of extension rods to

change the length of the micrometer depending on the distance between the rollers. This instrument was used to align all sets of roller except the one in span B, where there is an obstruction (connecting member of frame of the rig) between roller B and roller C. There was a need for a modified micrometer which would go over that beam (obstruction) and aid in setting roller C parallel to roller B.

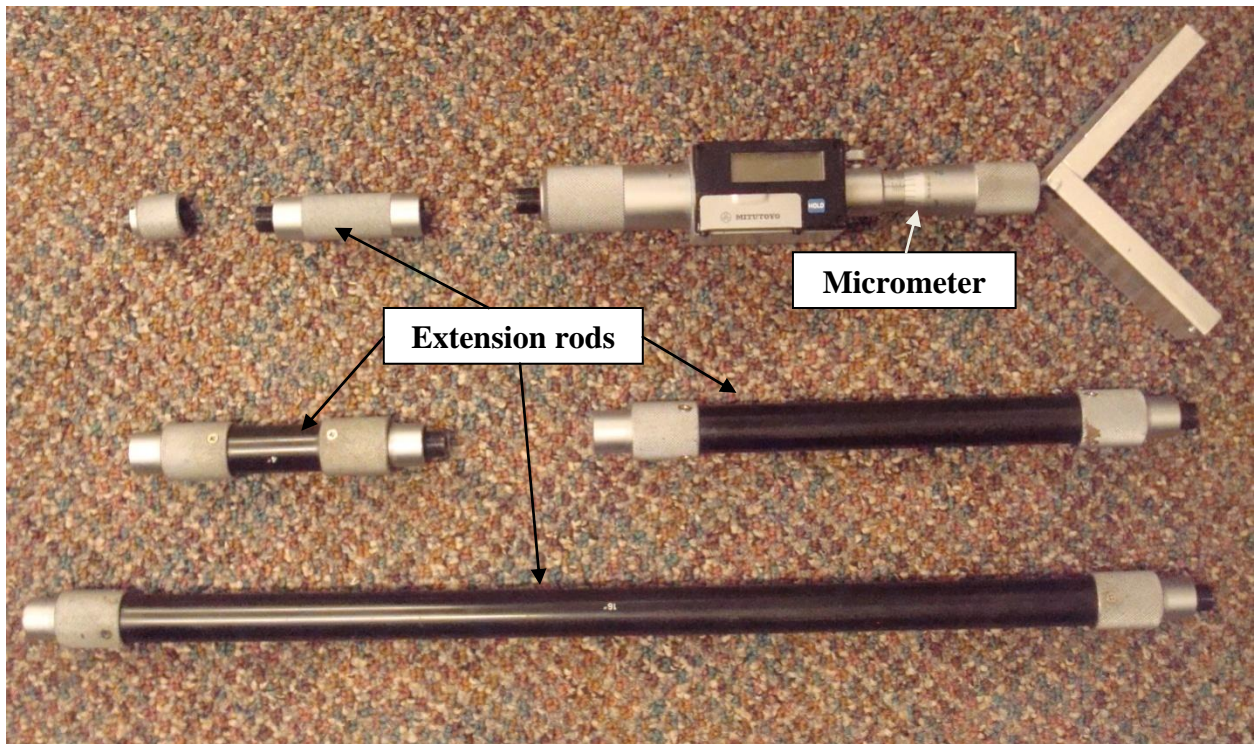


*Figure 3.22 Crow's foot micrometer with its extension rods*

**Custom made micrometer:**

Shown in figure (3.23) is a custom made micrometer for the need mentioned above. One end sits on roller B and the micrometer end touches the roller C. Then roller C is adjusted till the distance between both the rollers is same over their entire widths.

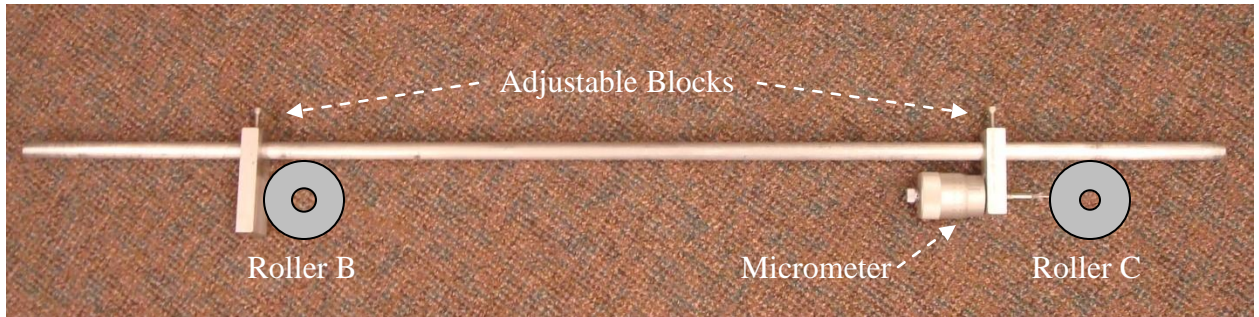


*Figure 3.23 Custom made micrometer for aligning roller B and roller C*

**Level:**

The Rails on which the LDV arm and the roller C assembly slides were made parallel to a ground reference during the set up of the rig. A spirit level shown in the figure (3.24) was used for this purpose. The frame of the rig has four adjustable screws fixed to the bottom of each foot. These screws were adjusted to make the rails horizontal.



*Figure 3.24 18' Starrett® Machinists' Level*

**3.7 A Summary of the Capabilities of the Machine:**

The setup was designed with the intention of studying the effect of misalignment in a multispan web system. The LDVs were setup to move along the pre-entering span, entering span and over the roller B. The Keyence edge sensors were installed to measure the lateral movement of the web at the end of the entering span, which is the maximum deflection in the web due to misalignment. To keep track of the moment transfer into the

pre-entering span another edge sensor was positioned upstream to roller B. The capabilities of the new test rig can be illustrated as follows:

**a) Moment can be measured anywhere in the entering span, on roller B, and in the pre-entering:**

Figure (3.25) show all three areas in which the LDVs can be moved to take data. As discussed earlier, when roller C is misaligned in anti-clockwise/clockwise direction, there is some moment generated in span B. Friction forces between the roller B and the web material may prevent the moment from transferring into the upstream span (span A). To observe the moments in this span LDVs are moved to the position in figure 3.25(c). Figure 3.25(a) and 3.25(b) show the position of the LDV arm while taking readings in span B and over roller B, respectively.

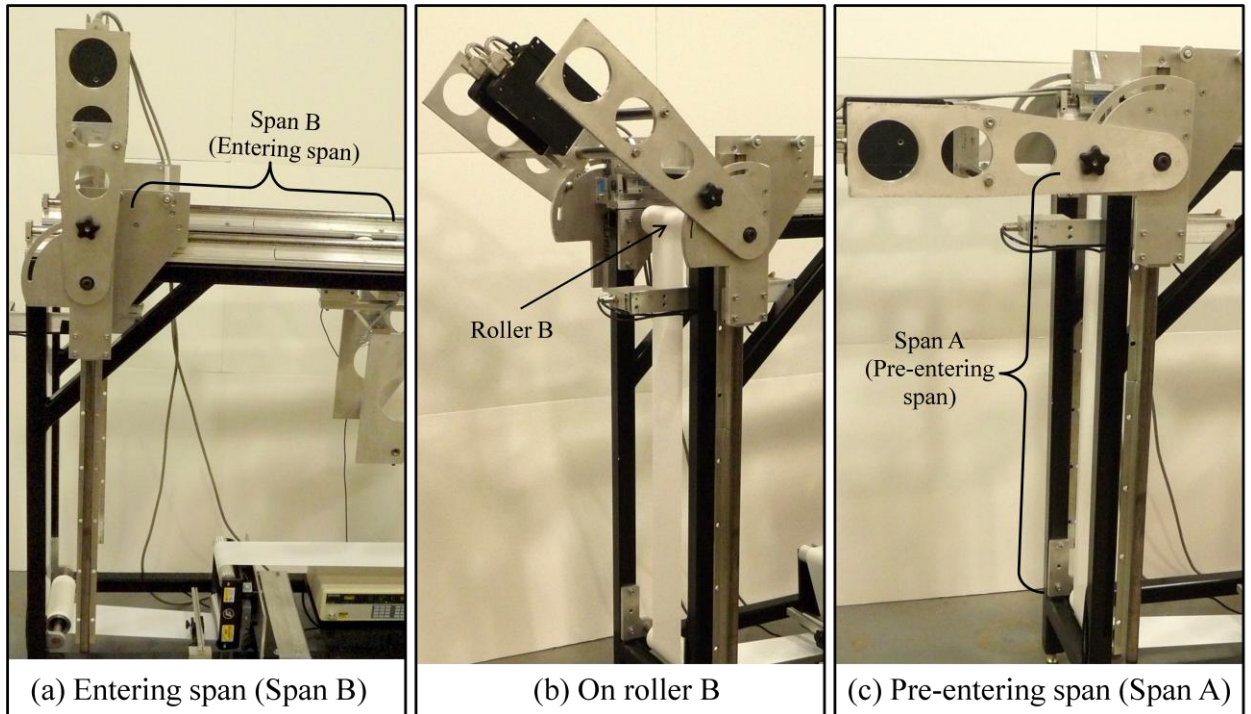


*Figure 3.25 LDVs taking data in all three spans*

**b) Monitoring edge deformation in the entering span:**

Misalignment of roller C at the end of span B leads to lateral motion of the web due to principal of normal entry. Figure (3.26) shows the web edge deformation in the entering span and the Keyence sensors employed to monitor it. As shown in figure, the direction of lateral movement of the web depends on the direction of rotation (counter-clockwise/clockwise) of the roller C.

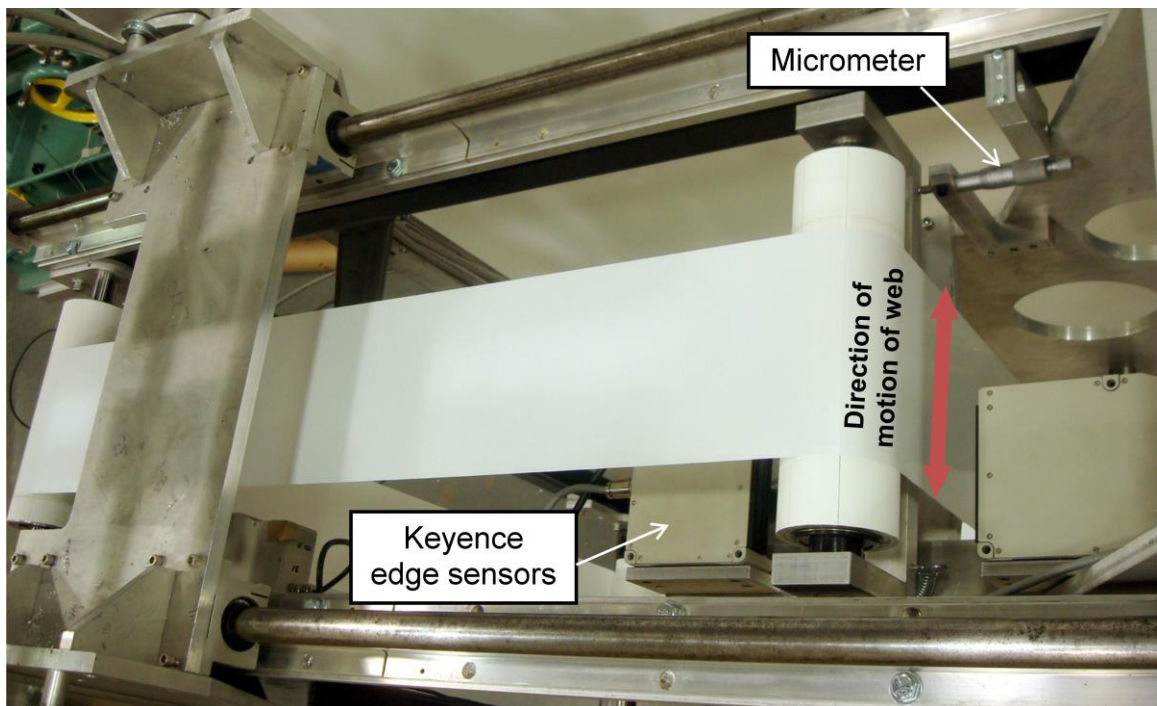


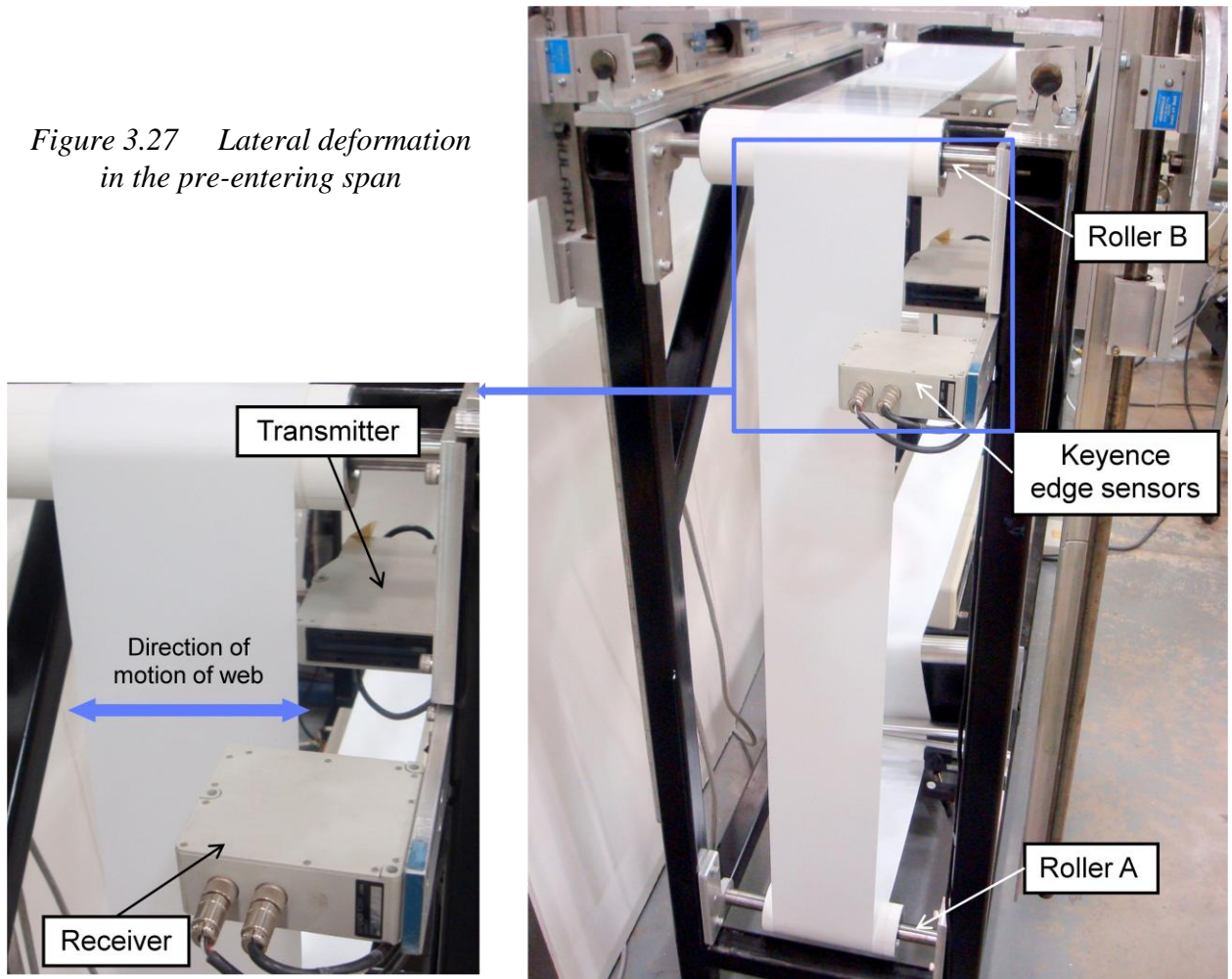
*Figure 3.26 Top view of the span B showing edge sensors*

**c) Monitoring Edge deformation in the pre-entering span:**

Figure (3.27) shows the position of the sensor in the pre-entering span. This sensor is used to record the edge deformation in the pre-entering span (A) occurring due to moment transfer from the entering span (B).



*Figure 3.27 Lateral deformation in the pre-entering span*



**d) Misalignment in the roller C:**

A linear variable differential transformer (LVDT) is installed to measure misalignment given to roller C. Figure (3.28) shows the placement of such a LVDT. This LVDT is connected to a computer, on which the misalignment values are recorded and saved as a text file.

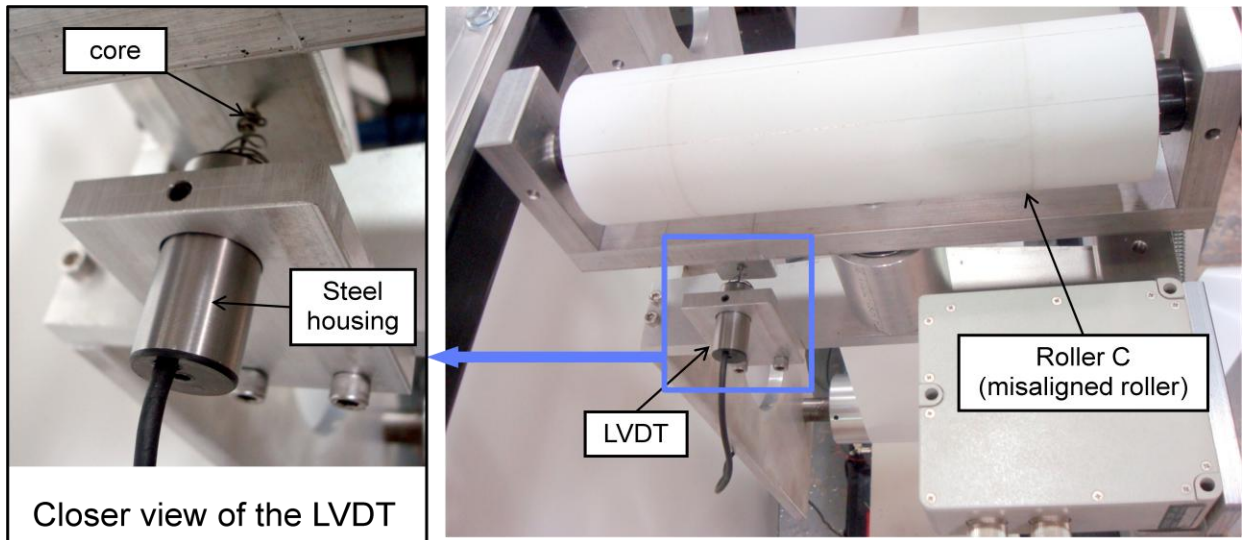


Figure 3.28 Position of the LVDT

### **3.8 Web Properties Testing:**

#### **3.8.1 Measurement of the Tangential Modulus of Elasticity:**

The modulus of elasticity may be measured by conducting tensile tests on smaller samples of webs, but in order to avoid the effects of localized strains and necking, these tests were carried out on full width samples of web with lengths far greater than width (6 inches). A web length of 50 feet was laid flat in a straight line on a smooth surface and one end of it was taped to the floor (figure 3.29). A tensile force was applied and measured by means of a hand held force gage (SHIMPO FGV100) and the resulting web deformation was recorded.

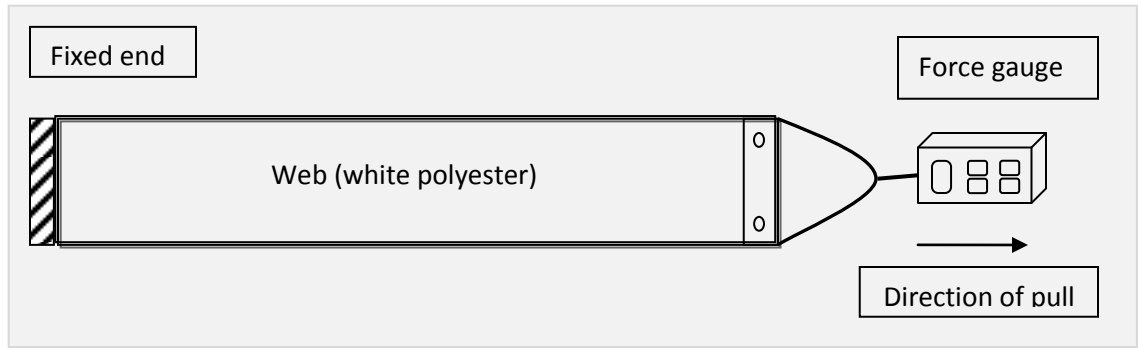


Figure 3.29 Schematic diagram showing Stretch test

A stress versus strain plot was generated in Microsoft Excel as shown in figure 3.30. A linear relationship was observed between stress and strain curves and hence Hooke's law was applied to obtain Modulus of Elasticity as  $\text{stress/strain} = 570 \text{ kpsi}$ . The slope was determined by fitting a straight line to the stress-strain curve.

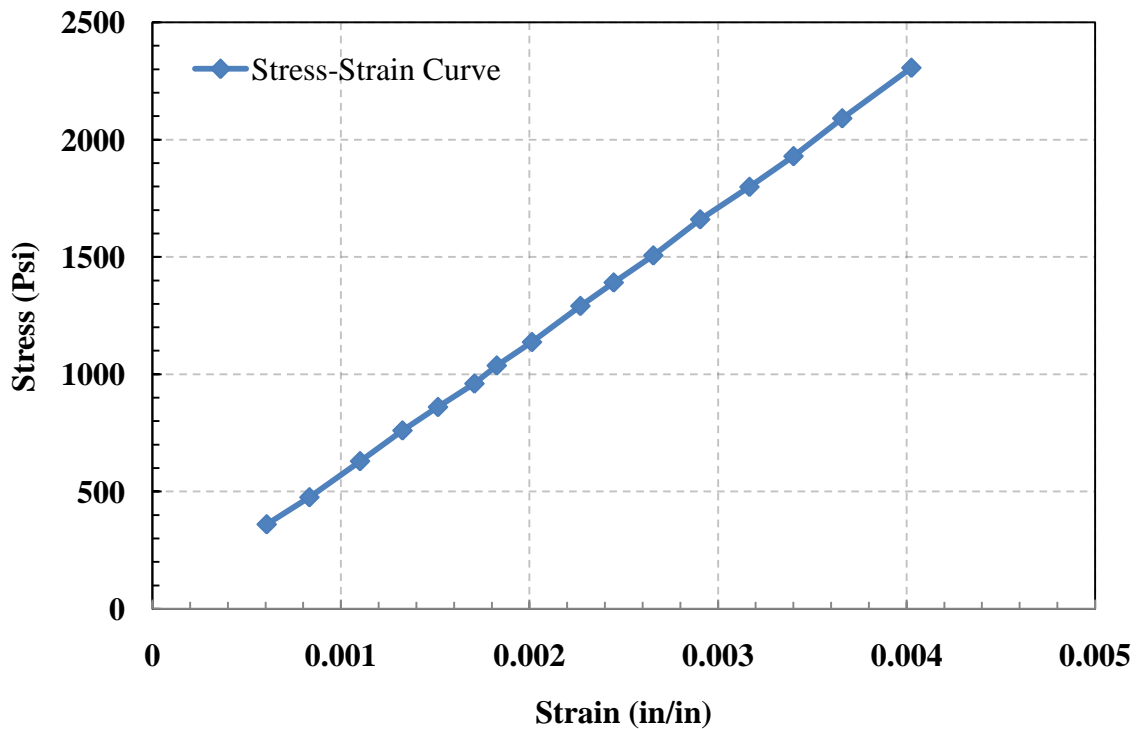


Figure 3.30 Stress-Strain relationship for White Polyester web

### 3.8.2 Measurement of Coefficient of Static Friction:

In order to measure the coefficient of static friction between the web and the roller, web of length 50 inches, subjected to a known dead weight was suspended from the roller with a wrap angle of  $\theta$ , and the other end of the web was clamped to a hand held force gage. The force gage here was used to measure the forces (peak forces) required to cause movement between the web and the roller when subjected to the respective weights. The setup for this experiment is shown in figure 3.31.

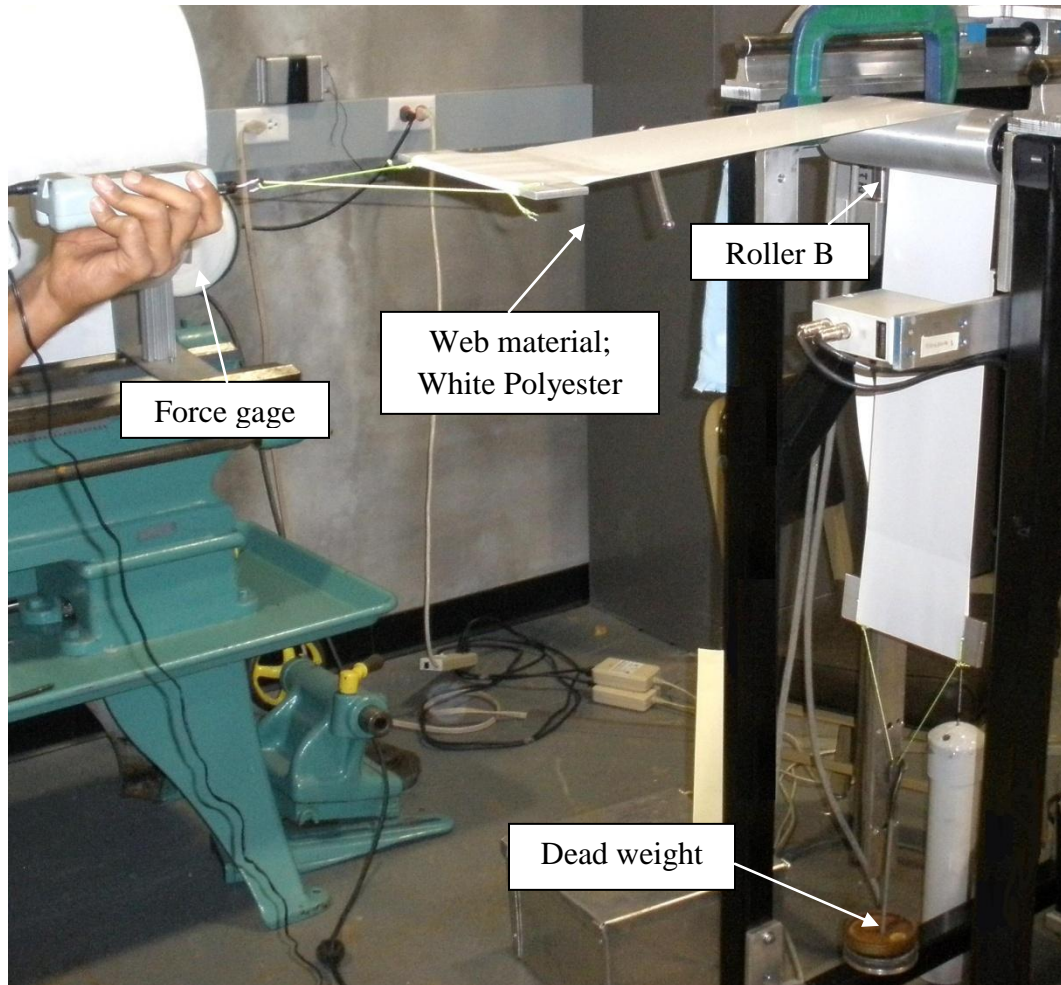


Figure 3.31 Setup for measurement of Co-efficient of Static Friction

The Co-efficient of Static Friction is determined using the equation:

$$\frac{T1}{T2} = e^{(\mu\theta)}$$

Where,

$\mu$  is static Coefficient of Static Friction (dimensionless).

T2 is force required to cause movement between roller and web (lbs).

T1 is the weights the web is subjected to (lbs).

$\theta$  is the wrap angle (rad).

Roller was constrained from rotating about its centroidal axis and the web was pulled with a force gauge and the peak force was recorded. Multiple tests were performed by varying dead weight and the average coefficient of static friction was determined to be 0.33.

### **3.8.3 Surface Roughness Tests (on roller B):**

Whenever a web passes over a roller, there is a possibility of air entrainment between the roller and the web surface. It causes loss of traction which is a function of web tension, web velocity, and roller radius. The phenomenon of air entrainment is simple. Air is entrained in between the web and the roller. As the web moves onto the roller, they both drag in their respective air layers, trapping a thin film between web and roller.

Knox and Sweeney [11] developed an expression for the air film lubrication thickness for a web approaching a roller as follows:

$$h_0 = 0.65R \left[ \frac{12\eta V}{T} \right]^{\frac{2}{3}}$$

where,

$R = 3.00\text{in}$  (radius of the roller)

$\eta = 4.463 * 10^{-11} \text{lb}\cdot\text{min}/\text{in}^2$  (kinematic viscosity of air) at  $27^\circ\text{C}$

$V = \text{web velocity (ft/min)}$

$T = \text{tension in the web (lb/in)}$

Other research [12] has shown when the air film lubrication thickness ( $h_0$ ) becomes comparable to the combined roughness of the web and roller surface in contact that the friction coefficient will begin to diminish. The combined roughness may be stated as:

$$R_{q,\text{eff}} = \sqrt{R_{q,\text{web}}^2 + R_{q,\text{roller}}^2}$$

where,  $R_q$  denotes the root-mean-square roughness of the web and the roller. It is not the intention of this research to study lateral web behavior resulting from cases where the friction coefficient is being affected by entrained air. Hence we will restrict our research to test conditions in which the air film thickness ( $h_0$ ) is less than the effective RMS roughness of the surfaces in contact ( $R_{q,\text{eff}}$ ).

In this case the effective roughness is dominated by the roller surface roughness. To find the surface roughness value  $R_q$  of the roller, a surface roughness test was employed (Mitutoyo SURFTEST 402). As it can be seen in figure (3.32), the tester has a detector stylus whose tip traces the surface of the roller. Then the roughness values ( $\mu\text{in}$ )

are displayed on the touch panel. The roughness test was performed at various locations on the roller and the average roughness was found to be 80.85  $\mu\text{in}$ .

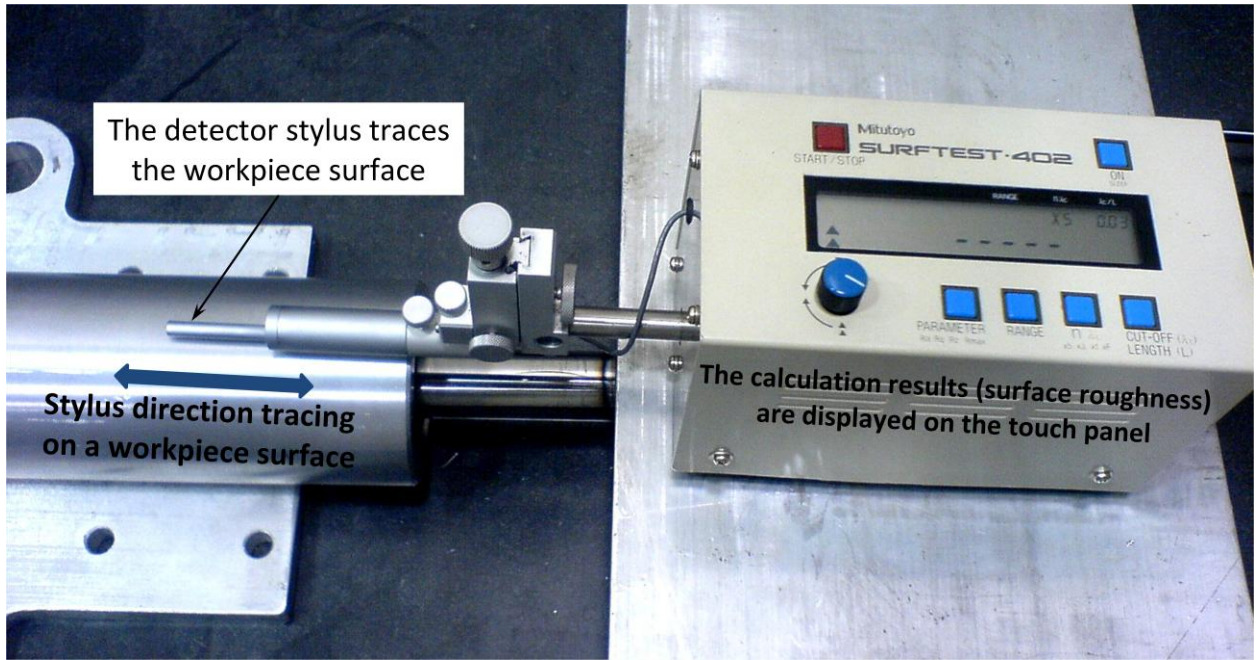


Figure 3.32 Surface roughness tester

In an attempt to eliminate air entrainment from decreasing the friction coefficient between the web and the roller B, it was ensured that the air film is smaller than the rms roughness of the roller ( $R_q = 80.85 \mu\text{in}$ ). The Knox Sweeney expression was used to find what speeds could be used at various tensions. Table 3.3 shows speeds obtained for various web tensions.

TENSION (lb)	SPEED (ft/min)
9	191
10	212
11	234
12	255
13	276
14	296
15	319

Table 3.3 Allowable tensions at various speeds

Most of the tests were conducted at 13 lbs or 2.167 pli of tension. The tests were run at speeds less than 100ft/min and thus from the table (2.3), it can be said that air entrainment should not have decreased the friction coefficient.

### **3.9 Evaluating different misalignment values for roller C**

After setting up the rig and troubleshooting the problems it had, it was the time to start the experimentation. As discussed in the previous section, various tests were conducted to find all the necessary parameters required for the experiment. All the specifications of the test are shown in Table 3.4.

<b>TEST SPECIFICATIONS</b>	
Material type	200 gage Hostaphan® polyester (Mitsubishi Polyester Film)
Young's modulus (E)	570 000 psi
Width of web (w)	6 inches
Thickness of web (t)	0.002 inches
Length of test span A ( $L_A$ )	43.75 inches
Length of test span B ( $L_B$ )	33.5 inches
Distance between LDVs ( $\Delta y$ )	5 inches
Tension in web (T)	13 lb
LDV Type	BETA LaserMike LS200
Pulse rate of each LDV	1000 counts/foot
Standoff distance of LDV	12 inches

*Table 3.4 Test specifications*



Then the misalignments (given to roller C) were chosen such that there were cases where there was no span interaction, cases where there was known to be span interaction and finally cases in between. The moment at the roller in span B is denoted by  $M_{bi}$  (Equation 2.6) and  $M_r$  (Equation 2.1) is the critical moment that  $M_{bi}$  must exceed for moment transfer into span A to begin. From chapter 2:

$$M_{bi} = \left[ \frac{2EI}{L_b} + \frac{TL_b}{6} \right] \theta_c$$

$$M_r = \frac{\mu T \beta W}{4}$$

Using the specifications set in the table 2.4 the following three misalignment values for roller C were calculated:

Case 1:	$M_{bi} = (1/6) M_r$	<ul style="list-style-type: none"> <li>When, no span interaction occurs</li> </ul>
Case 2:	$M_{bi} = (1/2) M_r$	<ul style="list-style-type: none"> <li>When, web starts slipping over a part of roller B's surface, but no moment is transferred into span A</li> </ul>
Case 3:	$M_{bi} > M_r$	<ul style="list-style-type: none"> <li>When, slippage occurs on roller B resulting in span interaction</li> </ul>

With the above relations misalignments used in tests and analyses were calculated as  $\theta_1 = 0.074^\circ$ ,  $\theta_2 = 0.223^\circ$ , and  $\theta_3 = 0.446^\circ$ .

Tests were conducted for all the three cases and the results are discussed in the following chapter.

## CHAPTER IV

### Experimental Results and Discussion

This chapter deals with the results obtained from the experimental setup. Results from the data recorded by LDVs and Keyence sensors are compared with the theory put forward by Good [2]. A comprehensive discussion of the results is conducted. Some significant modifications made to the experimental setup and corrections made while recording data are also discussed in this chapter.

As discussed earlier in the last chapter, LDVs were moved in span A, span B and over roller B to record data. For the first two cases ( $\theta_1$  and  $\theta_2$ ), data was recorded at three different locations in span B and at four different positions on roller B (at entry point, at exit point and two other positions in between). But, for the third case when misalignment was  $\theta_3$ , there is some moment transferred into span A so, moment measurements were made in span A also.

Each of the LDV was set to yield an output of 1000 pulses/foot. As discussed in section 3.2, these LDVs have some offset due to calibration errors. To find the offset between the set of LDVs, data is recorded when the misalignment given to roller C is

zero. This value of difference is accounted while performing moment calculations from the data recorded by LDVs. LDV counts are recorded for every 100 feet of web passed beneath it. At every point in a span, 10 such readings are taken and average of the values is considered for calculations.

Plots showing comparison between theoretical moments and experimental moments are obtained from the data recorded. So, there was a need to calculate theoretical moments at various positions in span B for all the three misalignment cases. Following section deals with the method of calculating these moments.

#### **4.1 Calculating Moments:**

Initially, while performing preliminary set of tests on modified Shelton machine as discussed in section 3.3, theoretical moments were calculated using concepts of Strength of materials. Force acting on the web due to misalignment given to roller C was considered for these calculations. But later, a modified equation based on theory developed by Good, et al. [2] was employed. This equation (4.5) considers the effect of shear and tensions while calculating moments in a web span.

As discussed in the previous chapters, a web between an upstream roller and a misaligned downstream roller behaves as a cantilever beam subjected to a lateral end load. The stiffness matrix for a beam stiffened by tension (as given by equation 2.2 of chapter 2) is:

$$\begin{Bmatrix} f_{yi} \\ M_i \\ f_{yj} \\ M_j \end{Bmatrix} = \begin{bmatrix} \frac{12EI}{L^3} + \frac{6T}{5L} & \frac{6EI}{L^2} + \frac{T}{10} & -\frac{12EI}{L^3} - \frac{6T}{5L} & \frac{6EI}{L^2} + \frac{T}{10} \\ \frac{6EI}{L^2} + \frac{T}{10} & \frac{4EI}{L} + \frac{2TL}{15} & -\frac{6EI}{L^2} - \frac{T}{10} & \frac{2EI}{L} - \frac{TL}{30} \\ -\frac{12EI}{L^3} - \frac{6T}{5L} & -\frac{6EI}{L^2} - \frac{T}{10} & \frac{12EI}{L^3} + \frac{6T}{5L} & -\frac{6EI}{L^2} - \frac{T}{10} \\ \frac{6EI}{L^2} + \frac{T}{10} & \frac{2EI}{L} - \frac{TL}{30} & -\frac{6EI}{L^2} - \frac{T}{10} & \frac{4EI}{L} + \frac{2TL}{15} \end{bmatrix} \begin{Bmatrix} v_i \\ \theta_i \\ v_j \\ \theta_j \end{Bmatrix} \quad (4.1)$$

For span B when there is no moment transfer occurring into upstream span,  $v_i$ ,  $\theta_i$  and  $M_j$  are zero. As discussed earlier in chapter 2, when there are no span interactions  $v_i$  and  $\theta_i$  are zero. Also it is known that the moment ( $M_j$ ) in the web at the entry point to roller C is zero [1]. From the 4<sup>th</sup> row of the matrix,  $v_j$  can be derived as:

$$v_j = \left[ \frac{\frac{4EI}{L_b} + \frac{2TL_b}{15}}{\frac{6EI}{L_b^2} + \frac{T}{10}} \right] \theta_j \quad (4.2)$$

From the 3<sup>rd</sup> row, the lateral steering force,  $f_{yj}$  can be derived as:

$$f_{yj} = \left[ \frac{12EI}{L_b^3} + \frac{6T}{5L_b} \right] v_j - \left[ \frac{6EI}{L_b^2} + \frac{T}{10} \right] \theta_j \quad (4.3)$$

Equations (4.2) and (4.3) can be combined to calculate the lateral force at the roller C due to a misalignment ( $\theta_j$ ) of roller C:

$$f_{yj} = \left[ \left( \frac{\frac{4EI}{L_b} + \frac{2TL_b}{15}}{\frac{6EI}{L_b^2} + \frac{T}{10}} \right) \left( \frac{12EI}{L_b^3} + \frac{6T}{5L_b} \right) - \left( \frac{6EI}{L_b^2} + \frac{T}{10} \right) \right] \theta_j \quad (4.4)$$

Then the moment at various locations in span B is given by:

$$M(x) = f_{yj}(L_b - x) - T[v(L_b) - v(x)] \quad (4.5)$$

where,  $x$  is the distance of that location from roller B. Figure 4.1 shows a free body diagram of the cantilever beam. The stiffness matrix is developed based on applied loads being defined in the global coordinates.

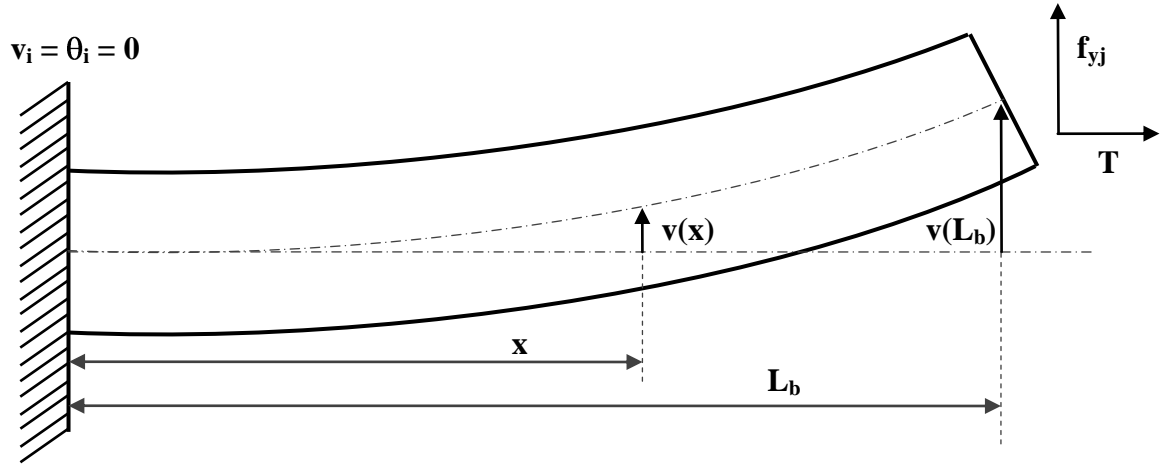


Figure 4.1 Free body diagram web in span B

Experimental moment values from the data recorded are calculated as shown in section 3.3.

In Figure 4.2, theoretical moments are compared with experimental moments in span B when misalignment given to roller C is  $0.074^\circ$  ( $\theta_1$ ). The misalignment was calculated earlier to be insufficient to induce moment transfer into span A. The origin on the x-axis denotes the exit tangent point of the web on roller B and the length of the span is 33.5 inches. It can be seen from the graph that there is no moment transferred into span A, as the experimental moment values are close to theoretical values near the roller B when  $x=2$ . Had the experimental moment been less than the theoretical moment, this would have been evidence that moment transfer was already occurring.

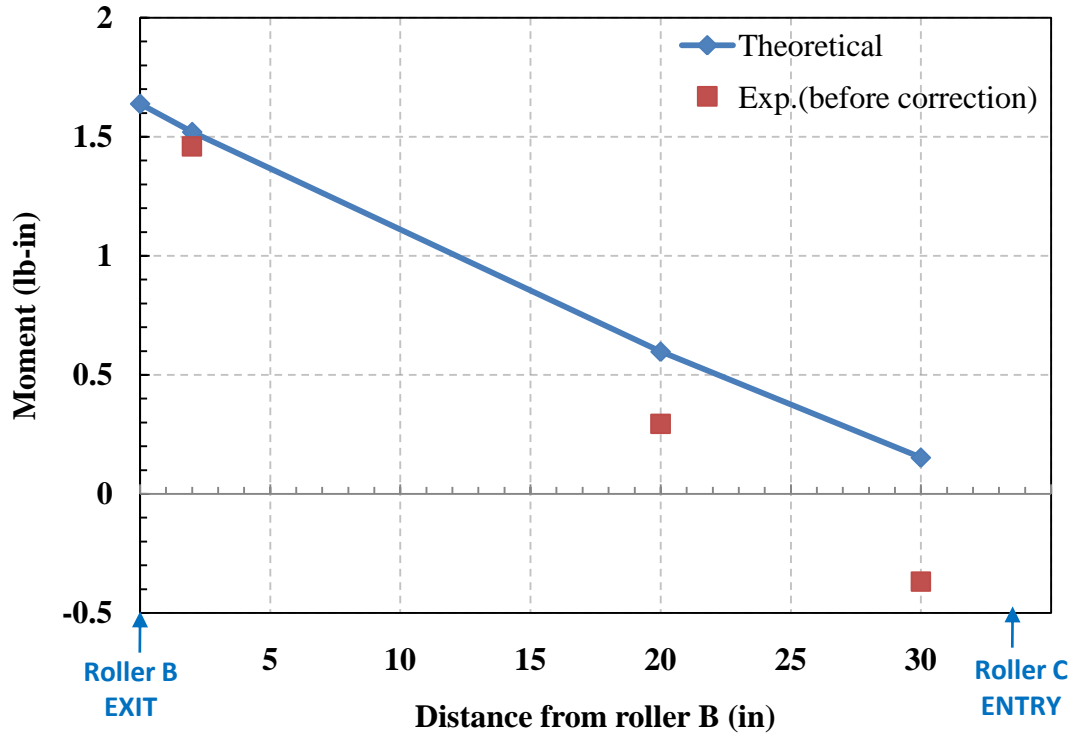


Figure 4.2 Plot of moments before correcting cosine error

While moving from roller B to roller C in span B, the theoretical moment changes linearly from maximum to zero whereas the experimental values in spite of following a linear path appear to intercept zero before the web reaches roller C. A possible explanation for this behavior is a cosine error involved in the measurements from the LDVs. This will be discussed in following section.

#### **4.2 Cosine error in measurements and correction:**

An investigation was done for all possible potential sources of error (as seen in figure 4.1) in the web moment calculated from the differential LDV measurements. When the test setup was designed initially, there was no provision to allow the LDVs to rotate with the web in case of any misalignment. Thus the lasers on the two LDVs strike the web at one MD location, as shown by the line AB in figure 4.3.

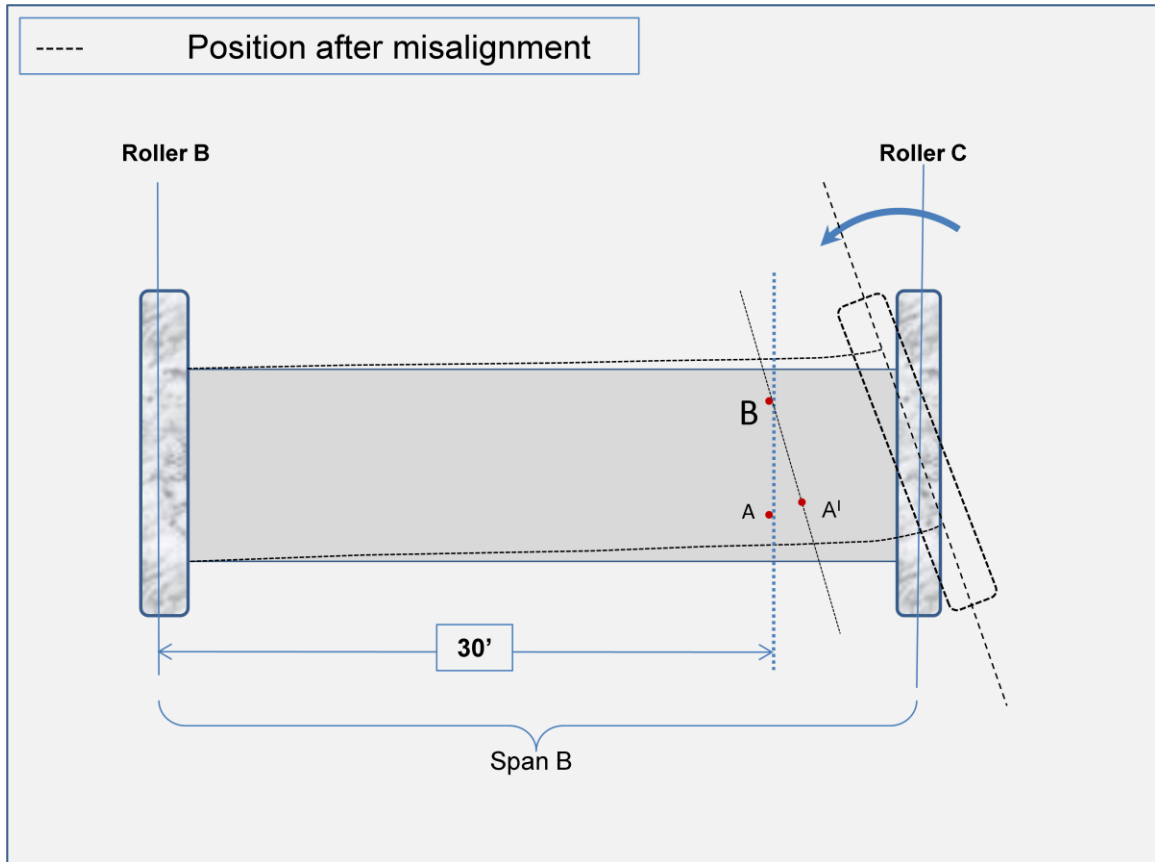


Figure 4.3 Cosine error in LDV measurements

There is a so-called “cosine error” involved with the LDV measurements. If the web velocity is not aligned with the MD then the LDVs will measure only the MD component of that velocity.

Points A and B refer to the position of the LDVs before aligning them with the slope of the beam. To correct the cosine error in the measurements, LDV A was adjusted to the position  $A^1$ , as shown in the figure 4.3. Line  $BA^1$  is now perpendicular to the web line. This correction in the position of LDV A was done at all the positions wherever the data was recorded.



To induce this correction in LDV A, a screw was installed beside the carriage to which LDV arms were fixed (figure 4.4). Calculations were done to find the amount of correction required at each measurement position in span B. A dial indicator was used to measure the twist that was induced with the screw. The base of the dial indicator was fixed to the frame of the test setup with its pointer touching the carriage carrying LDVs. So, whenever point A was needed to be moved to  $A^I$ , LDV carriage was pushed with the help of the installed screw.

Figure 4.5 shows one of the cases in which correction was made while recording LDV data. Plot shows the improvement in the value of experimental moment at a distance of 30 inches from roller B, when  $\theta = 0.074^\circ$ .

Similarly, data was recorded for all three cases of misalignment, incorporating cosine error correction in the LDV measurements.

Hereafter in this chapter, the experimental moments have been corrected for cosine error.

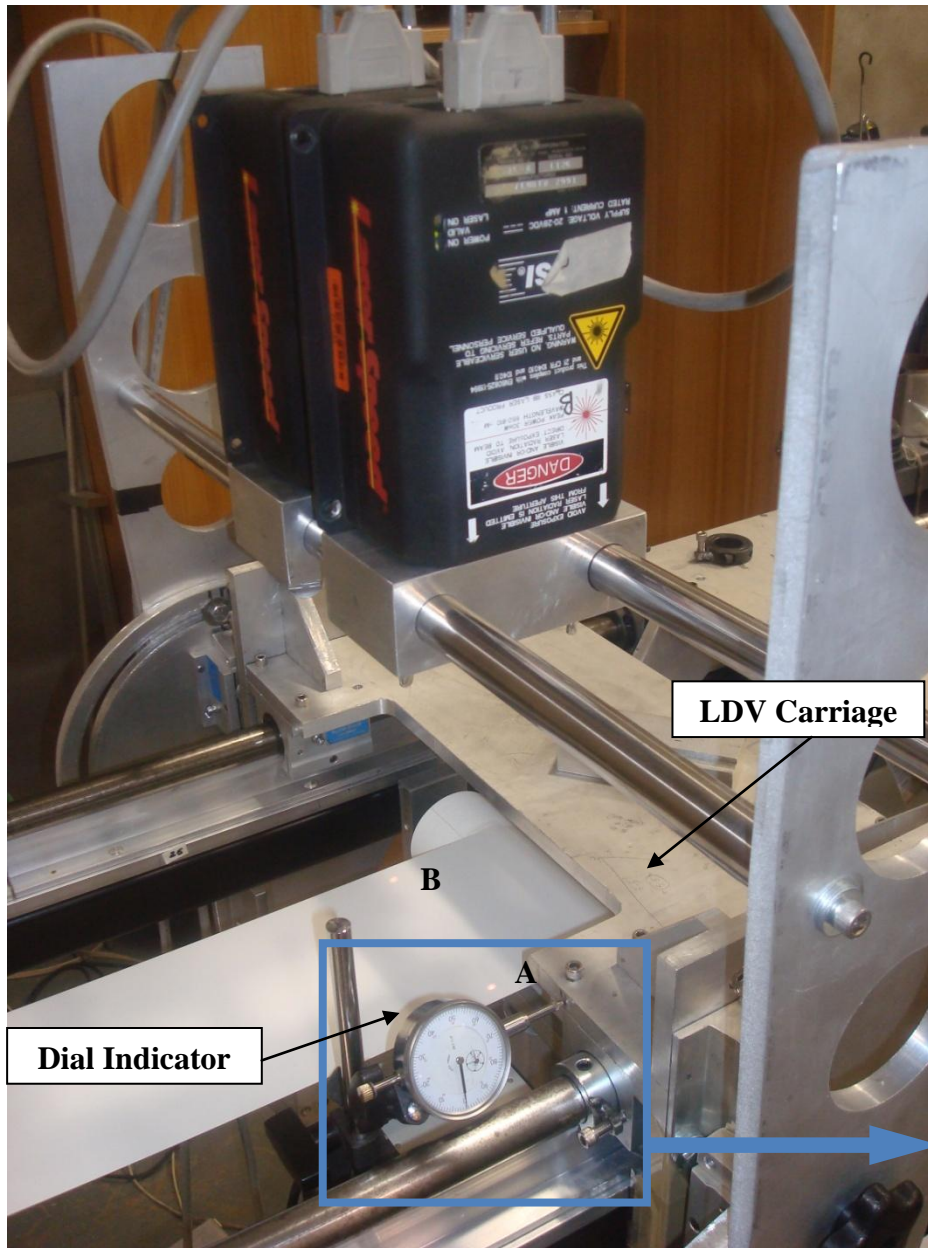
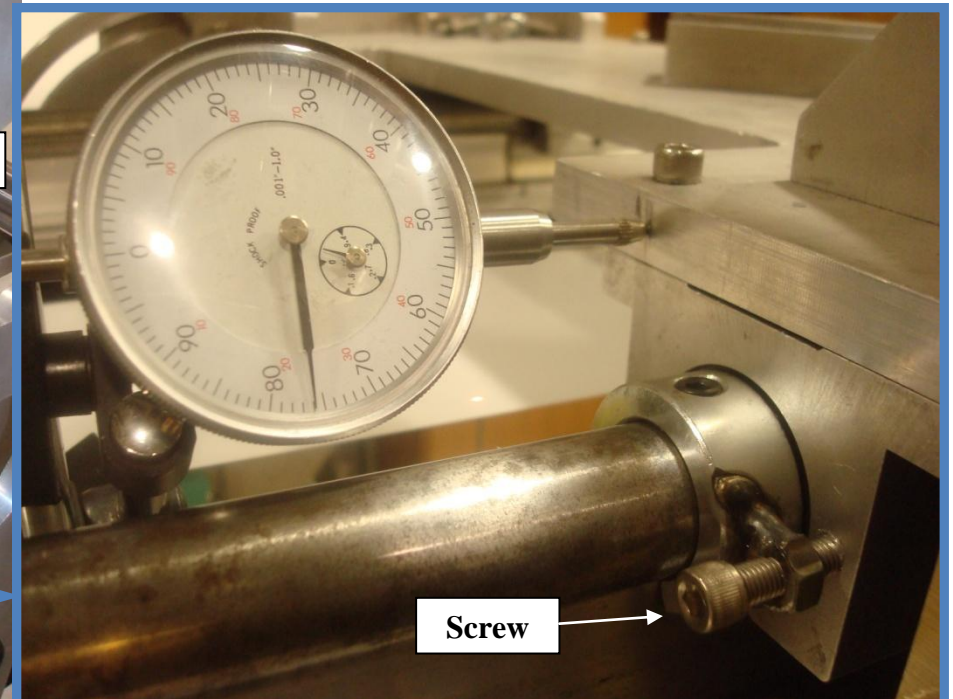


Figure 4.4 Modification in test setup to correct cosine error

(Bottom) Close view of screw assembly



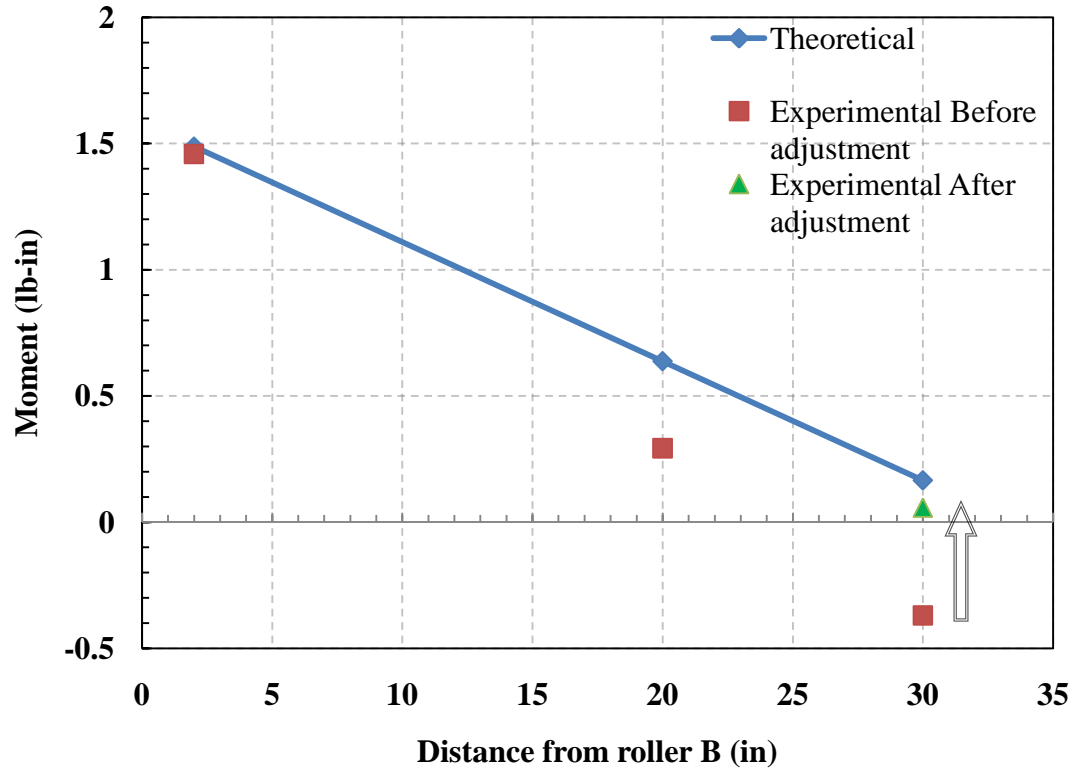


Figure 4.5 Moment at 30' from roller B in span B at  $\theta=0.074$  degrees

Following three sections lay out the results in span B (for  $\theta_1$ ,  $\theta_2$  and  $\theta_3$ ), on roller B (for  $\theta_1$ ,  $\theta_2$  and  $\theta_3$ ) and in span A (for  $\theta_3$  only).

### 4.3 Results in span B

Figure 4.6, 4.7 and 4.8 show the comparison between theoretical moments, initial experimental moments (recorded before correcting cosine error) and corrected experimental moments for first, second and third case, respectively. The theoretical moments are calculated from equation 4.5.

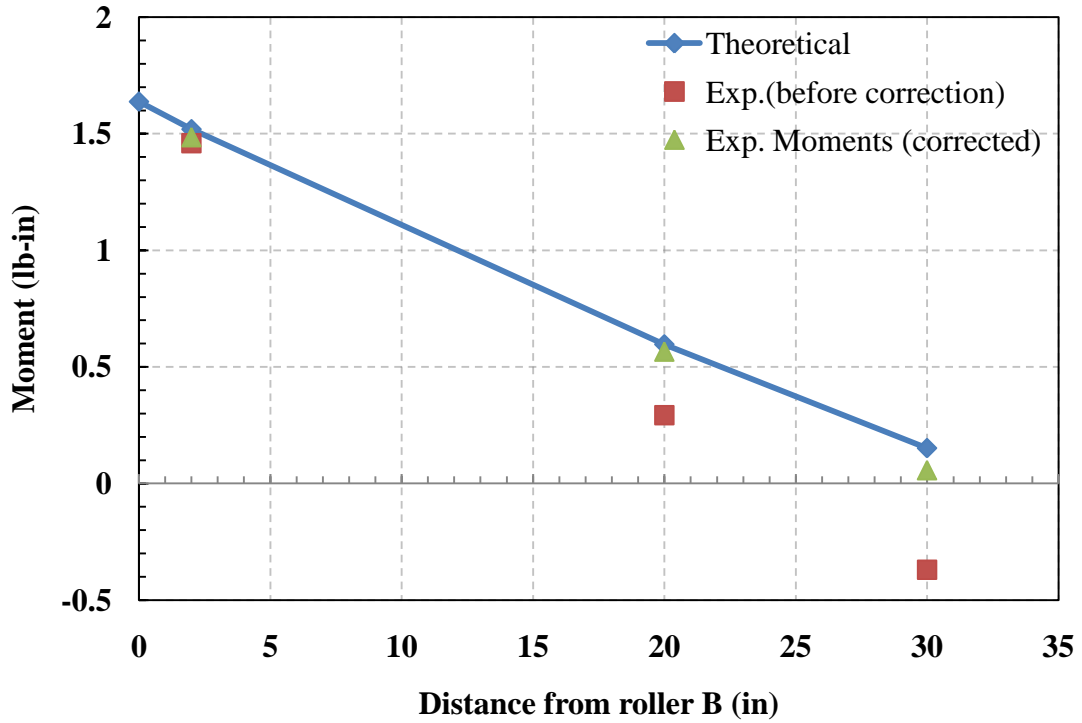


Figure 4.6 Moments in span B, when  $\theta=0.074$  degrees

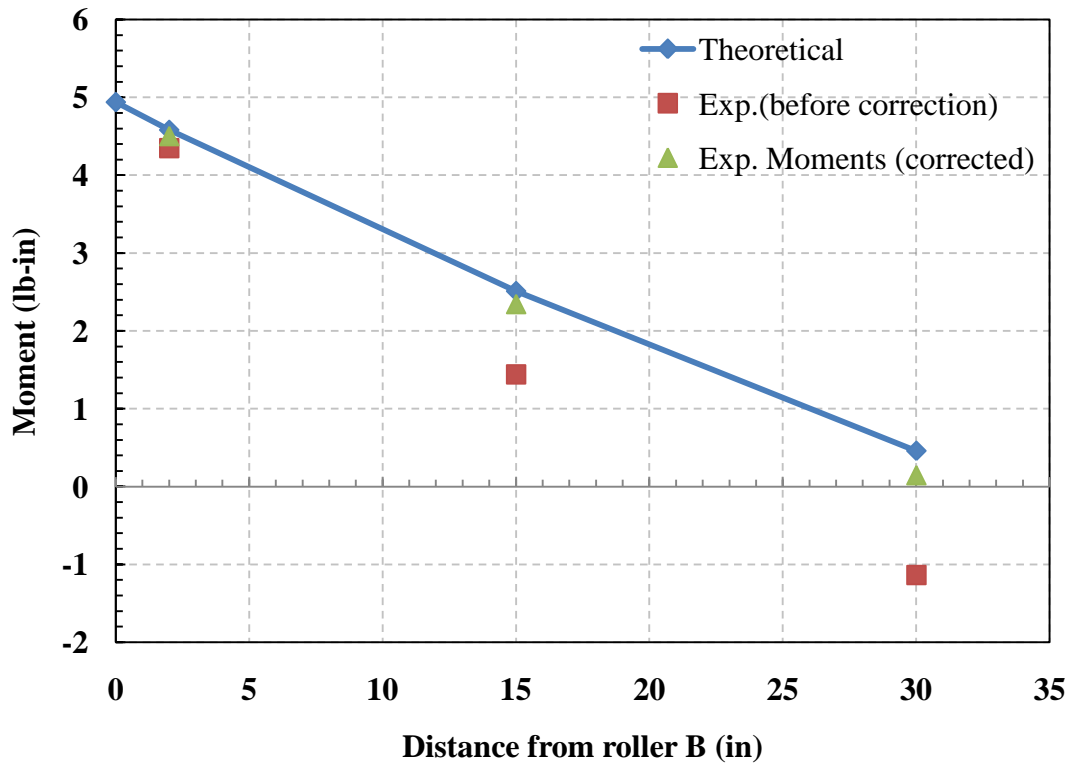


Figure 4.7 Moments in span B, when  $\theta=0.223$  degrees

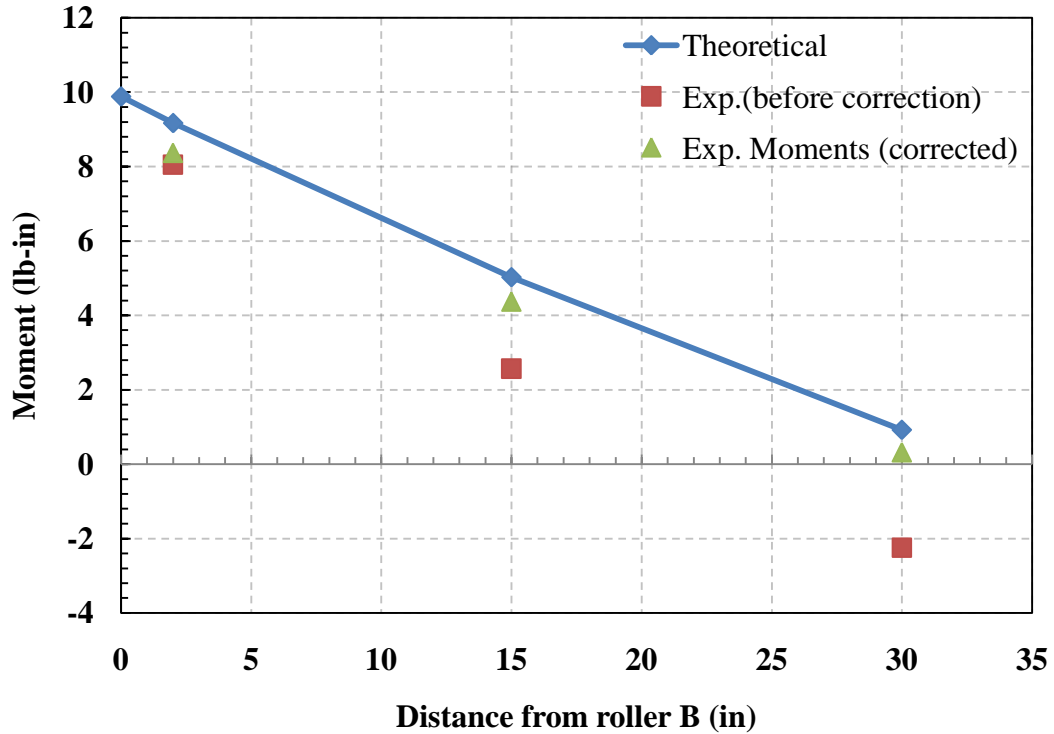


Figure 4.8 Moments in span B, when  $\theta=0.446$  degrees

For the first case when  $\theta=0.074^\circ$ ,  $M_{bi}$  is equal to  $(1/6) M_r$  and in the second case when  $\theta=0.223^\circ$ ,  $M_{bi}$  is equal is half of  $M_r$ . Moments plots for these two cases (figure 4.6 and figure 4.7) show that there is no moment transferred into span A, as the experimental moment values are close to theoretical values throughout span B.

When  $\theta=0.446^\circ$ ,  $M_{bi}$  is equal to  $M_r$ . From figure 4.8, it can be observed that the corrected experimental moments are less than that given by theory at all test stations. This one indication that moment has began to transfer into span A. It also means that slippage is occurring over the majority of the contact area between the web and roller B.

To predict the amount of slippage between roller and the web, it is necessary to study the behavior of moments on the roller B. The following section presents test results obtained at various locations on roller B.

#### 4.4 Results on roller B:

Four locations were chosen on roller B to make LDV measurements. Figure 4.9 shows all four locations on roller B. Table 4.1 gives the position of the LDVs in inches, starting from the entry point to roller B (location 1).

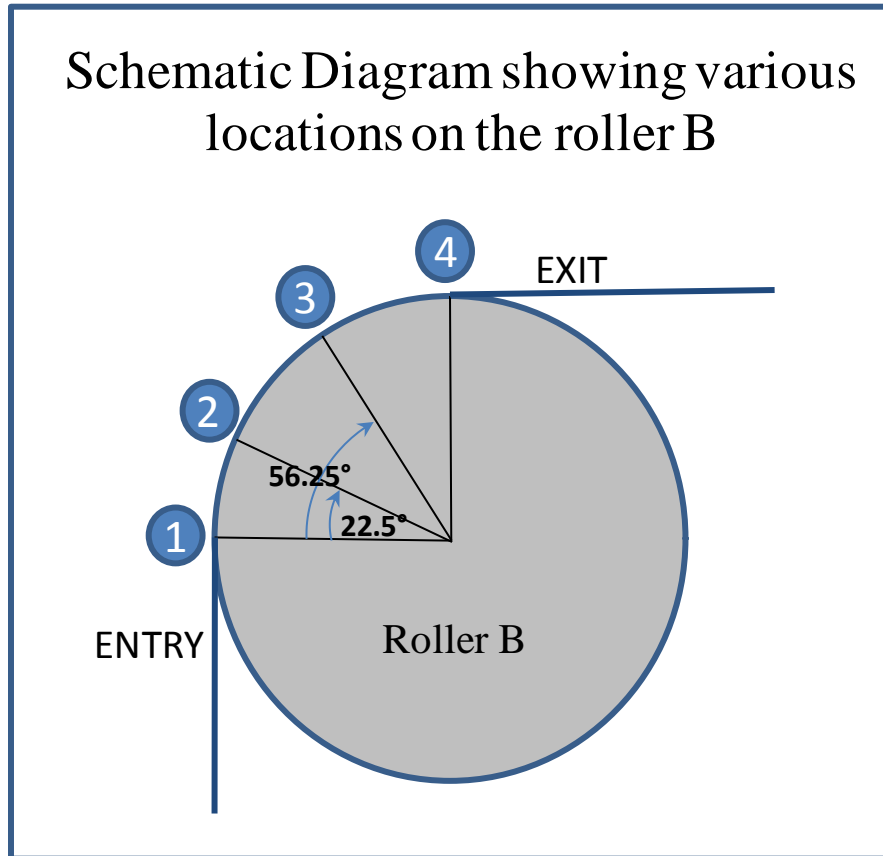


Figure 4.9 Different locations on roller B

Location on Roller B	Distance from Entry point (inches)
1	0
2	0.589
3	1.47
4	2.356

Table 4.1 Test positions on roller B

Figure 4.10 provides some of the first evidence of web behavior on rollers. The moments at the exit (wrap position 2.356") are slightly larger than the maximum values presented in figures 4.6, 4.7, and 4.8 which were taken 2" downstream of the exit. Theoretically the maximum value of the internal bending moment should exist as the web exits roller B when roller C is misaligned.

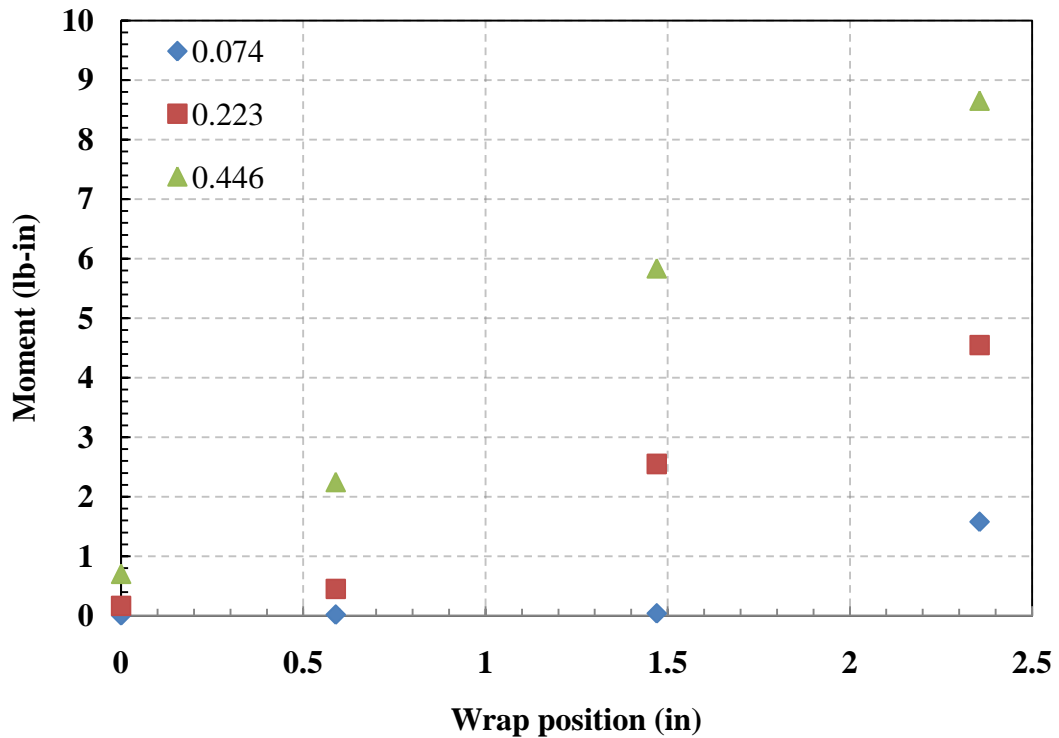


Figure 4.10 Moments on roller B

In figure 4.10 we can observe how the moment in the web is reacted by frictional moments. Any moment in the web will require a finite amount of wrap position before it can be reacted by frictional moments. Even for the moments induced by the least amount of misalignment ( $\theta = 0.074^\circ$ ) it appears that a web wrap of 0.9" was required before the moment was completely reacted and hence the web moment became zero. At the next level of misalignment ( $\theta = 0.223^\circ$ ) about 2" of wrap was required to react the moment.

This was expected because this misalignment was selected to produce moments that would require about  $\frac{1}{2}$  of the moment ( $M_r$ ) that could be reacted in friction. Finally at the third level of misalignment ( $\theta = 0.446^\circ$ ) it is apparent that slippage is occurring across the entire wrap of the web about the roller. Again this was by design.

It is also noteworthy that the moment in the web appears to decrease linearly from the exit of the web from roller B to an upstream location. When  $\theta=0.446^\circ$ , moment has some considerable value at position 1 on roller B (at entry point), so it is understood that there is some moment transferred into upstream span and hence it is important to find moments in span A also. Hence, moments obtained from the LDV data in span A are discussed in the following section.

In addition the data from the sensor (S1) installed upstream to roller B to measure lateral deformation in web, confirms that there were no span interactions for  $\theta_1$  and  $\theta_2$ , unlike  $\theta_3$ . The data shown in section 4.6 compliments this.

#### **4.5 Results in span A:**

As discussed earlier, span interactions were occurring only when the misalignment given to roller C was  $0.446^\circ$  (for  $\theta_3$ ). A plot of the moments in span A for this case is shown in figure 4.11.



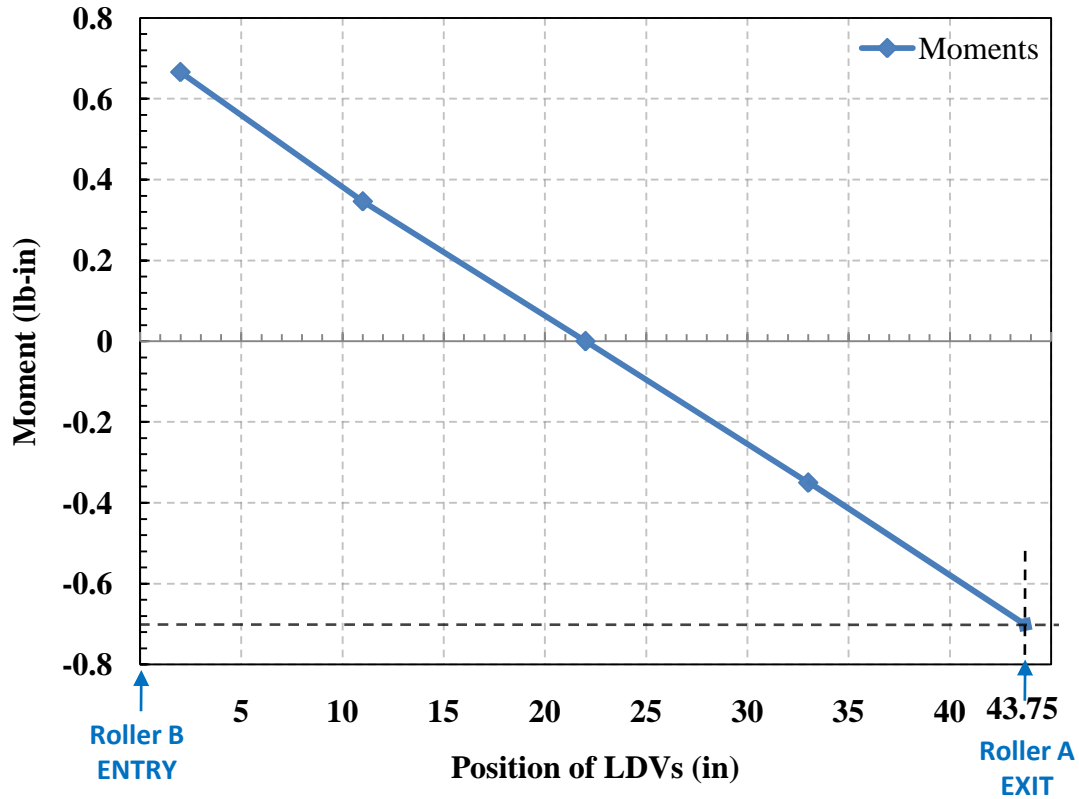


Figure 4.11 Moments in Span A (0.446°)

The length of the span A is 43.75 inches. Data was recorded at four different locations in span A. At 2in, 11in, 22in and 33in away from roller B. Moments decreased linearly as the LDVs were moved from roller B to roller A, in span A and moment value is zero halfway through the span. Of note here as well is that if moment is extrapolated to roller A, we see that:

$$M_{ai} = - M_{aj} \tag{4.6}$$

This is noteworthy because this is also true for a beam which is fixed fully at one end and allowed to translate laterally but not rotate at the other end per figure 4.12. If a side load is applied as shown, the same moment variation results and also becomes zero midspan.

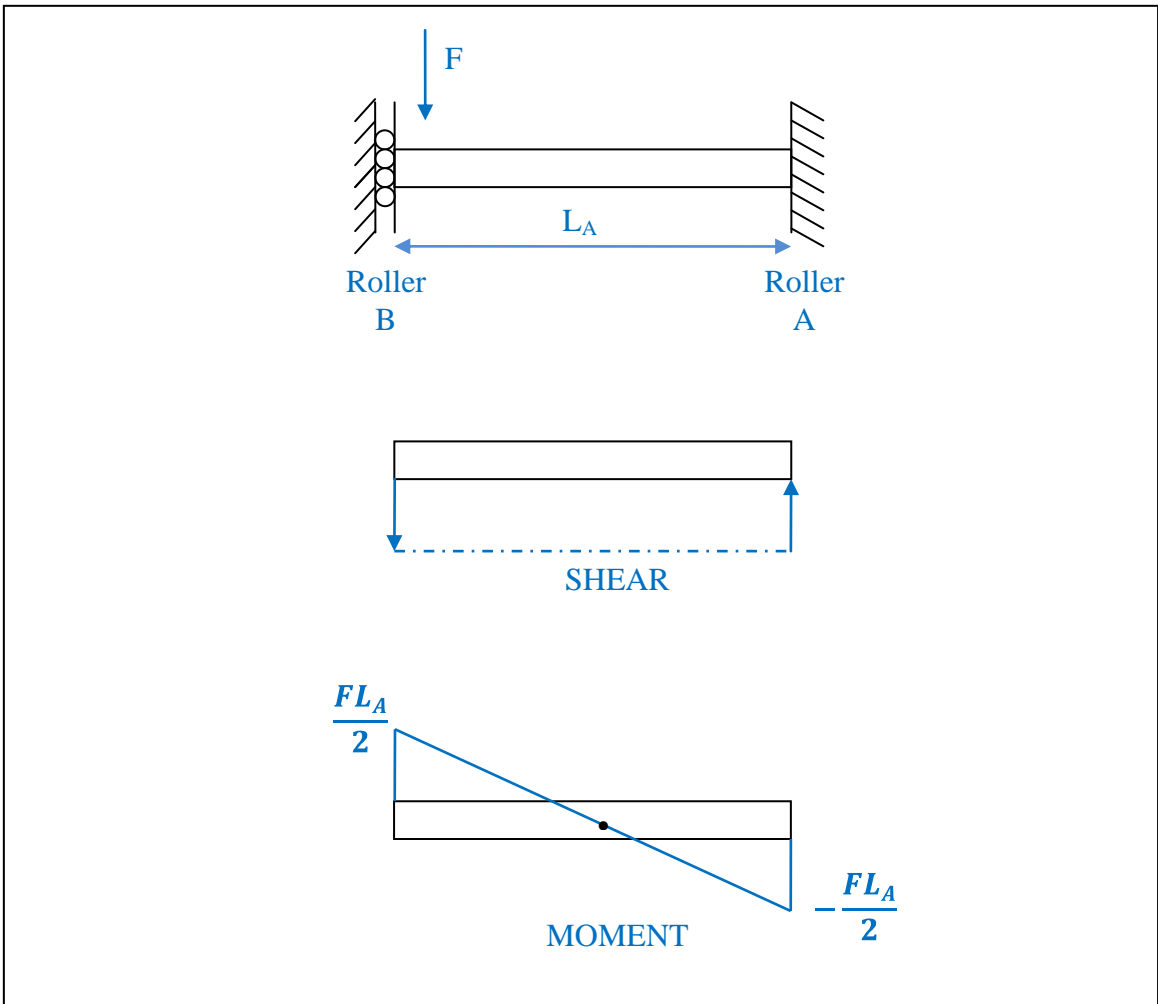
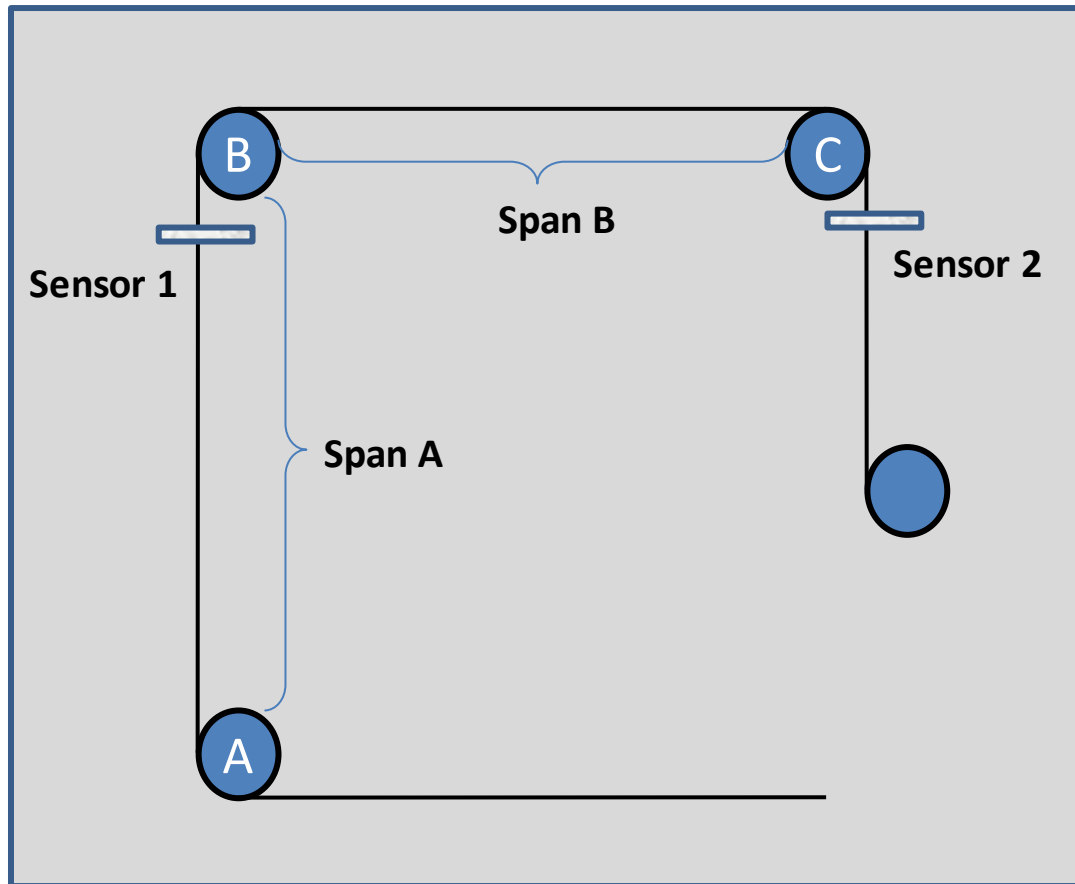


Figure 4.12 Shear and moment diagram for a constrained beam

This is important because it allows us to infer that the web is achieving normal entry to roller B under conditions of moment transfer.

#### 4.6 Results from Keyence sensors

As discussed in the section 3.5, two Keyence edge sensors were installed on the test setup. These sensors were employed to monitor edge deformations in the pre-entering span (sensor S1) and the entering (sensor S2) span. Figure 4.13 shows placement of S1



*Figure 4.13 Placement of sensors*

and S2 on the test setup. Figure 4.14 shows the data recorded from both the sensors for all three misalignments. Values in the blue arrows are the changes (in angles, S1 readings and S2 readings) occurring when misalignment goes from zero through  $\theta_3$ .

$\theta_c$	Angle (°)	S1 (in)	S2 (in)
Zero	0	0	0
	-0.074	0	-0.026
$\theta_1$	-0.074	0	-0.026
	-0.149	0	-0.064
$\theta_2$	-0.223	0	-0.090
	-0.223	+0.019	-0.078
$\theta_3$	-0.446	0.019	-0.168

Figure 4.14 Data recorded from S1 and S2

As discussed in the previous chapters, a web between an upstream roller and a misaligned downstream roller has been assumed to behave as a cantilever beam subjected to an end load. The maximum deflection in such a beam is given by:

$$v_j = \left[ \frac{\frac{4EI}{L_b} + \frac{2TL_b}{15}}{\frac{6EI}{L_b^2} + \frac{T}{10}} \right] \theta_j \quad (4.7)$$

Table 4.2 shows the comparison between lateral displacements of the web calculated using above formula and the displacements calculated from the data recorded by the sensor S2 (from figure 4.13).

Lateral Deflection on roller B	Misalignment (Degrees)		
	0.074	0.223	0.446
Calculations	0.029	0.088	0.176
Experimental	0.026	0.090	0.187

*Table 4.2 Lateral deflection on roller B*

From the data deflection obtained from the sensors S1 and S2, the following deductions can be supported:

- Data recorded from sensor S1 shows that the lateral deflection in the web due to misalignment of roller B is zero when  $\theta=0.074^\circ$ . Thus whatever slippage that occurs is limited to the region of the web near the exit of roller B and no slippage occurs to span A.
- For the case when  $\theta=0.223^\circ$ , there is additional slippage occurring on roller B but it is insufficient to overcome the whole of the frictional force between the roller B and web. So there is no transfer of moment from span A to B and no deformation in span A.
- When  $\theta=0.446^\circ$  ( $M_{bi} > M_r$ ), there is some moment interaction occurring between the spans and it can be seen from the readings of the sensor S1 (figure 4.14).
- As soon as we start misaligning roller B, the web starts moving laterally due to the normal entry principle of the web. This is witnessed from the data of sensor S2. The deflection in the web increases with the value of misalignment.

## **CHAPTER V**

### **A New FEM Model**

#### **5.1 Introduction**

The aim of this research is to study the various cases of moment transfer occurring due to a downstream misaligned roller from the data taken by LDVs. In order to ensure the accuracy of the results obtained from the data taken by LDVs, an attempt has been made to develop a FEM model for comparison. As discussed in the earlier chapters the web traversing rollers A, B and C can be considered as a simply supported beam. Misalignment in roller C is equivalent to a load at the end of the beam. Concepts of Finite Element Analysis have been employed to create a model to find the moments and lateral deformations in the web due to a misaligned roller. A comparison of the results is shown in the next chapter.

Previously, three amounts of misalignments were calculated for roller C, such that there is no slippage on roller B, a little slippage occurring on it and finally a case where there were moment interactions between spans. In this chapter, two more cases were also

considered with even greater values of misalignments. Misalignment values were higher than  $\theta_3$  and hence there were span interaction occurring between spans A and B for both the cases. Table 5.1 shows all five cases.

Case 1	$M_{bi} = (1/6) M_r$	$\theta_1 = 0.074^\circ$
Case 2	$M_{bi} = (1/2) M_r$	$\theta_2 = 0.223^\circ$
Case 3	$M_{bi} = M_r$	$\theta_3 = 0.446^\circ$
Case 4	$M_{bi} = 1.125 M_r$	$\theta_4 = 0.502^\circ$
Case 5	$M_{bi} = 1.25 M_r$	$\theta_5 = 0.558^\circ$

*Table 5.1 Various Misalignment cases*

## **5.2 Defining the Model**

Figure 5.1 presents an idea of the model. Length of the web in span A, on roller B and in span B is represented by simply supported beam. The beam has three segments for each of the three spans. The web on roller B is further divided into 10 portions to be able to choose the portion of the web over which slippage would occur. So, the beam now has a total of 13 nodes, 1<sup>st</sup> being the fixed end (at the exit point of roller A), 13<sup>th</sup> node is at the free end of the beam (at the entry point of roller C) and other 11 nodes are on the web on roller B. Rotation was given to roller C (i.e. at node 13).  $L_A$ ,  $L_B$ , and  $L_{RB}$  are lengths of span A, span B and length of the wrap on roller B, respectively. Length of the each element on the roller B is denoted by  $LRBE$ .

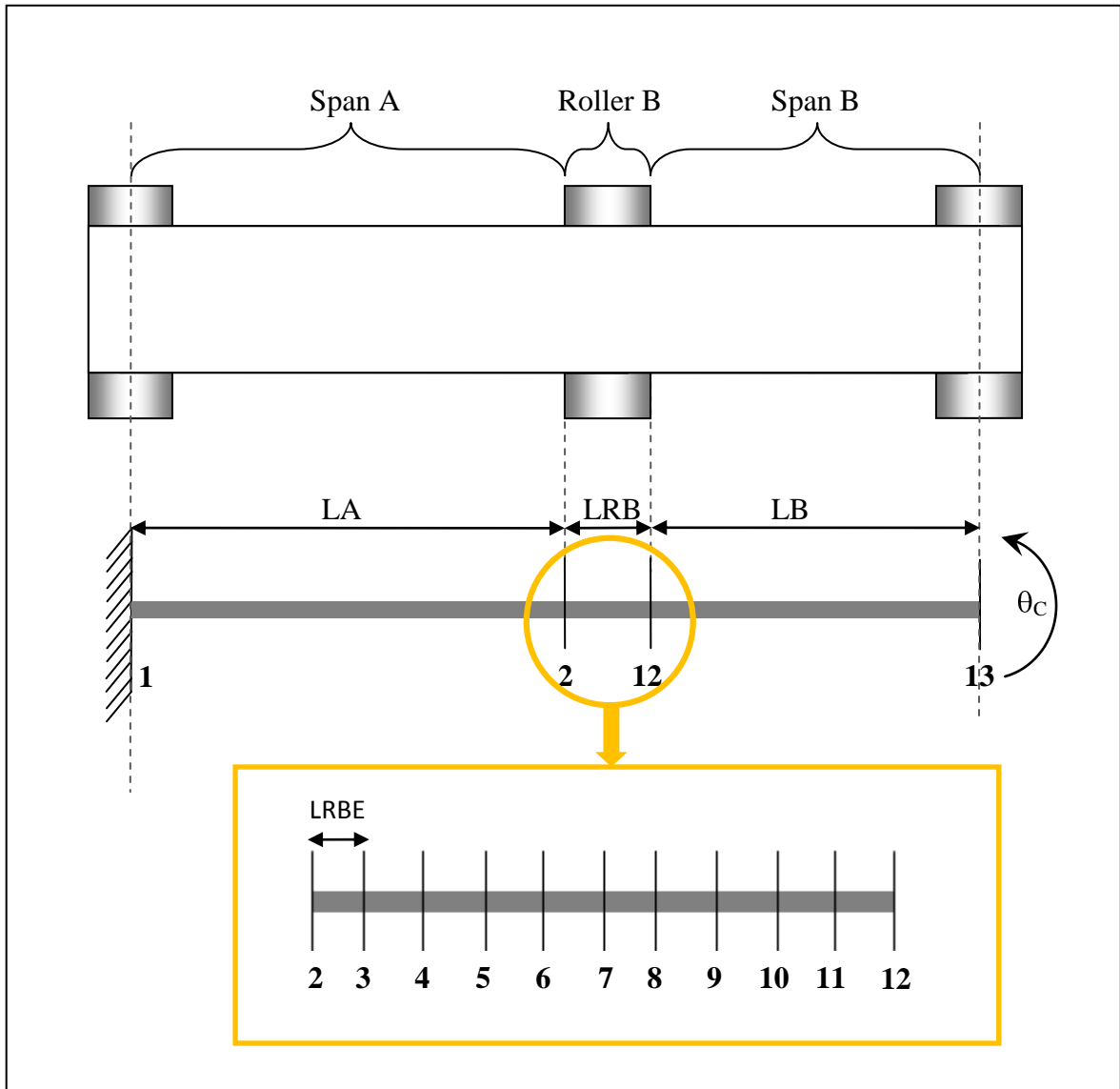


Figure 5.1 Distribution of nodes on the web

As discussed in chapter 2, Przemieniecki [5] developed a stiffness matrix for beams stiffened by tension. Figure 2.3 shows such a beam element. Stiffness matrix for that beam element is given by equation 2.2 as:



$$\begin{Bmatrix} f_{yi} \\ M_i \\ f_{yj} \\ M_j \end{Bmatrix} = \begin{bmatrix} \frac{12EI}{L^3} + \frac{6T}{5L} & \frac{6EI}{L^2} + \frac{T}{10} & -\frac{12EI}{L^3} - \frac{6T}{5L} & \frac{6EI}{L^2} + \frac{T}{10} \\ \frac{6EI}{L^2} + \frac{T}{10} & \frac{4EI}{L} + \frac{2TL}{15} & -\frac{6EI}{L^2} - \frac{T}{10} & \frac{2EI}{L} - \frac{TL}{30} \\ -\frac{12EI}{L^3} - \frac{6T}{5L} & -\frac{6EI}{L^2} - \frac{T}{10} & \frac{12EI}{L^3} + \frac{6T}{5L} & -\frac{6EI}{L^2} - \frac{T}{10} \\ \frac{6EI}{L^2} + \frac{T}{10} & \frac{2EI}{L} - \frac{TL}{30} & -\frac{6EI}{L^2} - \frac{T}{10} & \frac{4EI}{L} + \frac{2TL}{15} \end{bmatrix} \begin{Bmatrix} v_i \\ \theta_i \\ v_j \\ \theta_j \end{Bmatrix}$$

Elemental stiffness matrix for each of the 12 elements were written and combined to obtain a global stiffness matrix for the beam.

Problem was modeled in a MS Excel workbook with all the inputs on worksheet 1 and the code on worksheet 2. Inputs for the problem are shown in table 5.2.

Definition of the constants used in the Model	
LA (Length of span A)	43.75 inches
LB (Length of span B)	33.5 inches
RB (Angle of contact)	1.45 inches
WB (angle of contact on roller B)	1.570796327 radians
W (width of the web)	6 inches
h (thickness of the web)	0.002 inches
Eo (Young's modulus of web material)	570,000 psi
Mu (coefficient of static friction between roller and the web)	0.33
T (tension)	13 lb
LRB (Length of web on roller B)	2.277654674 inches
LRBE(Length of each element on roller B)	0.227765467 inches

Table 5.2 Inputs for the model

### 5.3 Applying Boundary Conditions

Next step in the process is to handle the various boundary conditions at all the nodes. Following three approaches were engaged to satisfy these boundary conditions [14]:

#### 1. Elimination Approach

As discussed earlier there are a total of 13 nodes with two degrees of freedom (dofs) at each node. In the elimination approach, the global stiffness matrix  $\mathbf{K}$  is reduced by deleting rows and columns corresponding to fixed dofs. Global stiffness matrix ( $\mathbf{K}_{eff}$ ) before elimination process is of the form:

$$K_{eff} = \begin{bmatrix} \mathbf{v1} & \mathbf{q1} & \mathbf{v2} & \mathbf{q2} & \dots & \mathbf{v13} & \mathbf{q13} \\ K_{1,1} & K_{1,2} & K_{1,3} & K_{1,4} & \dots & K_{1,25} & K_{1,26} \\ K_{2,1} & K_{2,2} & K_{2,3} & K_{2,4} & \dots & K_{2,25} & K_{2,26} \\ K_{3,1} & K_{3,2} & K_{3,3} & K_{3,4} & \dots & K_{3,25} & K_{3,26} \\ \vdots & \vdots & \vdots & \vdots & \vdots & \vdots & \vdots \\ K_{26,1} & K_{26,2} & K_{26,3} & K_{26,4} & \dots & K_{26,25} & K_{26,26} \end{bmatrix}$$

All 13 nodes have 2 dofs, say  $v_i$  and  $q_i$  ( $i = 1$  to  $13$ ). Hence,  $\mathbf{K}_{eff}$  is a matrix with 26 rows and 26 columns. 1<sup>st</sup> node of the simply supported beam is fixed and  $\mathbf{K}_{eff}$  can be reduced by deleting first two rows and columns (corresponding to  $v_1$  and  $q_1$ ). In the above matrix these rows and columns are shown in yellow. The resulting stiffness matrix is of the form:

$$K'_{eff} = \begin{bmatrix} \mathbf{v1} & \mathbf{q1} & \mathbf{v2} & \mathbf{q2} & \dots & \mathbf{v13} & \mathbf{q13} \\ K_{3,3} & K_{3,4} & K_{3,5} & K_{3,6} & \dots & K_{3,25} & K_{3,26} \\ K_{4,3} & K_{4,4} & K_{4,5} & K_{4,6} & \dots & K_{4,25} & K_{4,26} \\ \vdots & \vdots & \vdots & \vdots & \vdots & \vdots & \vdots \\ K_{26,3} & K_{26,4} & K_{26,5} & K_{26,6} & \dots & K_{26,25} & K_{26,26} \end{bmatrix}$$

## 2. Lagrange Constraints

This method of applying boundary conditions was used to input the rotation at the free end of the beam. There is some misalignment induced at the roller C. This constraint equation at node 13 is:

$$q_{13} = \theta_i \times \frac{\pi}{180} \text{ rad}$$

where,  $i=1$  to 5, for all five misalignment cases. To deal with this kind of boundary condition an additional constraint equation is added to the stiffness matrix.

$$[C]_{m \times n} \{Q\} - \{r_0\} = 0$$

where, C is matrix of coefficients,  $r_0$  is the vector of misalignment to be enforced, m is number of constraints (here,  $m=1$ , for every case) and n is the number of dof in {Q} (here,  $n=24$ , for every case, since elimination deleted 2 dofs). After applying Lagrange constraints the stiffness matrix is of the following form:

<b>v1</b>	<b>q1</b>	<b>v2</b>	<b>q2</b>	<b>...</b>	<b>v13</b>	<b>q13</b>	
$K_{3,3}$	$K_{3,4}$	$K_{3,5}$	$K_{3,6}$	$\dots$	$K_{3,25}$	$K_{3,26}$	<b>0</b>
$K_{4,3}$	$K_{4,4}$	$K_{4,5}$	$K_{4,6}$	$\dots$	$K_{4,25}$	$K_{4,26}$	<b>0</b>
.	.	.			.	.	.
.	.	.			.	.	.
.	.	.			.	.	.
$K_{25,3}$	$K_{25,4}$	$K_{25,5}$	$K_{25,6}$	$\dots$	$K_{25,25}$	$K_{25,26}$	<b>0</b>
$K_{26,3}$	$K_{26,4}$	$K_{26,5}$	$K_{26,6}$	$\dots$	$K_{26,25}$	$K_{26,26}$	<b>1</b>
<b>0</b>	<b>0</b>	<b>0</b>	<b>0</b>	$\dots$	<b>0</b>	<b>1</b>	<b>0</b>

## 3. Penalty Approach

For the second case of misalignment slippage starts occurring in between roller surface and the web material but there is no moment transfer into the upstream span. In

such a case, penalty method of handling boundary conditions was used to choose the portion of the web on roller B over which the slippage occurs.

Generally, penalty method is applied to specified displacement boundary conditions. Let us consider a case where,

$$Q_1 = a_1, \quad Q_2 = a_2, \quad Q_3 = a_3, \quad \dots, \quad Q_r = a_r$$

Then the structural stiffness matrix '**K**' is modified by adding a large number '**C**' to each of the 1<sup>st</sup>, 2<sup>nd</sup>, 3<sup>rd</sup>, ... and r<sup>th</sup> diagonal element. Also, the global load vector **F** is modified by adding  $Ca_1$  to  $F_1$ ,  $Ca_2$  to  $F_2$ , ..., and  $Ca_r$  to  $F_r$ . Then  $\mathbf{KQ} = \mathbf{F}$  is solved for the displacement **Q**, where **K** and **F** are modified stiffness and load matrices.

In our case, for every node on roller B, boundary condition is applied to constraint the lateral movement of the web, so the 'a' can only be zero. Whenever we want to cut loose some nodes on roller B, there will not be any constraints for those nodes. As  $a=0$ , there will not be any change in the force matrix. Resulting stiffness matrix is of the form:

<b>v1</b>	<b>q1</b>	<b>v2</b>	<b>q2</b>	...	<b>v13</b>	<b>q13</b>	
$(K_{3,3}+C)$	$K_{3,4}$	$K_{3,5}$	$K_{3,6}$	...	$K_{3,25}$	$K_{3,26}$	<b>0</b>
$K_{4,3}$	$(K_{4,4}+C)$	$K_{4,5}$	$K_{4,6}$	...	$K_{4,25}$	$K_{4,26}$	<b>0</b>
⋮	⋮	⋮	⋮	...	⋮	⋮	⋮
$K_{25,3}$	$K_{25,4}$	$K_{25,5}$	$K_{25,6}$	...	$(K_{25,25}+C)$	$K_{25,26}$	<b>0</b>
$K_{26,3}$	$K_{26,4}$	$K_{26,5}$	$K_{26,6}$	...	$K_{26,2}$	$(K_{26,26}+C)$	<b>1</b>
<b>0</b>	<b>0</b>	<b>0</b>	<b>0</b>	...	<b>0</b>	<b>1</b>	<b>0</b>

Reaction forces at each support are calculated as,  $R = -Cq$ .

#### **5.4 Executing the Problem**

Fixed end of the beam is always constrained for all the five cases of misalignment. First two rows and columns were eliminated from the global stiffness matrix, as discussed in previous section. Lagrange method was used to give different amounts of misalignments at the 13<sup>th</sup> node. ‘Solver’ was used to force the moment at the roller C to zero. Penalty method was used to constraint the nodes on roller B (to select the portion over which slippage was occurring) depending on the amount of misalignment. For larger values of  $\theta_c$ , when  $M_{bi} > M_r$  (for  $\theta_3$ ,  $\theta_4$  and  $\theta_5$ ) all the 11 nodes on roller B are unconstrained. For the first two cases ( $\theta_1$  and  $\theta_2$ ), reactions are calculated at each node to find the number of constrained nodes. Initially, all the nodes on roller B are constrained and reactions are calculated and the nodes were cut loose on the exit side of roller until the reaction was observed to a value close to zero.

Forces (opposite to the direction of the total force at the end of the beam) were applied at all the unconstrained nodes, which when added would be equal to the end force in magnitude (but opposite in sign).

This new FEM model was executed for all the five cases and the lateral deformations obtained were compared to those obtained from the Keyence sensors in the following section.

## **5.5 Results from FEM model**

As discussed in the previous sections, all the five cases of misalignments were implemented in the FEM model. Boundary conditions for each of these cases were applied to input the angle of misalignment and to constrain the nodes on roller B, depending on the level of misalignment.

It has been already conferred from the behavior of moments in the span A (for  $\theta_3$  case) in section 5.5, that the web tries to achieve normal entry to roller B under conditions of moment transfer. In such a situation, continuity of the bending stresses from one side of the tangent line of entry to roller B to the other side of the line should be maintained. This has been taken care of in the FEM model.

Lateral deformations in the web at all 13 nodes are obtained from the model, for all the cases and are shown in Figure 5.2. It can be observed that for smaller misalignment cases ( $\theta_1$  and  $\theta_2$ ), the value of misalignment is not enough to induce any lateral movement in the web on roller B and the only deflection is in span B with a maximum value at roller C. Hence the nodal deformations in nodes 2 through 12 ( $v_1, v_2, v_3 \dots v_{13}$ ) are zero. For larger misalignments ( $\theta_3, \theta_4$  and  $\theta_5$ ), the web on roller B starts slipping as the frictional forces between the web and the roller are insufficient to prevent moment interaction into span A. The values of nodal deflections at each node increases with the amount of misalignment. Table 5.3 shows the values of nodal displacements at each node on the web.

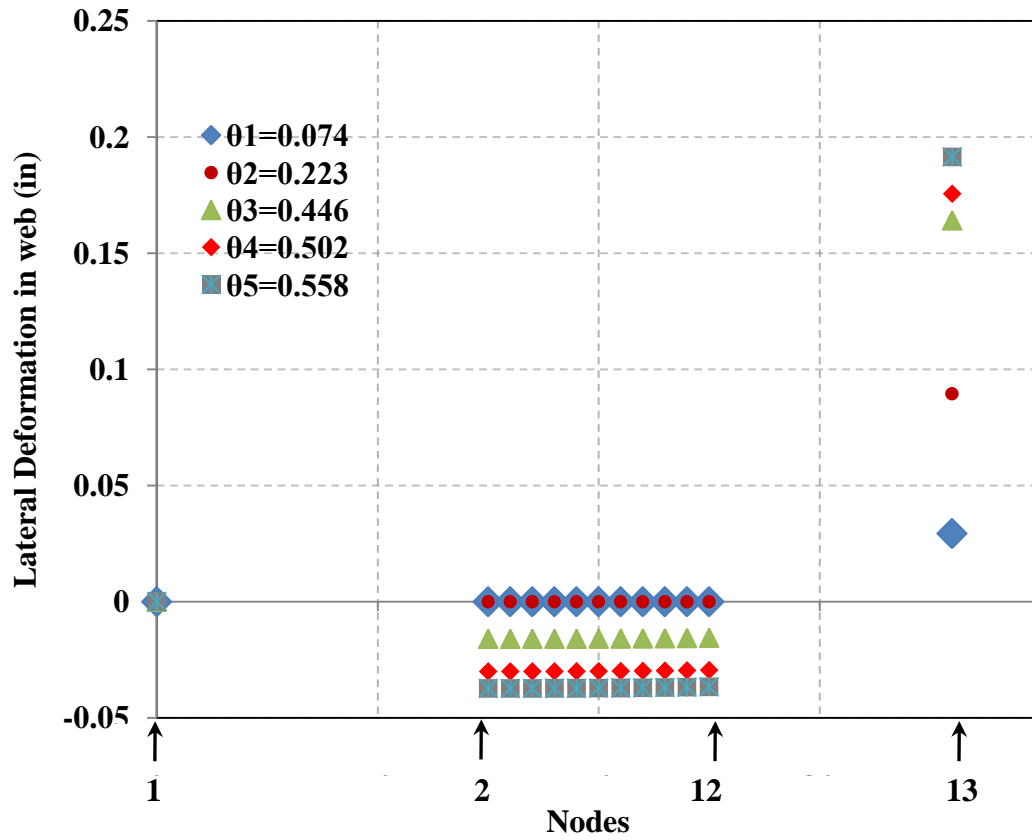


Figure 5.2 Lateral deformations at various nodes

Node	$\theta_1=0.074^\circ$	$\theta_2=0.223^\circ$	$\theta_3=0.446^\circ$	$\theta_4=0.502^\circ$	$\theta_5=0.558^\circ$
1	0	0	0	0	0
2	-3.1243E-48	-7.6882E-32	-0.01599	-0.03011	-0.0374
3	-6.33141E-44	-1.55802E-27	-0.01599	-0.0301	-0.03739
4	-1.28312E-39	-3.15741E-23	-0.01598	-0.03009	-0.03738
5	-2.60038E-35	-6.36995E-19	-0.01597	-0.03008	-0.03736
6	-5.26994E-31	2.75451E-16	-0.01595	-0.03005	-0.03733
7	-1.06801E-26	6.02086E-08	-0.01592	-0.03001	-0.03728
8	-2.16438E-22	1.35847E-06	-0.01588	-0.02995	-0.03722
9	-4.36695E-18	6.11897E-06	-0.01582	-0.02988	-0.03713
10	1.97601E-17	1.65492E-05	-0.01575	-0.02978	-0.03703
11	4.04193E-07	3.48403E-05	-0.01566	-0.02967	-0.03689
12	2.73442E-06	6.31665E-05	-0.01554	-0.02953	-0.03674
13	0.029328699	0.089507105	0.16416	0.1756	0.19136

Table 5.3 Lateral deformations at various nodes

Keyence sensors were installed on the test setup to monitor web edge deformation in entering and pre-entering span. They were capable of recording lateral deflection in the web at the entry point of roller B ( $v_2$  in FEM model) and at roller C ( $v_{13}$  in FEM model). This allows us to compare the output from Keyence sensors to the web nodal deflections obtained from the FEM model. Such a comparison of the lateral deformations in the web is shown in Table 5.4.

		$v_{aj}$	$v_{bj}$
$\theta_1=0.074^\circ$	Keyence	<b>0</b>	<b>0.0264</b>
	FEM Model	<b>0</b>	<b>0.0293</b>
	GOOD	<b>0</b>	<b>0.0292</b>
$\theta_2=0.223^\circ$	Keyence	<b>0</b>	<b>0.0903</b>
	FEM Model	<b>0</b>	<b>0.0895</b>
	GOOD	<b>0</b>	<b>0.088</b>
$\theta_3=0.446^\circ$	Keyence	<b>-0.019</b>	<b>0.1681</b>
	FEM Model	<b>-0.016</b>	<b>0.1642</b>
	GOOD	<b>0</b>	<b>0.176</b>
$\theta_4=0.502^\circ$	Keyence	<b>-0.0283</b>	<b>0.1864</b>
	FEM Model	<b>-0.0301</b>	<b>0.1756</b>
	GOOD	<b>-0.0193</b>	<b>0.1979</b>
$\theta_5=0.558^\circ$	Keyence	<b>-0.0352</b>	<b>0.2022</b>
	FEM Model	<b>-0.0374</b>	<b>0.1912</b>
	GOOD	<b>-0.0385</b>	<b>0.2201</b>

*Table 5.4 A comparison of web edge deflections*

Good [2] in his paper on “Shear in multispan web systems” (presented during IWEB 4) studied multispan interactions in web lines due to a misaligned downstream roller. He presented expressions to calculate maximum lateral deformations in span A and span B. Lateral deflection in span B was given by ( $v_{13}$  in FEM model):



$$v_{bj} = \left[ \frac{4EI}{L_b} + \frac{2TL_b}{15} \right] \theta_{bj} \quad (5.1)$$

and lateral deflection in span A at roller B ( $v_2$  in FEM model) is given by:

$$v_{aj} = -\frac{M_{aj}}{\frac{6EI}{L_b^2} + \frac{T}{10}} \quad (5.2)$$

where,

$$\begin{aligned} M_{aj} &= 0 && \text{when } M_{bi} < |M_r| \\ M_{aj} &= -[M_{bi} - M_r] && \text{when } M_{bi} > M_r \text{ and } M_{bi}(+) \\ M_{aj} &= -[M_{bi} + M_r] && \text{when } |M_{bi}| > M_r \text{ and } M_{bi}(-) \end{aligned} \quad (5.3)$$

As  $v_{bj}$  depends on the level of misalignment, it can be deduced for all five cases whereas,  $v_{aj}$  can be calculated for only last two cases of misalignment ( $\theta_4$  and  $\theta_5$ , where  $M_{aj}$  is non-zero) and is zero for other cases.

Results from the FEM model compare well with the data recorded by Keyence sensors. Good's model of predicting lateral deformations is also proved to be in accordance with tests and FEM model.

Moments were obtained on roller B from the FE model. Previously LDVs were used to observe the nature of moments on the roller B and all the moments for the all three misalignment cases was found to be decaying linearly on the roller B (Figure 4.10). Plot for the moments at the same locations on roller B obtained from FE model is shown in Figure 5.3.

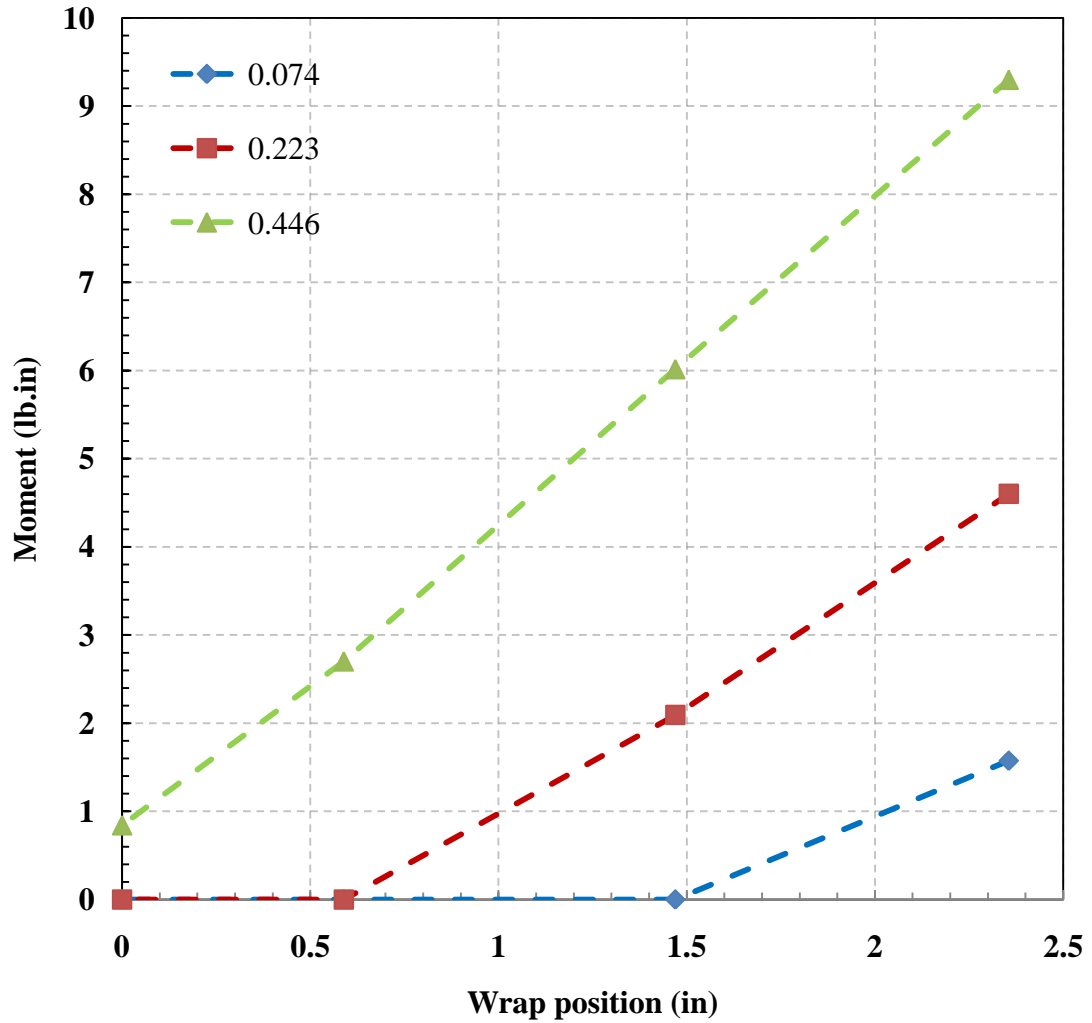


Figure 5.3 Moments on roller B from FE model

The moments seem to decrease linearly and as the moments values were close to ones calculated from the LDVs. When these results are compared with the results obtained from the LDVs (Figure 4.10), it is evident that the results obtained from the LDVs are valid.

## CHAPTER VI

### Summary and Conclusions

#### 6.1 Summary

The focus of this research has been on analyzing moments and moment transfer in a multispan web system due to a misaligned downstream roller. An experimental setup was built to examine various cases of misalignment and the results were discussed in the previous chapter. This chapter lays out the conclusions drawn from the research.

The attempt to develop a machine, capable of taking moment measurements in pre-entering and entering spans and on the intermediate roller B were successful. The test setup also has the ability to record lateral deflection in the web at roller B and roller C, for varying values of misalignment. A rig was also developed to calibrate the set of LDVs used for recording data. Use of LDVs has successfully helped in determining amount of moment associated with slippage which was then verified by a newly developed FEM model for various misalignment cases.

#### 6.2 Conclusions

As expected, for the cases when  $\theta=0.074^\circ$  and  $\theta=0.223^\circ$ , LDV results were consistent with the theory (figure 4.6 and figure 4.7). There is no moment transfer occurring into pre-entering span. For  $\theta=0.446^\circ$ , there is some moment interaction in span A.

Equation 2.1, which gives the critical moment (the moment at which span interaction starts), appears to be a good predictor of the misalignment required for moment transfer.

FEM model was proved to be capable of predicting the maximum lateral deformations in span A and span B for all the five cases of misalignments (Figure 5.2). It was able to detect the portion of roller B over which slippage was occurring and the amount of moment associated with that slippage. Comparison of the results with experimental data and Good [2] theory proves the models capability (Table 5.4).

In case of span interactions, it can be concluded that normal entry is achieved at roller B (Figure 4.1)

Moments decayed linearly on roller B, whenever there was moment transfer from span B to span A (Figure 4.10 and Figure 5.3)

### **6.3 Future Work**

In this research, a setup was developed to give various misalignments to roller C, to record LDV data for moment calculation and to measure lateral deformations near ends of entering and pre-entering spans. An explicit finite element model (using ABAQUS®) can be developed to for the same setup with similar geometry and loading conditions. It would help understand multi-span interactions in a better way.

Attempt to correct the cosine error in the measurements from LDVs due to misalignment, by aligning LDVs perpendicular to the motion of the web in span B, was effective. This process of correction can be automated (with a feedback control system) in such a way that the LDVs can align them automatically with the web, whenever there is some rotation in roller C.

## REFERENCES

1. Shelton, J. J., "*Lateral Dynamics of a Moving Web*," PhD Thesis, Oklahoma State University, 1969.
2. Good, J.K., "*Shear in Multispan Web Systems*," Proceedings of the Fourth International Conference on Web Handling, Oklahoma State University, pp. 264-286, 1997.
3. Lorig, E.T., "*Automatic Self-Centering Rolls and Pulleys*," 1950 AISE Convention, Cleveland, Ohio
4. Gehlbach, L.S., Good, J. K., and Kedl, D.M., "*Prediction of Shear Wrinkles in Web Spans*," TAPPI Journal, Vol 72, No. 8, pp. 129.-134, Aug. 1989.
5. Przemieniecki, J.S., "*Theory of Matrix Structural Analysis*," McGraw-Hill, 1968.
6. Dobbs, J.N., and Kedl, D.M., "*Wrinkle Dependency on Web Roller Slip*," Proceedings of the Fourth International Conference on Web Handling, Oklahoma State University, Stillwater, Oklahoma, June 18-21, 1995
7. Shelton, J.J., "*Interaction Between Two Web Spans Because of a Misaligned Downstream Roller*," Proceedings of the Eighth International Conference on Web Handling, Oklahoma State University, Stillwater, Oklahoma, June 5-8, 2005
8. Beisel, J.A., "*Prediction of Single Span Web Buckling and Experimental Verification*," M.S. Thesis, Oklahoma State University, July 2000
9. Webb, D.K., "*Prediction of Web Wrinkles Due to Misalignment of a Downstream Roll in a Web Span*," M.S. Thesis, Oklahoma State University, Dec. 2004.
10. Good, J.K. and Beisel, J.A., "*Buckling of Orthotropic Webs in Process Machinery*," Proceedings of the Seventh International Conference on Web Handling, WHRC, Oklahoma State University, June 2003.
11. Knox, K.L. and Sweeney, T.L., "*Fluid Effects Associated with Web Handling*," Industrial Engineering Chemical Process Design Development, 1971, Vol. 10, No. 2, pp. 201-205

12. Good, J.K., D.M. Kedl, and J.J. Shelton, "*Shear Wrinkling in Isolated Spans*," Proceedings of the Fourth International Conference on Web Handling, Stillwater, OK, WHRC, Oklahoma State University, June 1997.
13. Beisel, J.A., "*Single Span Web Buckling Due to Roller Imperfections in Web Process Machinery*," PhD Thesis, Oklahoma State University, 2006.
14. Chandrupatla, T.R., Belegundu, A.D., *Introduction to Finite Elements in Engineering*, 3<sup>rd</sup> ed, Prentice-Hall, New Jersey, 2006
15. Yurtcu, H.H., "*Development of Nonlinear Finite Element Codes for Stability Studies of Web Material with Strain State Dependent Properties*," PhD Preliminary Examination, Oklahoma State University, January 2009.

## **APPENDICES**

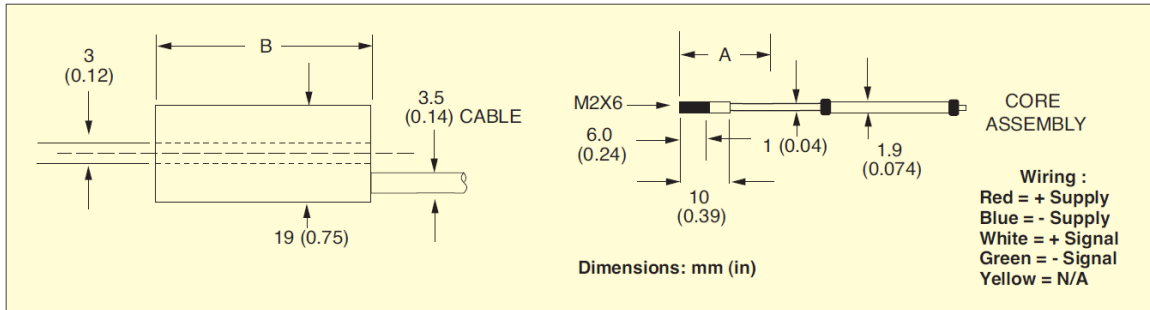
**APPENDIX – A**

**Data sheet for Miniature DC Output LVDT Displacement Transducer**

**(Model 400-5)**



## DIMENSIONS



Unit : mm (inch)

A = 20.5 (0.81)

B = 43 (1.69)

## SPECIFICATIONS

### ELECTRICAL

<b>Linearity</b>	0.3% FS	
<b>Sensitivity</b>	54 mV/V/mm	
<b>Excitation</b>	10 to 24 Vdc	
<b>Energizing Current at 10 Vdc</b>	LD400-5, 13 mA	
<b>Response Time</b>	3 ms	
<b>Frequency Response</b>	50 Hz for -3 dB	
<b>Ripple</b>	<1% FS	
<b>Thermal Effect</b>	<0.01% FC/°C; sensitivity: <0.025% FC/°C	
<b>Compensated Temperature Range</b>	-20 to 80°C (-4 to 176°F)	
<b>Operating Temperature Range</b>	-20 to 80°C (-4 to 176°F)	
<b>Electrical Connection</b>	2.9 m (9') shielded, color-coded cable	
<b>Sensitivity and Linearity Data</b>	Provided with a transducer output impedance of 2.4 kΩ into a calibration load of 20 kΩ at 20°C (68°F); variations in these parameters will change performance	

### MECHANICAL


<b>Threaded Core</b>	M2 thread
<b>Core Material</b>	Ni/Fe—Radio Metal 50
<b>Case Material</b>	400 Series stainless steel
<b>Weight: Body</b>	1.18oz Core 0.04oz
<b>Linear Stroke</b>	±5.0 (0.20) mm (in)

**APPENDIX – B**

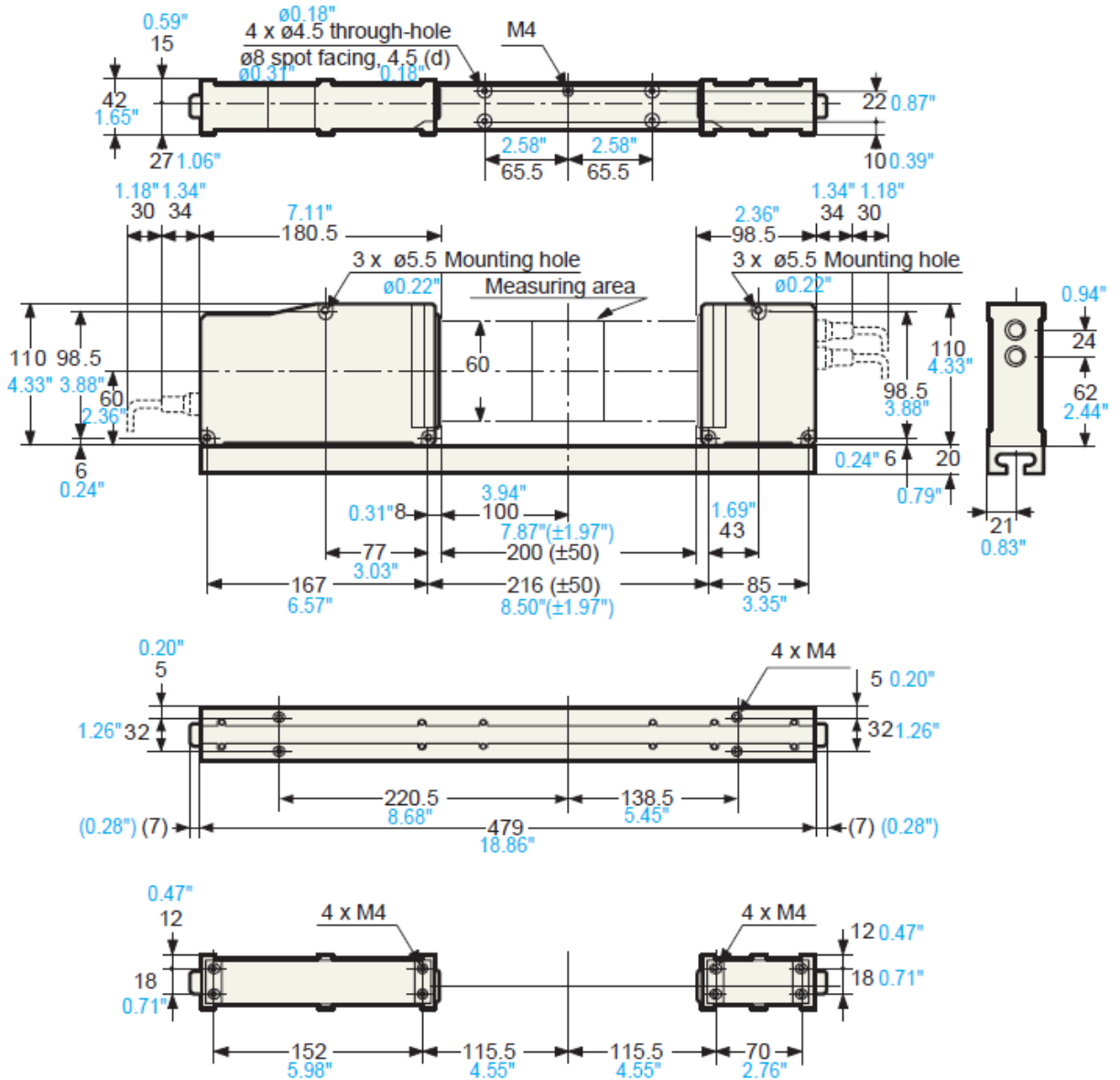
**Data Sheet for KEYENCE Sensor (Model LS 3060) and Controller**

## KEYENCE Sensor LS 3060 Specifications:

---

<b>Measuring Range</b>	<b>0.03" to 2.36"</b>	
<b>Controller</b>	mm/inch selectab	
<b>Minimum target width</b>	<b>0.03"</b>	
<b>T and R distance</b>	<b>7.87" ± 1.97"</b>	
<b>Light source</b>	Red semiconduct	
<b>Wavelength</b>	670 nm	
<b>Measuring accuracy</b>	± 3 µm max <b>0.01 Mil</b>	
<b>Repeatability</b>	0.5 µm <b>0.02 Mil</b>	
<b>Display resolution</b>	0.1 µm <b>0.004 Mil</b>	
<b>Laser scan rate</b>	400 scans/s	
<b>Laser scan velocity</b>	126 m/s <b>413.4'</b>	
<b>Laser scan range</b>	Approx. 65 mm <b>2.56"</b>	
<b>Measured value</b>	Main display: 7-segment green LED (8 digits) Sub display: 16 character x 2 line LCD (Backlight color: yellow-green)	
<b>Minimum display unit</b>	0.1 µm <b>0.004 Mil</b> / 0.2 µm <b>0.008 Mil</b>	
<b>Display range</b>	-999.9999 to 9999.9999	
<b>Target position indicator</b>	Green LED (7 levels)	
<b>Comparator output indicator</b>	Green LED x 3 (HI/GO/LO)	
<b>Laser emission indicator</b>	Green LED x 2 (HEAD 1/ HEAD 2)	
<b>Interface port</b>	RS-232C/GP-IB (optional)/ BCD (optional)	
<b>Power supply</b>	85 to 264 VAC, 50/60 Hz	
<b>Power consumption</b>	40 VA max.	
<b>Ambient temperature</b>	<b>Scanning head</b> 0 to +40°C <b>Controller</b> 0 to +40°C	
<b>Weight</b>	<b>Scanning head</b> Approx. 2.5 kg (base included) <b>Controller</b> Approx. 4.6 kg	

## KEYENCE Sensor LS 3060 Dimensions:

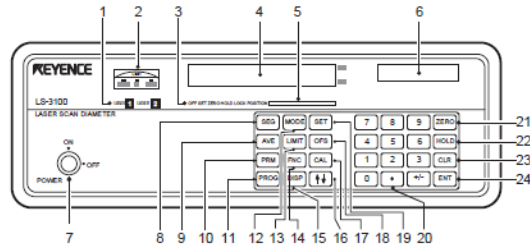


Unit: mm Inch

## Controller Parts:

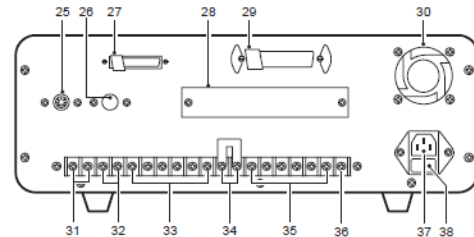
### Part Names and Functions

#### Front Panel



- 1 Laser emission indicator LED
- 2 Comparator output LEDs
- 3 Current setting indicator
- 4 Main display (CH1)
- 5 Target position indicator
- 6 Sub-display (CH2)
- 7 Key-operated power switch
- 8 SEGMENT key
- 9 AVERAGE key (for number of measurements)
- 10 PARAMETER key
- 11 PROGRAM key
- 12 MODE key
- 13 LIMIT key (for 3-level comparator output)
- 14 FUNCTION key
- 15 DISPLAY key
- 16 UP/DOWN key
- 17 CALIBRATION key
- 18 OFFSET key
- 19 SET key
- 20 Numeric keys
- 21 AUTO ZERO key
- 22 HOLD key
- 23 CLEAR key
- 24 ENTER key

#### Rear Panel



- 25 SCANNING HEAD connector
- 26 SCANNING HEAD connector (when 2 are installed)
- 27 RS-232C connector
- 28 Expansion I/O port (used when option board is installed)
- 29 36-pin connector (Control I/O)
- 30 Cooling fan
- 31 Analog voltage output terminals
- 32 Hold synchronous input terminals
- 33 Program selection input terminals
- 34 Laser emission control input terminals
- 35 Comparator limit output terminals
- 36 Frame ground terminal
- 37 Power supply connector
- 38 Fuse holder (2 A)

**VITA**

**Arjun Reddy Anugu**

**Candidate for the Degree of**

**Master of Science**

**Thesis:** ANALYSIS OF MOMENT TRANSFER IN MULTI-SPAN WEB SYSTEMS

**Major Field:** Mechanical Engineering

**Biographical:**

Personal Data:

Born in Hyderabad, Andhra Pradesh, India, on November 9<sup>th</sup>, 1985. Son of Gopal R. Anugu and Uma Anugu

**Education:**

2003-2010

Completed the requirements for the Master of Science in Mechanical Engineering at Oklahoma State University, Stillwater, Oklahoma in May, 2010.

2003-2007

Bachelor of Technology in Mechanical Engineering,  
Jawaharlal Nehru Technological University, Hyderabad, India

**Experience:**

2008-2010

Graduate Research Assistant,  
Web Handling Research Center, Oklahoma State University.

Name: Anugu Arjun Reddy

Date of Degree: May, 2010

Institution: Oklahoma State University

Location: Stillwater, Oklahoma

Title of Study: ANALYSIS OF MOMENT TRANSFER IN MULTI-SPAN WEB SYSTEMS

Pages in Study: 100

Candidate for the Degree of Master of Science

Major Field: Mechanical Engineering

Scope and Method of Study:

Webs pass over numerous rollers in web processing machinery. A common problem is the formation of troughs and wrinkles in webs. Any out-of-plane web deformation in a span is called a trough and if this trough passes over a roller it may form a wrinkle. A major reason for the formation of troughs and wrinkles is the misalignment of the downstream roller in a span. As a result of misalignment moments are developed in the span upstream of the misaligned roller. The moment must be reacted by the frictional forces between the web and the upstream roller, where the moment is largest. If these frictional forces are not adequate a portion of the moment will be passed into the next span upstream. The focus of this research is to study moment transfers from one span to an upstream span and study the moments on the contact patch on the intermediate roller for the first time. An experimental setup was built to quantify amount of moments transferred for various amounts of misalignments. A finite element model was also developed to verify the experimental results.

Findings and Conclusions:

Laser Doppler Velocimeters (LDVs) were used to study the span interaction in web systems due to a misaligned downstream roller. The LDV is an industrial instrument capable of measuring the length of the material moving beneath them. The LDV's capability to measure length was used to calculate relative strain in a web span which can be related to moment. Moment measurements were made in entering span, pre-entering span, and on the roller dividing those two spans. Moments calculated from the experiments were verified by a newly developed FE model. The FE model estimated the amount of slippage associated with each level of misalignment and it proved to be a good predictor of the nature of web/roller interactions resulting due to a downstream misaligned roller.

ADVISER'S APPROVAL: Dr. J.K. Good

---